AD

AD 685833

Research and Development Technical Report
ECOM- 0423-2

APPROXIMATE JOINT PROBABILITY DISTRIBUTIONS OF THE TURBULENCE ALONG A HYPOTHETICAL MISSILE TRAJECTORY DOWNWIND OF A SINUSOIDAL MODEL RIDGE

TECHNICAL REPORT

By

E. J. PLATE

F. F. YEH

R. KUNG

February 1969

DISTRIBUTION STATEMENT

This document has been approved for public release and sale; its distribution is unlimited.

ECOM

UNITED STATES ARMY ELECTRONICS COMMAND · FORT MONMOUTH, N.J.

CONTRACT DAAB07 68-C-0423
FLUID DYNAMICS AND DIFFUSION LABORATORY
FLUID MECHANICS PROGRAM
COLLEGE OF ENGINEERING
COLORADO STATE UNIVERSITY
FORT COLLINS, COLORADO 80521

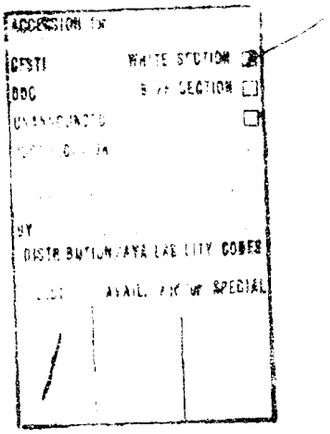

NOTICES

Disclaimers

The findings in this report are not to be construed as an official Department of the Army position, unless so designated by other authorized documents.

The citation of trade names and names of manufacturers in this report is not to be construed as official Government indorsement or approval of commercial products or services referenced herein.

Disposition

Destroy this report when it is no longer needed. Do not return it to the originator.

Technical Report ECOM 0423-2

Reports Control Symbol
OSD-1366
February 1969

APPROXIMATE JOINT PROBABILITY DISTRIBUTIONS OF THE TURBULENCE ALONG A HYPOTHETICAL MISSILE TRAJECTORY DOWNWIND OF A SINUSOIDAL MODEL RIDGE

by

Erich J. Plate, F. F. Yeh & R. Kung

Prepared for

U. S. Army Materiel Command

Contract No. DAAB07-68-C-0423

February 1969

DISTRIBUTION STATEMENT

This document has been approved for public release and sale; its distribution is unlimited.

Fluid Dynamics and Diffusion Laboratory

College of Engineering
Colorado State University
Fort Collins, Colorado

CER68-69EJP-FY-RK-1

Technical Report

APPROXIMATE JOINT PROBABILITY DISTRIBUTIONS OF THE TURBULENCE ALONG A HYPOTHETICAL MISSILE TRAJECTORY DOWNWIND OF A SINUSOIDAL MODEL RIDGE*

by

Erich J. Plate*, E. E. Yeh

and

R. . .g

ABSTRACT

The wind field is investigated which is encountered by a missile traveling along a hypothetical trajectory downwind of a two-dimensional ridge. Reasons are given for studying this situation in a wind tunnel. The problem is reduced to the determination of turbulence spectra and of joint probabilities for the joint occurrence of two velocities simultaneously along the trajectory which corresponds to mean flow conditions.

In the theoretical part an attempt is made to obtain approximations to the joint probability density distributions which yield to experimental evaluation. The experimental part is concerned with measurements of profiles of mean velocities and turbulent intensities and with the determination of turbulence data for evaluating spectra and joint probability distributions.

---

*A preliminary version of this report has been presented at the Unguided Ballistic Missile Meteorology Conference, Las Cruces, Oct. 31 - Nov. 2, 1967.

TABLE OF CONTENTS

LIST OF SYMBOLS

A	Real constant
D	Dissipation number
E	Mean output (d.c.) of voltage from hot-wire anemometer
K	Universal constant
L	Length, dimension of the missile
R_τ	Autocorrelation coefficient
T	Average observation time
$\overline{U}$	Local mean velocity in X direction
X_c	Location of end point of the mean wind trajectory
X_e'	Deviation from X_e
e	Fluctuating (a.c.) output of voltage form
f	Frequency
$f(u')$, $f(v')$, $f(w')$	Probability density of u', v', w'
$f(\vec{v}') = f(u',v',w')$	Joint probability density of u', v', w'
$f(\vec{V}_n'/\vec{V}_{n-1}')$	Conditional probability density of $\vec{V}_n$ given $\vec{V}_{n-1}'$
h	Height of the obstruction
k	Wave number
k_s	Reference wave number
m_u', m_v', m_w'	Mean values of u', v', w'
p_a	Static pressure at static tap position
p_b	Static pressure at dynamic tap position
u',v',w'	Turbulent fluctuations in x, y, z directions
$\overline{u'v'}$	Covariance of u' and v'
$\vec{v}\ (\vec{s})$	Mean velocity vector
$\vec{v}\ (\vec{s},t)$	Velocity vector

$\vec{v}'(\vec{s},t)$	Fluctuating velocity vector
x,y,z	Coordinate system
z_o	Roughness height
α, β	Flow attacking angles on the crossed hot-wire
ε	Dissipation energy calculated from the spectra
ε'	Dissipation energy calculated from differential circuit
$\mathcal{J}_s$	Space integral scale
θ	Rotating angle of coordinating axes
λ_g	The microscale of the turbulence
ν	Kinematic viscosity
ρ_a	Density of air
ρ	Correlation coefficient of two random variables
$\sigma u', \sigma v', \sigma w'$	Variance of u', v', w'
ϕ	Angle deviation of the flow from the free stream direction
ω	Angular frequency

LIST OF TABLES

LIST OF FIGURES

Chapter I

INTRODUCTION

1.1 The Problem

One of the major problems in predicting the target hitting capabilities of unguided rocket propelled missiles flying in the atmospheric boundary layer is the interaction between the missile and the turbulent wind field along its flight path. In the analysis of missile weapon systems, especially those used in short range (0-1 km) applications, predicting target hit probability caused by gust winds, involves prior knowledge of the wind field along the missile's trajectory. We can formulate this problem as follows: if the trajectory of a missile is given by a deterministic curve determined by mean-wind conditions, we must find the probability distribution of the perturbations of the trajectory end point if the missile encounters random velocity fluctuations during its travel along the trajectory. The fluctuations influence the flight path in two ways. Vibrations, caused by the gust spectrum might occur, and the missile might be deflected from its course by large velocity fluctuations. For obtaining instantaneous wind measurements to calculate trajectories in a turbulent wind field, the present experimental study was undertaken.

We chose the wind field which exists in the wake downwind of a two-dimensional obstruction with air flow separation at the downwind slope, as shown in Fig. 1. The sinusoidal obstruction used in this study represents the model of a ridge. The wind field which exists in the wake of a ridge is of interest in military combat applications since ridges have been used as part of a defensive line against an attacking force. If missile launchers are emplaced along a ridge, the target impact dispersion of missiles caused by the turbulent winds on the lee side of the ridge will play a considerable role in battlefield strategy.

A full account of this wind field is difficult to obtain in the field. The number of data points at which wind speed information is required is large, and the variability of wind speeds in natural environments would require elaborate and costly experimental equipment. Therefore, it was suggested to study the wind fields that might be encountered downwind of a sinusoidally shaped hill in the controlled environment of a laboratory where many needed data can be taken one after another instead of simultaneously, and where the reliability of measuring instruments and data analysis equipment has reached a high level.

In this report, we shall concentrate only on the problem of obtaining an approximation to the joint probability distribution for a sequence of instantaneous velocity vectors along some hypothetical trajectories. The analytical considerations are based on assuming certain models for joint probability distributions. The validity of these distributions for the disturbed flow field downstream of a ridge is demonstrated by means of experimental data obtained in the wind tunnel. The observations were made for a steady mean velocity field obtained by

blowing air parallel to a flat plate perpendicularly onto a model ridge of sinusoidal shape.

1.2 Considerations on Modeling

The crucial problem in applying laboratory results for practical applications in a natural environment is the question of scaling laboratory conditions up to field dimensions. For flows of undisturbed boundary layers, such as the wind along a boundary of constant roughness over a long fetch, the modeling has been achieved beyond reasonable doubt by scaling according to the ratio of the roughness heights, and by keeping the shear velocities constant. With these conditions met, both the mean velocity conditions and the turbulence structure are approximately scaled. For a boundary layer flow which is disturbed by a sharp edged obstacle, Plate and Lin (1965) have presented an argument, based on the boundary layer integral momentum equation, that the same parameters together with the drag coefficient of the obstacle (as referred to some convenient velocity, such as the geostrophic wind velocity), suffice to model the mean velocity field. As far as the turbulence structure is concerned, no equivalent conclusions are as yet forthcoming, but some work by Plate and Lin (1966) has pointed at the possibility that the modeling of the dissipation number is an additional requirement. Moreover, no conclusions have yet been reached on how the turbulence structure would be affected if this number is not modeled accurately. Work is in progress on this point at Colorado State University. It is reasonable to suspect that modeling requirements will result in a scale factor for the dissipation rates which does not differ very much from that for the mean velocity.

With this assumption made, translation of laboratory data to field data is a simple problem, provided that the drag coefficient of the obstruction can be estimated. The procedure would be to determine the roughness length and the geometrical pattern of the natural situation, and then to prepare a scale model of it in the laboratory, setting the roughness length in the laboratory at a convenient level by artificial roughening of the wind tunnel boundary. As long as the dimensions of the obstruction are such that it lies well within the lowest 1000 to 2000 ft of the atmosphere, and as long as the wind velocity is such that the gross Richardson number of the prototype is not essentially different from zero, and as long as the model is sharp edged, so that the separation line is fixed, the condition in the laboratory should be similar to that in the field:

$$\left(\frac{h}{z_o}\right)_{model} = \left(\frac{h}{z_o}\right)_{field} \qquad (1)$$

In this equation, h is the height of the obstruction and z_o is the roughness height.

For an obstacle which is not sharp edged, such that the separation line moves with change in velocity, the Reynolds number affects the drag coefficient, and compensations will have to be made for this effect. A possibility exists in artificially tripping the boundary layer on the

obstruction so as to induce turbulence locally and fix the boundary layer separation line. However, such refinements have not been used in this study, which is intended to furnish qualitative information rather than quantitative design data and, in that case, it is unnecessary to substantiate the small improvements in similarity which can be had by artificially inducing separation on the model hill. Thus, the problem of scaling need not concern us in this study, especially since a comparison with field data is not possible at this time. We shall, therefore, formulate our problem in more detail without regard to scaling.

Chapter II

THEORETICAL CONSIDERATIONS

The two essentially different problems which arise in considering the interaction of missiles and turbulent wind fields are that of missile flight stability, and that of impact dispersion. The difference of these two problems can best be illustrated by considering the flight of a missile through a homogeneous velocity field of infinite extent. A missile which flies at constant speed encounters a spatially random velocity field which is, with respect to a coordinate system traveling with the missile, converted into a random and stationary time series of the continuous variable: velocity. If the missile has a transfer function $H(\omega)$, then the missile response velocity spectrum $\phi_m(\omega)$ is related to the impact wind-gust spectrum $\phi_w(\omega)$ by the relation of

$$\phi_m(\omega) = \left| H(\omega) \right|^2 \phi_w(\omega) \tag{2}$$

Thus, since the transfer function $|H(\omega)|$ is a deterministic function, and since $\phi_w(\omega)$ for an infinitely long stationary record denotes the exact average behavior of the wind field, $\phi_m(\omega)$ is also an exact average measure of the missile response. If none of the response amplitudes exceed the stability limit of the missile, then only some fluctuations of the missile occur; if some do exceed the stability limit, the missile might change course drastically and miss its target by a wide margin. The stability can usually be evaluated on the basis of the average behavior expressed by Eq. 2. In this paper, we shall provide experimental data on wind spectra, which can be used for missile stability calculation purposes.

In contrast to stability, the dispersion of a missile results from an integrated effect of all the velocities which are acting on the missile in its course along the missile trajectory. Since these velocities are fluctuating from instant to instant, and can be described only in a probabilistic way, the missile dispersion cannot be predicted deterministically. Instead, the missile dispersion problem is the problem of determining the probability distribution of the missile trajectory end point as a function of the sequence of all the velocities which the missile encountered along the trajectory. The distribution of the end point of the missile then becomes a function of the joint probability distribution for all the velocities along the missile trajectory.

In this report, we shall disregard the characteristics of the missile and shall concentrate on an attempt to describe the joint probability distribution for the velocities along some hypothetical missile trajectories in a simplified manner. The theoretical ideas will be developed in this chapter. They lead to a program of measurements of probability distributions which was performed in the Fluid Mechanics Laboratory of Colorado State University.

Since it is impossible to obtain the true joint probability distribution for all velocity vectors along any trajectory, a simplifying procedure has to be adopted. We proceed by introducing some simplifying assumptions which represent the turbulence encountered by the missile by the instantaneous turbulence existing along the mean trajectory. Furthermore, the trajectory is subdivided into sections and it is assumed that the turbulence in each section can be represented by the turbulence at the end points of the sections. For the ensuing sequence of velocities at the section end joints, the joint probability density function is then constructed and broken down into a product of functions which can be determined by means of available experimental techniques. No attempt will be made to apply the ensuing functions to the missile dispersion problem.

2.1 Basic Assumptions

The problem of evaluating the instantaneous missile trajectory is approached in the following way. Let the mean trajectory of a missile be given, and use the reference coordinate system as shown in Fig. 1 for our problem. Then on its travel along the trajectory the missile encounters mean velocities and a sequence of gusts, both described by a velocity vector $\vec{v}(\vec{s};t)$, where t is the time of flight, and $\vec{s}$ is the position vector of the trajectory. The velocity vector consists of a mean velocity $\bar{\vec{v}}(\vec{s})$ and a fluctuation in velocity $\vec{v}'(\vec{s};t)$. The position vector consists of a mean position vector $\bar{\vec{s}}$ corresponding to an absence of all velocity fluctuations (i.e., the trajectory due to mean wind only) and a small deviation $\vec{s} - \bar{\vec{s}}$ due to the sequence of fluctuating velocities which the missile has encountered during the time t.

Now, let the travel time until impact be equal to t_i and the end point of the mean wind trajectory be located at x_e. Then due to the sequence of wind fluctuations encountered during its flight, the missile is deflected in the impact area by a total deviation r'_e from the target distance x_e. Due to the random nature of the fluctuations encountered, the r'_e will also be randomly distributed. The probability distribution of the quantity r'_e is the desired quantity to which the results of this study must be applied.

The meteorological problem associated with finding the probability distribution of r'_e is to make available knowledge of the instantaneous velocity field which the missile might encounter on its course. Clearly, this problem cannot be solved by presently available techniques. Instead, it is proposed to obtain joint probability distributions for the simultaneous occurrence of a sequence of velocity vectors along the missile trajectory. In general, this requires specifying joint probability distributions of the joint occurrence of velocities at infinitely many different points in space and time. In order to reduce this problem to tractable dimensions, a number of assumptions have to be made.

The first assumption is that the distance of any instantaneous trajectory from the mean trajectory calculated on the basis of the mean wind distribution is small, so that

$$\vec{v}'(\vec{s};t) \approx \vec{v}'(\bar{\vec{s}};t) \quad . \tag{2}$$

In this manner, it is no longer necessary to consider the whole space but one can concentrate on the single trajectory. Obviously, the validity of this assumption depends both on the relative magnitude of v' with respect to $\bar{v}$, and on the response characteristics of the missile, and will have to be tested each time.

The second assumption concerns the time distribution. We assume that the missile travels much faster than the velocity fluctuates, so that

$$\vec{v}'(\vec{s};t) \approx \vec{v}'(\vec{s};t_o) \tag{3}$$

where t_o denotes the start time. This assumption implies that during the flight time the relation holds:

$$\vec{v}'(\vec{s};t)\ \vec{v}'(\vec{s};t_o) \approx \vec{v}'(\vec{s};t_o)\ \vec{v}'(\vec{s};t_o)$$

or that, in the average for n different starting times t_o :

$$\frac{1}{n}\sum_{i=1}^{n} \vec{v}'(\vec{s};t)\ \vec{v}'(\vec{s}'t_{oi}) \approx \frac{1}{n}\sum_{i=1}^{n} (\vec{v}'(\vec{s};t_{oi}))^2 .$$

If the flow is stationary, and if the ergodic hypothesis is valid, then we can restate this requirement as:

$$R_\tau \approx 1 \tag{4}$$

where

R_τ is the autocorrelation function defined by:

$$R_\tau = R(t_x - t_o) = \frac{1}{T}\int_o^T \frac{\vec{v}'(\vec{s};t_o + (t_x - t_o)) \cdot \vec{v}'(\vec{s};t_o)dt_o}{\vec{v}'^2(\vec{s}, t_o)} \tag{5}$$

where

T is an observation time taken long enough to ensure a stable average, and

$t_x - t_o$ is the time during which the missile has traveled from x_o to x^* .

---

* To convert actual travel times to model travel times, the scaling law $\left(\frac{tu^*}{z_o}\right)_{\text{model}} = \left(\frac{tu^*}{z_o}\right)_{\text{field}}$ must be used, which, for $u^*_{\text{model}} = u^*_{\text{field}}$ reduces to $t_m = t_{\text{field}} \frac{z_{o\ \text{model}}}{z_{o\ \text{field}}}$.

For small times $t_x - t_o$ Eq. 4a becomes:

$$R_{\cdot} \sim 1 - \frac{(t_x - t_o)^{\cdot}}{\lambda_g^{\cdot}} \tag{4b}$$

where λ_g is the microscale of the turbulence. The scale λ_g can be replaced to a good approximation by the scale λ_g of the u-component of the turbulence

$$\lambda_g^{-2} = \frac{1}{2\,\overline{u'^2}} \left(\frac{\partial \overline{u'}}{\partial t} \right)^2 \Bigg|_{t=0} . \tag{5}$$

Consequently, it follows that $t_x - t_o \ll \lambda_g$ for the assumption Eq. 3 to be valid.

2.2 Simplifications of the Probabilistic Problem: connecting probabilities along trajectories.

We base our calculations on assumptions Eq. 2 and Eq. 3, and, thus, we have reduced the meteorological aspects of the problem to finding simultaneous instantaneous velocity distributions along the mean trajectory $\bar{x}$. To avoid the implied necessity of determining velocities simultaneously at infinitely many different points, we adopt the following probabilistic specification of the velocity field. The required quantity is the joint probability density distribution

$$f_j = f(\vec{v}'_o , \vec{v}'_1 , \vec{v}'_2 \ldots . \vec{v}'_n) \tag{6}$$

for all n points along the mean trajectory. The experimental distribution of f_j requires simultaneous measurements at all n points of the trajectory, i.e., it requires an infinite array of probes placed along the trajectory. Evidently, this is an impossible task, so that instead, the trajectory is cut into n finite intervals, of length Δx , at whose end points turbulent quantities are measured. In each interval $\Delta x = x_{i+1} - x_i$ the instantaneous velocity is assumed constant and equal to:

$$\vec{v}'_i = u'_i \vec{i} + v'_i \vec{j} + w'_i \vec{k} \tag{7}$$

when the components u'_i , v'_i and w'_i are average values of the velocity components at the two end points. From the values of $\vec{v}'_i$, the trajectory is calculated.

The problem to be solved then is to convert probability distributions between adjacent points in such a way that a meaningful approximation for Eq. 6 is found. We want to investigate three smiple cases of possible approximations for Eq. 6.

a. Consider first the assumption that $f(v'_{i+1})$ and $f(v'_i)$ are statistically independent. This condition corresponds to velocities which vary comparatively rapidly along the trajectory, in the sense that $R_x \approx 0$ where R_x is the spatial correlation coefficient obtained from the definition

$$R_x = R(x_{i+1}-x_i) = \frac{1}{\Delta x}\int_{x_i}^{x_{i+1}} \frac{\vec{v}'(t_o,x-x_i)\ \vec{v}'(t_o,x_i)\,dx}{\sqrt{\overline{v'^2(t_o,x_i)}}\cdot\sqrt{\overline{v'^2(t_o,x_{i+1})}}} \quad . \tag{8}$$

However, the assumption of rapidly varying velocities is in contradiction to the assumption of a velocity vector which is constant throughout the travel interval Δx, unless Δx is chosen in such a way that a meaningful relation between it and the space integral scale $\mathcal{J}_s$ exists, where:

$$\mathcal{J}_s = \int_{x_i}^{\infty} R_x\,dx \quad . \tag{9}$$

Also, in order to be of influence on the flight pattern, $\mathcal{J}_s$ must be large compared to the length dimension L of the missile, such that a condition for the validity of this assumption might be defined as:

$$\Delta x \approx \mathcal{J}_s \quad \text{and} \quad \frac{L}{\mathcal{J}_s} \ll 1 \quad \text{say} \quad <0.1 \tag{10}$$

Under these circumstances, Eq. 6 reduces to

$$f(\vec{v}'_o\ ,\ \vec{v}'_1\ \ldots\ \vec{v}'_{n-1}\ ,\ \vec{v}'_n) = f(\vec{v}'_o)\ f(\vec{v}'_1)\ldots\ldots f(\vec{v}'_{n-1})\ f(\vec{v}'_n) \tag{11a}$$

or in terms of conditional probability densities:

$$f(\vec{v}'_i \mid \vec{v}'_{i-1}\ ,\ \vec{v}'_{i-2}\ldots\ldots) = f(\vec{v}'_i) \tag{11b}$$

This equation can be evaluated conveniently, if the probability density distributions $f(\vec{v}'_i)$ are given. These correspond to joint probability densities for those variables u'_i, v'_i and w'_i, which will be discussed below in Section 2.3.

b. As a second possibility, we considered the condition

$$\mathcal{J}_s > x_e - x_o$$

in which case the correlation coefficient defined by Eq. 8 assumes a value very near to 1. This implies that the velocities $\vec{v}'(t_o, x_i)$ $\vec{v}'(t_o, x_{i+1})$ are very nearly proportional, so that

$$\vec{v}'(t_o, x_{i+1}) \approx A\vec{v}'(t_o, x_i) \tag{12}$$

where A is a (vector) constant. Furthermore, the jpdf defined by Eq. 6 becomes:

$$f(\vec{v}'_o , \vec{v}'_1 \ldots . \vec{v}'_{n-1}, \vec{v}'_n) = f(\vec{v}'_o) \quad , \tag{13a}$$

or in terms of conditional probability densitic :

$$f(\vec{v}'_i \mid \vec{v}'_{i-1}, \vec{v}'_{i-2} \ldots..) = 1 \tag{13b}$$

Again, the discussion of a method for calculating $f(\vec{v}'_o)$ is postponed until Section 2.3.

c. The assumption of a and b bracket the possibilities for simplifying the joint probability density functions of the turbulence along the trajectory. An intermediate method, based on the assumption that the eddy structure of the turbulence is highly elongated, (as is usually the case in turbulent flows) would combine assumptions of independence of the motions perpendicular to the mean wind direction with an assumption of some dependency of the components in the wind direction along the trajectory. The simplest way is obtained if a Markoff dependency can be found to relate probability density distributions along the trajectory, i.e., if

$$f(\vec{v}'_i \mid \vec{v}'_{i-1} , v'_{i-2}.....\vec{v}'_1, \vec{v}'_o) = f(\vec{v}'_i \mid \vec{v}'_{i-1}) \tag{14}$$

when $f(\vec{v}'_i \mid \vec{v}'_{i-1})$ is the conditional probability density for the occurrence of $\vec{v}'_i$ when $\vec{v}'_{i-1}$ has already occurred.

The elongated eddy structure leads us to assume that what happens at point x_i depends on the happenings at x_{i-1} only through the u'_i-component, i.e., the components v'_i and w'_i are independent of all components at the point x_{i-1} except inasmuch as they depend on u'_i, which in turn depends only on the component u'_{i-1} and not on v_{i-1} and w_{i-1}. Write Eq. 14 in the form:

$$f(\vec{v}'_i \mid \vec{v}'_{i-1}) = f(u'_i \mid u'_{i-1})\, f(v'_i \mid u'_i) \cdot f(w'_i \mid u'_i, v'_i) \tag{15}$$

where $f(w'_i \mid u'_i, v'_i)$ denotes the conditional probability density for finding w'_i when both u'_i and v'_i are assumed to occur also.

We can now summarize the results for the three approximations of Eq. 6 as follows:

Independence (Case a)

$$f(\vec{v}'_i \mid \vec{v}'_{i-1}, \vec{v}'_{i-2}, \ldots. v_o) = f(\vec{v}'_i)$$

so that

$$f(v_i, v_{i-1}, v_{i-2}\ldots.\vec{v}'_o) = f(\vec{v}'_i)\, f(\vec{v}'_{i-1}) \ldots . f(\vec{v}'_o)$$

Dependence (Case b)

$$f(\vec{v}'_i \mid \vec{v}'_{i-1}, \vec{v}'_{i-2} \ldots\ldots) = 1$$

so that

$$f(v_i, v_{i-1}, v_{i-2} \ldots\ldots) = f(\vec{v}'_o)$$

Markoff dependency (Case c)

$$f(\vec{v}'_i \mid \vec{v}'_{i-1}, \vec{v}'_{i-2}, \ldots\ldots) = f(\vec{v}'_i \mid \vec{v}'_{i-1})$$

so that

$$f(v_i, v_{i-1}, v_{i-2} \ldots\ldots v_o) = f(\vec{v}'_o)\ f(\vec{v}'_1 \mid \vec{v}'_o) \ldots\ldots f(\vec{v}'_i \mid \vec{v}'_{i-1})$$

which simplifies further for the elongated eddy case to Eq. 15.

2.3 Simplification of the Probabilistic Problem: joint probability densities at a point

All three cases discussed above require the determination of probability density distributions of the form: $f(\vec{v}'_i)$. Since $\vec{v}'_i$ is a vector consisting of three components, $f(\vec{v}'_i)$ is actually a joint probability density function for the joint occurrence of u'_i , v'_i and w'_i . Such a triple joint probability density function is too difficult to determine experimentally. We, therefore, write

$$f(u'_i, v'_i, w'_i) = f(u'_i)\ f(v'_i \mid u'_i)\ f(w'_i \mid u'_i, v'_i) \tag{16}$$

in the form

$$f(u'_i, v'_i, w'_i) = f(u'_i)\ f(v'_i \mid u'_i)\ f(w'_i) \tag{17}$$

and Eq. 14 in the form

$$f(v'_i \mid v'_{i-1}) = f(u'_i \mid u'_{i-1})\ f(v'_i \mid u'_i)\ f(w'_i) \tag{18}$$

which are based on the following assumptions:

a. The velocity component w'_i is statistically independent of all other velocity components.

b. The connection between adjacent points takes place only through u'_i and is at most first order Markovian.

Assumption a. is partly justified because the homogeneity of the turbulence in planes parallel to the ground, in a two-dimensional flow field, requires that the time average product $u'_i w'_i = 0$ which is a necessary, but not a sufficient condition for statistical independence.

The first part of assumption b. is postulated without any firm basis except for the motion of an elongated eddy stated previously. For the second part, however, we have some support, both from meteorological data as well as for the laboratory case of the present study.

For a Markoff dependency to exist, it is a necessary and sufficient condition that, if the variables u'_i are stationary with respect to i and Gaussian, and are also jointly Gaussian distributed, then the cross correlation between u'_i , u'_{i+1} , u'_{i+2} is an exponential function in the parameter i (p. 96, Feller (1964) p. 234, Doob (1953)) i.e., in the continuous parameter case

$$R(x) = e^{-\lambda x} R(0) \qquad x \geq 0 \tag{19}$$

where λ has a non-negative real part, if $R(x)$ is known to be continuous. Conversely, a sequence with stationary Gaussian distributions satisfying Eq. 18 is Markovian and Eq. 14 can thus be used.

The applicability of a Markoff process to turbulence data is thus insured if it can be shown that

a. the space correlations are homogeneous, i.e., independent from where the correlation starts.

b. the space correlations are exponential.

c. the probability density distributions for the functions representing u' are Gaussian.

Some proof for the validity of these conditions for our laboratory flows will be given in the next chapter. For atmospheric turbulence in neutrally stratified atmospheric boundary layers over homogeneous terrain, these conditions are approximately satisfied. In the older meteorological literature (for reference see Pasquill (1961)) the autocorrelation functions were usually found to be exponential. Together with Taylor's hypothesis, according to which time correlations can be translated into space correlations by means of the substitution $t = \frac{x}{\bar{U}}$, (where $\bar{U}$ is the local mean velocity), it can thus be shown that space correlations are exponential. Meteorologists have in recent times (Lumley and Panofsky (1964)) preferred to use different analytical representations of the correlation functions, for the simple reason that the spectrum corresponding to an exponential autocorrelation decreases at large values of angular frequencies ω proportional to ω^{-2} , whereas the spectral shape should contain an inertial subrange, with a drop-off proportional to $\omega^{-5/3}$. The difference between 5/3 and 2 is, however, not large enough to give a strong reason for discarding the assumption of an exponential decay of the autocorrelation function. For our prediction purposes, it does, therefore, seem to be justified to assume that an exponential autocorrelation function exists in neutrally stratified atmospheric boundary layers over homogeneous terrain. In a later section we shall show that an approximately exponential space correlation function which is homogeneous along trajectories parallel to the ground can be found even in

the highly disturbed flow field downwind from a model ridge. Since we also find that almost all velocity components follow Gaussian distributions, the Markoff dependency postulated for Eq. 15 is reasonably well established experimentally.

2.4 Some Considerations on Gaussian Two Variable Joint Probability Density Functions.

When the joint probability density functions of the quantities of turbulence at one point are Gaussian, then this distribution function is fully specified by the means and the turbulence quantities $\overline{u'^2} = \sigma_u^2$, $\overline{v'^2} = \sigma_v^2$, $\overline{w'^2} = \sigma_w^2$ as well as by the cross correlations, for example, $\overline{u'v'}$. These quantities are most important also in describing the dynamic conditions of the turbulent flow, i.e., they represent stresses, and it is, therefore, of interest to show the connection between the probability density functions and the stresses.

Theoretically, if all the probability densities of individual turbulent components are distributed in a Gaussian form, then:

$$f(u') = \frac{1}{\sqrt{2\pi}\,\sigma_{u'}} e^{\frac{-(u'-m_{u'})^2}{2\sigma_{u'}^2}}$$

$$f(v') = \frac{1}{\sqrt{2\pi}\,\sigma_{v'}} e^{\frac{-(v'-m_{v'})^2}{2\sigma_{v'}^2}} \qquad (20)$$

$$f(w') = \frac{1}{\sqrt{2\pi}\,\sigma_{w'}} e^{\frac{-(w'-m_{w'})^2}{2\sigma_{w'}^2}}$$

The joint densities of two turbulent components can be expressed by a joint Gaussian form, i.e.,

$$f(u',v') = \frac{1}{2\pi\,\sigma_{u'}\,\sigma_{v'}\sqrt{1-\rho^2}} e^{-Q(u',v')} \qquad (21)$$

for some constants $\sigma_{u'} > 0$, $\sigma_{v'} > 0$, $\rho < 1$, $-\infty < m_{u'} < +\infty$ $-\infty < m_{v'} < +\infty$, in which the function $Q(u', v')$ for any two real numbers u' and v' is defined by

$$Q(u', v') = \frac{1}{2(1-\rho^2)} \left[\left(\frac{u' - m_{u'}}{\sigma_{u'}} \right)^2 - 2\rho \left(\frac{u'-m_{u'}}{\sigma_{u'}} \right) \left(\frac{v'-m_{v'}}{\sigma_{v'}} \right) + \left(\frac{v'-m_{v'}}{\sigma_{v'}} \right)^2 \right]$$

where ρ is the correlation coefficient $\frac{\overline{u'v'}}{\sqrt{u'^2}\ \sqrt{v'^2}} = \rho$, $\sigma^2_{u'}$ and $\sigma^2_{v'}$ are the variances of u' and v', respectively, and $m_{u'}$ and $m_{v'}$ are the mean values. The curve $Q(u', v') =$ constant is an ellipse since $\rho < 1$.

In order to find the orientation of the ellipse, the coordinates u^* and v^* of the coordinate system parallel to the axes of the ellipse

$$\begin{aligned} u^* &= u' \cos\theta + v' \sin\theta \\ v^* &= -u' \sin\theta + v' \cos\theta \end{aligned} \tag{22}$$

are introduced. Applying the Jacobian transformation to the probability density, Eq. 20, we obtain

$$\begin{aligned} f(u^*, v^*) &= \frac{f(u',v')}{|J(u',v')|} \\ &= f(u^*\cos\theta - v^* \sin\theta,\ u^* \sin\theta + v^* \cos\theta) \end{aligned} \tag{23}$$

which follows from the fact that the Jacobian:

$$J(u',v') = \begin{vmatrix} \frac{\partial u^*}{\partial u'} & \frac{\partial u^*}{\partial v'} \\ \frac{\partial v^*}{\partial u'} & \frac{\partial v^*}{\partial v'} \end{vmatrix} = 1$$

For further simplicity, we may assume $m_{u'} = m_{v'} = 0$ then,

$$\begin{aligned} f(u^*,v^*) = \frac{1}{2\pi\sigma_{u'}\,\sigma_{v'}\sqrt{1-\rho^2}} \exp\Bigg\{ -\frac{1}{2(1-\rho^2)} \Bigg[\Bigg(\frac{\cos^2\theta}{\sigma_{u'}^2} - 2\rho\,\frac{\cos\theta\sin\theta}{\sigma_{u'}\sigma_{v'}} + \\ \frac{\sin^2\theta}{\sigma_{v'}^2} \Bigg) u^{*2} \\ -2\left(\frac{\cos\theta\,\sin\theta}{\sigma_{u'}^2} - \rho\,\frac{\sin\theta}{\sigma_{u'}\,\sigma_{v'}} - \frac{\cos\theta\,\sin\theta}{\sigma_{v'}^2} \right) u^*v^* \\ + \left(\frac{\sin^2\theta}{\sigma_{u'}^2} + 2\rho\,\frac{\cos\theta\,\sin\theta}{\sigma_{u'}\,\sigma_{v'}} + \frac{\cos^2\theta}{\sigma_{v'}^2} \right) v^{*2} \Bigg] \Bigg\} \end{aligned} \tag{24}$$

because of the symmetry of the ellipse with respect to the new axes, the term involving $u^* v^*$ should vanish, i.e.,

$$\frac{\cos\theta \sin\theta}{\sigma_{u'}^2} - \rho \frac{\sin^2\theta - \cos^2\theta}{\sigma_{u'} \sigma_{v'}} - \frac{\cos\theta \sin\theta}{\sigma_{v'}^2} = 0$$

or

$$\tan 2\theta = \frac{2\rho\sigma_{u'}\sigma_{v'}}{\sigma_{u'}^2 - \sigma_{v'}^2} \tag{25}$$

This can be written in terms of the turbulent stresses by means of the relations:

$$\rho = \frac{\text{cov}\,(u',v')}{\sigma_{u'}\,\sigma_{v'}} = \frac{\overline{u'v'}}{\sigma_{u'}\sigma_{v'}}$$

and

$$\sigma_{u'} = \sqrt{\overline{u'^2}} \quad , \quad \sigma_{v'} = \sqrt{\overline{v'^2}}$$

$$\therefore \tan 2\theta = \frac{2\overline{u'v'}}{\overline{u'^2} - \overline{v'^2}} \tag{26}$$

With this relationship, the joint density function of the turbulent components can be defined once we have the values of the associated turbulent stresses. For example, the Eq. 18 can be established by measuring $\overline{u_{i-1}'^2}$, $\overline{u_i'^2}$, $\overline{v_i'^2}$, $\overline{w_i'^2}$, $\overline{u_i' v_i'}$ and $\overline{u_{i-1}' u_i'}$. For its application, we have, however, to show that the individual components are Gaussianly distributed and that the joint probability distributions follow Eq. 19.

We notice in passing the equality between Eq. 26 and the inclination of the plane of zero shear stress in a plane stress state of classical mechanics, if u'^2 and v'^2 are the normal stresses and $\overline{u'v'}$ is the shearing stress (due to turbulence). Clearly, then, the angle θ denotes the orientation of a plane at a point in a fluid when the shear stress is zero, so that the joint probability distribution is found to be oriented with the long axis of the ellipse of constant correlation parallel to the zero shear stress plane.

Chapter III

EQUIPMENT AND PROCEDURES

3.1 The Experimental Setup

The experiments were performed in the U.S. Army Meteorological Wind Tunnel in the Fluid Dynamics and Diffusion Laboratory of Colorado State University. This facility is shown in Fig. 2. It is a recirculating wind tunnel with an 88 ft long test section with a 6 x 6 ft^2 cross section. For the experiments of this study, the model hill was placed at a distance of approximately 40 ft downstream from the inlet where the undisturbed boundary layer, stimulated by large roughness elements in the inlet region of the test section, had an undisturbed thickness of about 24 inches. The model hill consisted of a plexiglass section with a shape given by

$$y = h \cos \frac{\pi x}{L} \quad \text{for} \quad -\frac{1}{2} \leq \frac{x}{L} \leq \frac{1}{2} \tag{27}$$

where the base width L = 20 in. and the height h = 4 in. The velocity outside of the undisturbed boundary layer was 30 fps.

3.2 Measurement of Mean Velocity Profiles

Mean velocity profiles were measured both by hot wire anemometer and pitot tube, in order to obtain a cross check. In the upper part of the flow, continuous traverses of velocity were taken. In the lower part or in the separation region where the variability of velocity was large, point by point data were taken in order to determine the velocity profiles more precisely.

The hot wire measurement of mean velocity was made with a 4×10^{-4} inch diameter single wire which was held perpendicular to the local mean velocity vector $\bar{U}$. The hot wire anemometer used was made at CSU.

By means of the pitot tube, total head readings were obtained for calculating mean velocities. If there is no pressure gradient in the flow field, the local mean velocity can be calculated by

$$\frac{1}{2} \rho_a \bar{U}^2 = \Delta P_{AB} \tag{28}$$

ΔP_{AB} = pressure difference between the static tap and dynamic tap of a pitot static tube.

But in the neighborhood of the model ridge, large pressure gradients exist, not only in y-direction but also in x-direction. Since the static tap is one inch downstream from the dynamic tap on the pitot tube, a correction must be applied for the pressure gradient between the two taps. Since

$$\frac{1}{2}\rho_a U^2 = \Delta P_{AB} - (P_A - P_B) \qquad (29)$$

ρ_a = density of air at the room temperature

U = local mean velocity

ΔP_{AB} = the measured pressure difference

P_A = the static pressure at dynamic tap's position

P_B = the static pressure at static tap's position

$P_A - P_B$ = pressure difference between the static tap and the dynamic tap.

If $P_A - P_B$ is known, the local mean velocity at one point can be calculated from Eq. 29. At each point the value of $P_A - P_B$ can be obtained from Fig. 3. This figure was made by connecting the static tap and a reference tap to the pressure transducer (Transonic Type 120 Equibar). Since the static tap is one inch downstream from the dynamic tap, at one point the coordinates of the dynamic tap is known, say (x_1, y_1) then the static tap is $(x_1 + 1, y_1)$. When the coordinates of two points are known the pressure difference $P_A - P_B$ can be obtained from Fig. 3 and the corrected mean velocity at that point can be calculated by applying Eq. 29.

To measure the mean velocity profiles the pitot tube and the hot wire were mounted on a 24 inches vertical carriage. The dynamic tap of pitot tube and hot wire were held side by side at the same height. The velocity profiles were taken every two inches downstream from the crest up to $x = 18"$ and also at $x = 24", 36", 40"$.

The block diagram of set up is shown on Fig. 4. The calculation of the mean velocity is listed on Table I and the results are on Fig. 5.

When a hot wire was used to measure the mean velocity, the calibration curve of this wire was checked from time to time and the wire was recalibrated if excessive drift of an anemometer was detected. It was found that after a hot wire had aged several hours the drift of the wire was negligibly small.

3.3 Measurement of Turbulent Quantities

For coordinates of the flow field as shown in Fig. 1, the turbulent components at a point in x, y, z directions are u', v', w', respectively.

The u'-component was calculated from a single hot wire held parallel to z axis (Fig. 6). The v'-component was calculated from a crossed wire held in the x-y plane (Fig. 6).

In the subsequent discussion, we shall use the following notation:

$u = \sqrt{\overline{u'^2}}$, $v = \sqrt{\overline{v'^2}}$ and

$w = \sqrt{\overline{w'^2}}$ is the rms value of the fluctuating velocity component in the x, y, z direction, respectively

$\overline{uv}$ = covariance of the fluctuations u' and v'

$e_{1,2} = \sqrt{\overline{e_1'^2}}$, $\sqrt{\overline{e_2'^2}}$ are the rms values of the fluctuating voltages e_1' and e_2' measured with wire No. 1, or 2, respectively.

a. Calculating of u-component of turbulence.

To calculate the u-component at one point, say, (x_1, y_1) we need the following information:

1. the rms value of a single wire at (x, y),
2. the calibration curve of this wire,
3. the local mean velocity $\bar{U}$ at (x, y)
4. the slope of the calibration curve $\frac{dE}{dU}$ at $\bar{U}$ then:

$$e = \frac{dE}{dU} u$$

or

$$u^2 = \left(\frac{dU}{dE}\right)^2 e^2 \tag{30}$$

The u-component at a point (x, y) was calibrated by Eq. 30.

b. Calculating v and $\overline{uv}$ components of turbulence.

If the crossed wire is held in the x-y plane as shown in Fig. 7, then we find in general that

$$e_1 = \frac{1}{\cos \alpha} \frac{dE_1}{dU} \sqrt{\overline{(u'\cos \alpha + v'\sin \alpha)^2}}$$
$$e_2 = \frac{1}{\cos \alpha} \frac{dE_2}{dU} \sqrt{\overline{(u'\cos \alpha - v'\sin \alpha)^2}} \tag{31}$$

where $\frac{dE_1}{dU}$ and $\frac{dE_2}{dU}$ are the slopes of the calibration curve for wire 1 and wire 2, respectively, Equation 31 can be written as

$$e_1^2 = \frac{1}{\cos^2\alpha}\left(\frac{dE_1}{dU}\right)^2 (\overline{u'^2}\cos\alpha + 2\overline{u'v'}\cos\alpha\sin\alpha + \overline{v'^2}\sin^2\alpha)$$

$$e_2^2 = \frac{1}{\cos^2\beta}\left(\frac{dE_2}{dU}\right)^2 (\overline{u'^2}\cos\beta + 2\overline{u'v'}\cos\beta\sin\beta + \overline{v'^2}\sin^2\beta) \qquad (32)$$

In order to account for small deviations of mean velocity vectors from the horizontal we write:

$$\alpha = 45^\circ + \phi$$

$$\beta = 45^\circ - \phi$$

where ϕ is the small deviation of the angle between the mean velocity vector and the horizontal, as determined from the streamline pattern. Then, for small ϕ, so that rms in ϕ^2 can be neglected, and $\cos\phi \approx 1$, $\sin\phi \approx \phi$:

$$\cos\alpha = \cos(45^\circ + \phi) \doteq \frac{\sqrt{2}}{2}(1-\phi)$$

$$\cos^2\alpha \doteq \frac{1}{2} - \phi$$

$$\sin\alpha \doteq \frac{\sqrt{2}}{2}(1+\phi) \qquad (33)$$

$$\sin^2\alpha \doteq \frac{1}{2} + \phi$$

also

$$\cos\beta \doteq \frac{\sqrt{2}}{2}(1+\phi) \qquad \cos^2\beta \doteq \frac{1}{2} + \phi$$

$$\sin\beta \doteq \frac{\sqrt{2}}{2}(1-\phi) \qquad \sin^2\beta = \frac{1}{2} - \phi$$

Substituting Eq. 33 into Eq. 32 yields

$$e_1^2(\tfrac{1}{2} - \phi)\left(\frac{dU}{dE_2}\right)^2 = (\tfrac{1}{2} - \phi) + \overline{u'v'} + \overline{v'^2}(\tfrac{1}{2} + \phi)$$
$$\overline{u'^2}(\tfrac{1}{2} - \phi) + \overline{u'v'} + \overline{v'^2}(\tfrac{1}{2} + \phi) \qquad (34)$$

$$e_2^2(\tfrac{1}{2} + \phi)\left(\frac{dU}{dE_2}\right)^2 = \overline{u'^2}(\tfrac{1}{2} + \phi) + \overline{u'v'} + \overline{v'^2}(\tfrac{1}{2} - \phi) \qquad (35)$$

The difference of Eq. 34 and Eq. 35 then yields

$$\overline{u'v'} = \frac{1}{2}\left(\frac{dU}{dE_1}\right)^2 e_1^2(\tfrac{1}{2} - \phi) - \frac{1}{2}\left(\frac{dU}{dE_2}\right)^2 e_2^2(\tfrac{1}{2} + \phi) \qquad (36)$$
$$+ \phi(\overline{u'^2} - \overline{v'^2})$$

Inserting Eq. 36 into Eq. 34 leads to

$$v^2 = \frac{1}{2}\left[e_1^2\left(\frac{dU}{dE_1}\right)^2 + e_2^2\left(\frac{dU}{dE_2}\right)^2\right] - u^2 - \phi\left[e_1^2\left(\frac{dU}{dE_1}\right)^2 - e_2^2\left(\frac{dU}{dE_2}\right)^2\right] \tag{37}$$

Since, in our experiment both wires were of the same length, the slope of the calibration curves of both wires for the same U were the same, i.e., at a point $\frac{dU}{dE_1} = \frac{dU}{dE_2} = \frac{dU}{dE}$. Then Eq. 37 becomes

$$v^2 = \frac{1}{2}\left(\frac{dU}{dE}\right)^2 (e_1^2 + e_2^2) - u^2 - \phi\left(\frac{dU}{dE}\right)^2 (e_1^2 - e_2^2) \tag{38}$$

and Eq. 33 yields:

$$\overline{u'v'} = \frac{1}{2}\left(\frac{dU}{dE}\right)^2 e_1^2\left(\frac{1}{2} - \phi\right) - e_2^2\left(\frac{1}{2} + \phi\right) + \phi(u^2 - v^2) \tag{39}$$

Substituting Eq. 38 into Eq. 39

$$\overline{uv} = \frac{1}{4}(e_1^2 - e_2^2)\left(\frac{dU}{dE}\right)^2 - 2\phi v^2 \tag{40}$$

If $\phi = 0$ i.e., the velocity vector is in x-direction, Eq. 38 becomes

$$v^2 = \frac{1}{2}\left(\frac{dU}{dE}\right)^2 (e_1^2 + e_2^2) - u^2 \tag{41}$$

and Eq. 40 yields:

$$\overline{uv} = \frac{1}{4}(e_1^2 - e_2^2)\left(\frac{dU}{dE}\right)^2 \tag{42}$$

Equation 41 and 42 are the well-known equations on calculating $\overline{uv}$ and v^2 when the velocity vector is in the x-direction. But, in our study when the wind is flowing over the hill the velocity vector may deviate from the x-direction. Therefore, Eqs. 38 and 40 were used to calculate the $\overline{uv}$ and v^2 when $\phi \neq 0$. The angle ϕ at one point was estimated from the streamline pattern shown in Fig. 5. How the streamlines were determined will be discussed later.

For crossed wires, when $\phi = 0$ i.e., when the velocity vector is parallel to the x-axis, the angles of inclination between wire 1 and wire 2 and the x-axis are the same and equal to 45° (both wires were very carefully mounted perpendicular to each other). In order to make sure that both wire 1 and wire 2 were held under 45° to x-axis during the experiment, first, the wires were held in the free stream, when the (ambient) velocity is in x-direction. Then, the crossed wires were rotated 180° about the hot wire probe axis. If the outputs of the wires were different after this rotation, an adjustment in the angle of the probe with flow direction was made until the anemometer readings of both wires were invariant to rotation about the longitudinal axis.

The block diagram of the set up for measuring the turbulence is shown in Fig. 8. A single wire and a crossed wire were mounted side by side at the same height on a 24" vertical carriage. The elevation of wires could be read off as a voltage across a potentiometer geared to the positioning shaft and was either read out from a digital voltmeter (DVM) or plotted on an x-y plotter. At each section, data were taken at 55 test points shown in Fig. 9. Also, at each station x = constant continuous data profile plots were obtained on an x-y plotter. The test points were chosen so that they included:

a. points on the trajectory, i.e., points on the trajectories at the distances x of the measuring stations,

b. points near where the maximum change of rms value of u' occurred in each section.

At each of the test points the following data were taken:

a. The rms values, i.e., the fluctuations in voltage of a single wire and of two crossed wires. All three rms values were recorded by x-y plotters versus time and were also read directly from true rms meters as a reference.

b. 5-minute turbulence recordings for energy spectrum and probability analysis. A Mincom (Type C100) 7 channel FM tape recorder was used to record the turbulence for both single and crossed wires (3-channel simultaneous recording). The output of the CSU-made hot wire anemometer has a dc level of one volt and an rms value of the order of 0.05 volt. The dc level was too high and the rms value too low for best operation of the tape recorder. Therefore, an ac-amplifier was used to amplify the fluctuating voltage and to eliminate the dc level. Furthermore, an attenuator was connected between the amplifier and the tape recorder to adjust the recording voltage to 0.5 volt rms.

The interconnections of all instruments are shown in Fig. 8. The rms values of the wires obtained from the rms-meter (RMS II) before the amplifier and attenuator (A+A). The recording voltage was read from RMS II of Fig. 8.

Besides the data which have been taken at each test point, the continuous rms values for all three wires were also recorded on an x-y plotter. Figure 10 is a typical continuous rms profile of e_s for a single wire at x = 12" . For the same station the rms profiles of e_1 and e_2 for wire 1 and wire 2, respectively, are shown in Figs. 11 and 12.

As long as the rms values for single wires and corssed wires were known, the turbulence components u',v' and the turbulent shear stress $\overline{uv}$ could be calculated from Eq. 3, Eq. 11 and Eq. 13, respectively.

The measured rms values and the calculations of u^2 , v^2 and $\overline{uv}$ are shown in Table II. The profiles of these quantities are plotted in Fig. 13.

3.4 Determination of Streamline Locations

Mean streamlines can be drawn so as to be always tangential to the vectors of fluid velocity in a flow. Since a separation bubble existed near the downstream side of the model, it was found desirable to first determine a reference streamline in the outer part of the flow by joining the direction of mean velocity vectors from station to station, and to obtain lower streamlines by integration, i.e., the integral $\int u\, dy$ = constant below the reference streamline defined other streamlines.

The first streamline was found by using a hot wire in the following arrangement. The heat transfer from hot wire to air depends not only on the magnitude of the velocity, but also on the flow direction with respect to the wire. The heat transfer from the wire is maximum when the flow is perpendicular to the wire, minimum when the wire is parallel to the flow. By rotating the hot wire and plotting the output of the hot wire anemometer versus the rotating angle on an x-y plotter, a well-defined minimum was found which could be used to define the flow direction.

The starting point of the reference streamline was arbitrarily set at $x_o = 0$, $y_o = 9.1"$, the height of the second point was estimated by

$$y_1 = y_o - \ell_o \sin\Delta\alpha \tag{43}$$

$\Delta\alpha_o$ = the direction of local velocity vector to the free stream vector at first point

ℓ_o = the horizontal distance from the first point to the second point

y_o = height of the first point

In general the height of the point y_n at station x_n can be calculated from the n-1th point when the height y_{n-1} , the angle $\Delta\alpha_{n-1}$ and the distance ℓ_{n-1} are known. We have

$$y_n = y_{n-1} - \ell_{n-1} \sin\Delta\alpha_{n-1} \tag{44}$$

The first reference streamline was estimated in this manner, with the result shown on Fig. 5.

It is evident that this is not too satisfactory a method for determining the streamline. The method was difficult and time consuming, and wrought with error due to the fact that the error in estimating the height was cumulative. Therefore, a different method was used, where integration starts at the floor. It is clear that outside of the separation region the streamlines can be determined from velocity profiles by integrating up from the lower boundary.

According to continuity the flow rate between two streamlines at any section must be the same. It is known that the lower boundary is a streamline. The lower boundary consists of three parts

(a) before separating the surface of the model hill, upstream of separation

(b) between separation and reattachment, the upper boundary of the separation bubble

(c) after reattachment, the floor.

In our flow field the part (a) and (c) are fixed and are well known. Thus, a reference streamline can be found for regions (a) and (c) at some height up, and the streamline above the separation region (which is rather short) can be found by fairing between the two curves following the trend of the reference streamline measured by the previous method. The remainder of the procedure of streamline construction is as was outlined above. In this manner two streamlines are obtained, namely, (1) the measured streamline starting 5" above the crest, which was constructed from the reference streamline by applying the continuity equation, and (2) the lower boundary. Between these two streamlines the flow rates are q at any section. Some streamlines were interpolated between these two. The streamlines and the separation region are shown in Fig. 5.

3.5 Measurement of Turbulence Spectra

Spectra of the u'-component of the turbulent signal was obtained by means of a Bruel and Kjaer spectrum analyzer (Type B & K 2109), with occasional cross checks against results from a Technical Products Wave Analyzer (Type TP 62). The former has a proportional band width, passive filter system, while the latter works with active constant bandwidth filters. Both set-ups for this evaluation are shown in Fig. 14.

3.6 Measurement of Probability Densities

The probability density distribution of a single turbulent component was measured with a Technical Products probability analyzer (Type TP 647), Fig. 15. Joint probability densities were measured with two of the above analyzers coupled together so that one provided the gate for the joint probability density obtained from the other, Fig. 16.

Normalization and calibration of probability analyzers were based on a known input sine wave, whose rms value is close to that of the hot-wire turbulent signals. The probability density of a sine wave $e=A\sin\theta$ whose phase θ is a random variable uniformly distributed on the interval $-\frac{\pi}{2}$ to $\frac{\pi}{2}$, is given by:

$$f(e) = \frac{1}{\pi A}\left[1-\left(\frac{e}{A}\right)^2\right]^{-\frac{1}{2}} \qquad \text{for} \quad |e| \leq A \tag{45}$$

$$= 0 \qquad \text{otherwise}$$

Since the normalizing process has made all the amplitudes of different sine waves to be $A = \sqrt{2}\sqrt{e^2} = \sqrt{2}$ in such a way that $\sqrt{e^2} = 1$, the lowest point of the sine-wave probability density is found to be $f(o) = \frac{1}{\pi A} = 0.225$, which was used for calibrating the x-y plotter. An example is given in Fig. 17. As for the calculation after the analog analysis, the main problem was to convert the measured σ values into the real turbulent fluctuation units (in feet per second). A graphical integration based on the second-moment of the probability density was suggested as a proper approach, i.e.,

$$u_i^2 = \int_{-\infty}^{\infty} e_i^2 \, f(e_i) \, de_i \tag{46}$$

where u_i^2 is the square of the rms value at point i and e_i is the value obtained from the probability analyzer.

The experimental data for probability densities were plotted, both for probability densities of single quantities and for joint probability densities. Instead of establishing a 3-dimensional distribution of joint probability density, iso-probability density contour maps were plotted. Conditional density functions were evaluated according to the definition,

$$f(v'/u') = \frac{f(u',v')}{f(u')} = \frac{f(u',v')}{\int_{-\infty}^{\infty} f(u',v')dv'} \tag{47}$$

and thus, the conditional probability density is given as

$$f(v'/u' = u_o')dv' = \frac{\text{Prob}\left[u_o' < u' \leq u_o' + du',\ v_o' < v' \leq v_o' + dv'\right]}{\text{Prob}\left[u_o < u' \leq u_o' + du'\right]} \tag{48}$$

This equals the ratio of the mass in the differential element of Fig. 18 to the mass in the strip $(u_o', u_o' + du')$. Thus, for a given u_o', the density $f(v'/u' = u_o')$ is the u_o' - profile of joint density $f(u'v')$ normalized to make its area equal to 1, (Fig. 18).

3.7 Measurement of Space Correlation Coefficients Along the Trajectories

Space correlations along trajectories were taken by passing the outputs of two single hot-wire anemometers through a well-calibrated sum-and-difference circuit instead of an analog multiplier (Fig. 19). The calculations were only based on the rms values of inputs and outputs of the sum-and-difference circuit.

Let $u_1^2 = A_1^2 \cdot e_1^2$ $\qquad u_2^2 = A_2^2 \cdot e_2^2$

$S = C_S \sqrt{(e_1' + e_2')^2}$ $\qquad D = C_D \sqrt{(e_1' - e_2')^2}$

where A_1 , A_2 , are the calibration constants for hot-wire anemometers, 1 and 2, respectively, C_S , C_D , the calibration constants for sum (S) and difference (D) circuits. Then

$$R(x,\xi) = \frac{\overline{u_1'(x)u_2'(x+\xi)}}{u_1^2 \cdot u_2^2} = \frac{(S/C_S)^2 - (D/C_D)^2}{4\, e_1 \cdot e_2} \tag{49}$$

yields a relation for the space correlations when ξ is the distance of point 2 from point 1, and x is the location of point 1 in the reference coordinate system.

Chapter IV

THE EXPERIMENTAL RESULTS

The experimental work on this project was conducted in three phases. These were:

1. Measurements of the mean wind vertical velocity profiles and turbulent intensities at selected points on the lee side of a sinusoidal hill using the Army Wind Tunnel. This work has been reported by Plate and Lin (1965). Another more detailed flow pattern will be given in this chapter.

2. Determination of theoretical missile trajectories, corresponding to mean wind conditions if the missiles were fired from the lee side of a scaled-up version of the two-dimensional ridge.

3. Determination in the wind tunnel of the characteristics of the wind field at selected points along the scaled-down missile trajectories, in accordance with the theoretical development given in Chapter II.

A fourth phase, not reported here, will be to calculate the response of the missile to the experimental wind fields determined in phase 3.

4.1 Determination of Mean Missile Trajectories

This work was conducted at the USA Ballistic Research Laboratories, Aberdeen, Maryland, using the laboratory computing facilities and a six degree of freedom multi-stage rocket trajectory program.

The missile used for the mean trajectory calculation was a hypothetical gun-launched two-stage anti-tank missile. The gun launched the missile at 1200 f/s. After a short delay, a booster section ignited, the thrust from which accelerated the missile to a velocity of 2100 f/s. At that point, a sustainer motor ignited, the thrust from which kept the missile at a constant velocity until it reached a position about 1 km from the launcher. In computer simulations, this missile was shown to have a steady cross wind sensitivity of 0.36 mils angular deflection per ft/sec of cross wind.

For the simulation study, the two-dimensional ridge used in the tunnel was scaled up by a factor of 1200 to a ridge 400 ft high by 2000 ft long. It was then assumed that missile launchers were emplaced at the base of the ridge; halfway up the ridge, and at the top of the ridge. All the launchers were pointed at targets on the lee side of the ridge, the targets being 1 km from the launcher sites.

The trajectories of missiles were simulated first for the no-wind case and then for the case of the steady wind flowing over the ridge by interpolating in the data from Plate and Lin (1965).

The missile trajectory data from these simulations were then sent to Colorado State University to be used in further experimental work. The characteristics of the wind fields along the trajectories, shown in Fig. 3, generated in the above study, is discussed in this report.

4.2 Mean Velocities and Streamline Pattern

Mean velocity distributions are shown in Fig. 5. The solid lines indicate velocities measured with a pitot static tube, while the dashed lines refer to hot-wire measurements. On the whole, the agreement between the two sets is good, even without any corrections for turbulence. The small deviations might just as well be due to drift in the hot-wire characteristics, which could never be fully eliminated.

Characteristic of the flow field is the strongly accelerated flow above the crest of the model, which gives rise to the velocity maximum, and the very sharp velocity gradients in the neighborhood of the separation streamline. These velocity gradients interact with the turbulent shear stress to cause a large increase in the amount of turbulent energy of the flow.

Vertical mean velocities can be determined from the mean streamline pattern shown in Fig. 5. The streamline pattern also shows the separation region. Under the separation streamline, the velocity gradually decreases, reaches zero and reverses direction. This can be inferred from the fact that the discharge across any vertical section underneath the separation streamline must be zero. The experimental data, however, fail to show this behavior due to the fact that the pitot tube cannot measure any backflows, while the hot-wire cannot distinguish the flow directions.

4.3 Turbulent Intensities and Shear Stresses

The turbulent quantities $\overline{u'^2}$ and $\overline{v'^2}$, and the turbulent shearing stress $\overline{u'v'}$ were plotted against y in Fig. 13. The turbulent quantity $\overline{w'^2}$ was also determined at a number of points and generally behaved roughly like the u-component. The shear stresses $\overline{u\,w}$ were calculated and found to be negligibly small even in the bubble region. The profiles shown in Fig. 13 have a strongly peaked shape in the neighborhood of the separation streamline, especially for short distances from the separation point on the hill slope. In general, the intensity profiles of u component based on values which had not been corrected for the flow direction coincide with those obtained by Plate and Lin (1965) and thus the reproductibility of the turbulent flow field in the present tunnel is quite satisfactory.

4.4 Turbulence Spectra and Dissipation Rates

Turbulence spectra were evaluated for all points indicated in Fig. 9. The signal is plotted in the form $\overline{e_B^2}/B$ vs. f (Fig. 20 through Fig. 28). Here $\overline{e_B^2}/B$ is the energy density, per Hz, of the electrical signal

from the hot wire as passed through the filter of bandwidth B and of center frequency f of the spectrum analyzer. It differs from the energy level of the turbulent motion by a calibration factor given by the square of the slope of the calibration curve $\overline{U}$ vs. E of the hot-wire anemometer.

In the low frequency range, we notice a strikingly different spectrum shape close to the hill crest $(x = 0)$ as compared to the results at 16 inches downstream. At short vertical distances from the wall, the data close to the crest (Fig. 22) indicate a much slower drop-off with frequency than the set of data shown in Fig. 25. In fact, there seems to exist a well-developed region, between 40 and 200 cps, in which the energy level decreases almost linearly. This behavior is characteristic of strong interactions between mean flow and turbulence, i.e., of a flow when a large amount of turbulence generation due to large velocity gradient takes place. This behavior is not typical for other boundary layer flows of the U.S. Army Wind Tunnel.

Due to strong noise levels of the magnetic tape recorders, the part of the spectra corresponding to frequencies above 2000 Hz is not usable. For large frequencies, but below 2000 Hz, the shape of the spectrum is the same for all data. In fact, if the spectrum is plotted in the similarity form of the universal equilibrium law of Kolmogoroff, we find that the shape is identical for all data, and they collapse on a single curve. This is illustrated in Figs. 29, 30, 31, 32 and 33, in which the data of Figs. 22, 23, 25, 26 and 28 have been replotted in dimensionless form:

$$\phi \left(\frac{k}{k_s} \right) = N.F(f) \tag{50}$$

ϕ is the non-dimensional spectral density, $F(f)$ is the measured spectral density at frequency f, and N is a conversion factor:

$$N = \frac{u'^2 \, \overline{U}}{2\pi \varepsilon^{1/4} \nu^{5/4}} \tag{51}$$

Furthermore, K_s is the reference wave number based on the dissipation ε:

$$K_s = (\varepsilon \nu^{-3})^{1/4} \tag{52}$$

As an estimate for the dissipation ε we have used the isotropic relationship:

$$\varepsilon = 15 \, \nu \, \overline{\left(\frac{\partial u'}{\partial x} \right)^2} = 15 \, \nu \, \overline{U^{-2}} \overline{\left(\frac{\partial u'}{\partial t} \right)^2} \tag{53}$$

and also, the equivalent form

$$\varepsilon = 15 \, u'^2 \int_0^\infty K^2 f(K) \, dK \tag{54}$$

where K is the wave number

$$K = \frac{2\pi f}{\overline{U}} \tag{55}$$

and $\overline{U}$ is the mean velocity, as before. Dissipation rates calculated from Eqs. (53) and (54) are shown in Fig. 34.

In Figs. 29, 30, 31, 32 and 33 we have also indicated the -5/3 law of the inertial subrange and the universal shape of the high frequency and of the turbulence spectrum, in the form given by Sandborn and Marshall (1963). It is surprising to see that the high frequency end of the spectrum in the highly disturbed boundary layer of our case is presented exactly by the high frequency shape of the undisturbed turbulence in a boundary layer along a flat plate. Since Sandborn and Marshall have demonstrated the perfect agreement of their spectra with experimental results obtained in wind over ocean waves by Pond et al., (1963), it appears that this range of the spectrum is a universal feature of all turbulent flows.

But the same conclusion cannot be drawn for the turbulence spectrum in the inertial subrange. Pond et al., report that here a spectrum law of the form is valid

$$N \quad F(f) = k \left(\frac{K}{K_s}\right) \tag{56}$$

where k is a universal constant, about 0.46. For the data of this report, it is found very near the crest of the model hill, this "constant" is well enough verified, but at larger distances downstream, in the region which derives its turbulence from the initially strong gradients in the mean velocity across the separation streamline, the "constant" seems to be substantially higher. At 16" (Fig. 31) downstream from the hill crest, the best fitting -5/3 law has a constant k of about 0.85. It should be noted that in the velocity region where this is found the turbulence level decreases rapidly with distance, indicating that the amount of energy generated locally is lower than that dissipated, i.e., the ratio of dissipation to generation

$$D = \frac{\varepsilon}{\overline{u'v'}\,\frac{\partial \overline{U}}{\partial y}} \tag{57}$$

in this region is greater than one. This result thus is in qualitative agreement with a result of Margolis and Lumley (1964). It has as yet, however, not been shown that a universal relation exists between k and D. Experiments are at present underway at Colorado State University to investigate this point. That D might also be an important quantity in modeling of atmospheric turbulence has been pointed out by Plate and Lin (1966).

The low frequency end of the spectrum is governed by the process of energy extraction from the mean flow and depends on the local velocity field. Similarity forms can, therefore, not be expected for the whole spectrum. But the eddies associated with the low frequency end of the spectrum input cause the most important dynamic effect on a missile during its flight. Work is therefore in progress at CSU on relations between the low frequency end of the spectrum and the local mean velocity field.

4.5 Probability Density Distributions

Two different sets of probability densities are given for the points along the trajectories. These are probability densities of the v', of the ' components (Figs. 35-42), and joint probability densities of u' and v' ,(Figs. 43-50).

The density of each individual turbulent component seems quite well represented by a Gaussian (normal) curve except the mean value is not exactly zero. This is illustrated by plotting cumulative probability densities on probability papers (Figs. 51-54). The angle θ of the joint probability density contour as calculated by Eq. (26), which is based on the assumption of a zero mean density, is surprisingly close to the measured angle θ obtained directly from the two-dimensional contour of joint probability density (Table III). Most of probability densities also show the evidence of skewness. Numerical evaluation of the skewness factor is not necessary for this study, but the reason for this skewness could always be interpreted as the result of the preferred direction of fluctuation of the turbulence component due to the shear stresses. This phenomenon could be strongly show for those points along the separation streamline and somewhere within the bubble region because of the complex interactions of the three-dimensional turbulence.

Flatness of the probability density, which was suspected as the result of turbulent intermittency, was not obviously seen among our measurements which were usually performed in the fully turbulent boundary layer.

In order to check the statistical independence of w' from u' , joint probability density distributions $f(u', w')$ are measured. As mentioned in a previous section, the homogenuity of turbulence in plane parallel to the ground requires that $\overline{u'w'}$ be zero, which was confirmed by our experiments. But it is also necessary that for each value of u' , $f(w'|u')$ be independent of u' and equal to $f(w')$. To check this criterion (which gives a sufficient condition for statistical independence) we have plotted into one graph $f(w'|u')$ for different values of u' as well as $f(w')$. Some results are shown in Figs. 55-59. They indicate that u' and w' are not exactly jointly Gaussian, even though $\overline{u'w'}$ was found to be zero from hot wire measurements, which is not a sufficient condition to conclude that w' is independent of u' for the slightly non-Gaussian curves observed in this study.

We next checked joint probability density distributions $f(u'_i, u'_{i-1})$. Different results were obtained depending on the direction of the trajectory. For a trajectory of 60^0 azimuth these typical measurements

are shown in Figs. 60-62. The results indicate that no correlation exists for turbulence components u'_1 and u'_2. This is evident from the coincidence of the axes of the elliptical contours with one of the axes. It implies that the distance between the two points has been chosen too wide, so that the integral length scale is somewhat smaller than the distance between adjacent points.

For the case of 60^0 azimuth, the assumption of an elongated eddy structure with u_1' related only to u_2' is not justified. The only way of obtaining an impact dispersion probability distribution is found by assuming statistical independence between neighboring points along the trajectory, with the resulting inconsistency in the averaging procedure for the average velocity encountered by the missile in traveling from x_{i-1} to x_i.

When joint probability densities for u'_{i-1} and u_i' lying on a trajectory in the mean wind direction (0^0 azimuth) are considered, strong correlations are found as is demonstrated in Figs. 63-65. The results are even better illustrated by considering directly the space correlation functions along different trajectories, which are plotted in Fig. 66. Two trajectories were added, trajectory 2 which starts halfway down the hill slope, and trajectory 3 which starts at the crest of the ridge. For correlation functions which start at the hill directly, correlation distances are rather short: already at 1" downstream from the hill the correlation between u_o and $u_{1"}$ has decreased to a correlation coefficient $r = 0.2$, where

$$r = \frac{\overline{u_i' \, u'_{i-1}}}{\sqrt{\overline{u_i^2} \; \overline{u_{i-1}^2}}} \tag{58}$$

For correlations starting at larger values than $x = 4"$ the correlation coefficients for both trajectories seem to follow a fairly constant correlation curve, with approximately equal shape and furthermore, with a shape which is approximately exponential. The exponential curve which appears to give the best fit has been sketched into the experimental results. It is represented by the equation:

$$r = e^{-ax} \tag{59}$$

when a is a constant equal to $0.2\ in^{-1}$. This result implies that in the outer region (further downstream than 4" from the ridge) the joint probability distribution $f(u'_i, u'_{i-1})$ can be specified by the magnitudes u'^2_i and u'^2_{i-1} and by the curve expressed by Eq. (59), If u'_i and u'_{i-1} can be approximately represented by Gaussianity. The latter yields the numerator, and the former the denominator of Eq. (26) with u'_{i-1} taking the place of v', while u'_1 takes the place of u'. A difficulty in interpretation arises, however, if u_i happens to be equal, or

nearly equal to u_{i-1} . In that case, we may let $u_i^\dagger = Au_i$ and $u_{i-1}^\dagger = u_{i-1}$, where A is any positive constant factor in order to either enlarge or contract the values of u_i in such a way that $u_i^\dagger$ and $u_{i-1}^\dagger$ are numerically quite different from Eq. (21) and assuming again $m_{u_i} = m_{u_{i-1}} = 0$ for simplicity,

$$f(u_i^\dagger, u_{i-1}^\dagger) = \frac{f(u_i, u_{i-1})}{J(u_i, u_{i-1})} = \frac{1}{A} f\left(\frac{u_i^\dagger}{A}, u_{i-1}^\dagger\right) = \frac{1}{2\pi A \sigma_{u_i} \sigma_{u_{i-1}} \sqrt{1-p^2}}$$

$$\exp\left\{\frac{1}{2(1-p^2)}\left[\left(\frac{u_i^\dagger}{A\sigma_{u_i}}\right)^2 - 2p\left(\frac{u_i^\dagger}{A\sigma_{u_i}}\right)\left(\frac{u_{i-1}^\dagger}{\sigma_{u_{i-1}}}\right) + \left(\frac{u_{i-1}^\dagger}{\sigma_{u_{i-1}}}\right)^2\right]\right\} \quad (60)$$

Now, following the same procedure in deriving our Eq. (26), we may obtain

$$\text{Tan } 2\theta = \frac{2A\,\overline{u_i\, u_{i-1}}}{A^2\,\overline{u_i^2} - \overline{u_{i-1}^2}} \quad (61)$$

But this angle θ can only be used to specify $f(u_i^\dagger, u_{i-1}^\dagger)$, and of course, $f(u_i, u_{i-1})$ can also be specified by a little transformation technique.

For the region between 0 and 4" along the trajectory, it is necessary to know the coefficient α for each length section, which can approximately be found by linear interpolation. It is thereby assumed that the correlation function is exponential between point x_i and x_{i-1} . Thus, even though at larger distances the same exponential does not fit all the data, it is possible to make the assumption of Markoff dependency over a short reach, with at least engineering accuracy.

Conclusions

In the report we have given experimental evidence that the turbulence structure in the complicated flow field downstream of a model hill can be represented to a good approximation by Gaussian and jointly Gaussian probability distributions connected by space correlation functions which appear exponential. The joint probability densities are seen to be fully specified by the variances of the two variables and their first order cross correlation.

The results of this study indicate that it is possible to construct a model of the missile dispersion probability distribution by simply determining the variance of this distribution. Research towards this objective is currently under way at CSU.

TABLE I

Mean Velocity Calculation

x in	pt	y in	U_{HW}	$U_{P.T}$	x in	pt	y in	U_{HW}	$U_{P.T}$
2"	6	3.89	22.4	29.4	8"	18	1.35	3.6	-
	7	3.98	29.0	27.8		19	1.52	4.4	-
	8	4.09	31.8	33.3		20	1.9	7.9	10.1
	9	4.22	32.0	33.3		21	2.0	10.6	11.9
	10	4.68	31.8	32.9		22	2.16	13.6	15.5
	11	5.1		32.0		23	2.51	19.7	20.2
		6.0	31.4	31.3		24	3.12	22.6	23.3
		8.0	31.2	30.8		25	4.86	24.7	25.3
		10.0	31.0	30.7			6.	26.3	27.4
		15.0	31.0	30.3			8.	27.2	28.3
		20.0	30.9	30.6			10.	28.5	29.3
		24.0	30.7	30.2			15.	29.5	30.2
							20.	30.3	30.6
4"	12	3.35	16.2	19.2			24.	30.3	30.4
	13	3.49	26.5	25.4					
	14	3.60	27.3	5	10"		0.05	1.15	1.707
	15	3.84	29.0	29.8			.7	5.15	1.707
	16	4.63	29.0	29.7			1.15	7.96	8.18
	17	5.25	29.8	29.7			1.65	16.8	12.77
		6.0	29.5	30.1			2.2	22.5	17.
		8.0	30.3	30.			3.36	24.	23.35
		10.0	30.5	30.1			5.43	25.8	25.72
		15.0	30.5	30.3			8.	27.3	26.72
		20.0	31.	30.5			10.	28.5	28.2
		24.0	30.7	30.5			15.	29.5	30.06
							20.	30.6	31.
6"		2.46	10.2						
		2.53	16.6	8.18	12"	26	0.12	3.8	-
		2.81	24.1	17.06		27	0.73	5.9	5.12
		3.29	26.2	23.22		28	1.12	8.0	9.2
		4.0	27.4	24.58		29	1.50	11.1	13.3
		6.	28.6	26.77		30	1.75	14.4	15.
		8.	29.7	28.26		31	2.66	20.0	20.9
		10.	30.4	29.2		32	5.00	24.0	26.2
		15.	31.0	30.5			7.14	25.4	25.6
		20.	31.4	31.16			9.	27.	27.4
							12.	28.2	28.5
							15.	28.9	29.5
							23.3	29.9	30.3

TABLE I (Continued)

x in	pt	y in	U_{HW}	$U_{P.T}$	x in	pt	y in	U_{HW}	$U_{P.T}$
14"		0.05	2.7	-	24"	41	0.12	12.	12.81
		.18	4.14	-		44	1.06	15.8	17.31
		.4	6.0	6.15		45	1.20	16.2	16.85
		.62	7.96	8.86		46	2.73	18.8	20.25
		1.05	11.	12.31		47	6.16	23.9	23.85
		1.58	16.6	15.55			8.	25.7	25.2
		2.0	19.	17.16			10.	26.4	26.24
		2.67	21.35	19.62			12.5	27.55	27.65
		4.	22.64	22.44			15.	28.20	28.58
		8.	26.8	26.4			20.	29.3	29.4
		10.	27.5	27.64					
		15.	28.9	29.58	32"	48	0.14	14.	14.02
		20.	30.4	30.64		49	.50	16.5	16.85
						50	3.58	20.9	21.82
16"	33	0.12	5.8	9.66		51	6.74	24.	25.55
	34	.28	8.4	11.32			10.	26.55	26.8
	35	.69	10.2	13.87			12.5	27.1	27.3
	36	.96	10.8	15.17			15.	28.1	28.56
	37	1.56	13.8	18.07			20.	29.4	29.48
	38	2.2	18.2	19.62					
	39	3.32	20.	22.6	40"	52	0.1	14.5	15.4
	40	6.5	23.8	25.9		53	.2	16.5	16.57
		8.	25.8	26.98		54	4.16	22.2	22.4
		10.	27.8	28.5		55	6.32	23.9	24.44
		15.	28.8	30.			7.5	25.1	24.75
		20.	29.9	30.7			10.	26.2	26.3
							12.5	27.4	27.5
18"		.05	7.4	9.66			15.	28.0	28.2
		.13	9.55	11.45			20.	29.4	29.34
		.37	10.95	12.66					
		.95	14.05	13.44					
		2.	19.5	17.4					
		2.9	20.85	20.42					
		4.	22.3	22.6					
		8.	26.3	26.42					
		10.	27.7	27.76					
		15.	29.5	29.6					
		20.	30.2	30.64					

TABLE II

Turbulent Calculation

$$\overline{u'^2} = \left(\frac{dU}{dE}\right)^2 \overline{e'^2}$$

$$\overline{v'^2} = \frac{1}{2}\left[\overline{e_1'^2} + \overline{e_2'^2}\right]\left(\frac{dU}{dE}\right)^2 - \overline{u'^2} - \varepsilon\left[\overline{e_1'^2} - \overline{e_2'^2}\right]\left(\frac{dU}{dE}\right)^2$$

$$\overline{u'v'} = \frac{1}{4}\left[\overline{e_1'^2} - \overline{e_2'^2}\right]\left(\frac{dU}{dE}\right)^2 - 2\varepsilon\,\overline{v'^2}$$

$$\overline{w'^2} = \frac{1}{2}\left[\overline{e_1'^2} + \overline{e_2'^2}\right]\left(\frac{dU}{dE}\right)^2 - \overline{u'^2}$$

$$\overline{u'w'} = \frac{1}{4}\left[\overline{e_1'^2} - \overline{e_2'^2}\right]\left(\frac{dU}{dE}\right)^2$$

TABLE II (Continued)

x	pt	y	$\overline{u'^2}$	ε	$\overline{v'^2}$	$\overline{u'v'}$	$\overline{w'^2}$	$\overline{u'w'}$
2"	6	3.89	27.7	.227	18.51	-10.06	22.9	-.455
	7	3.98	26.5	.209	28.60	-11.89	13.9	-.071
	8	4.09	3.37	.175	5.635	- 3.36	5.93	-.0367
	9	4.22	2.46	.14	7.568	- 2.64	6.58	-.011
	10	4.68	1.88	.105	1.869	- 0.657	4.92	-.005
	11	5.10	1.70	.0872	1.398	- 0.354	4.99	-.014
		10.00	.69	.0349	0.6976	- 0.227	.230	-.0283
		15.00	.388	.0175	0.1157	- 0.0574	.076	-.0505
		17.00	.72	-	0.149	- 0.048	.081	+.056
		20.00	.019	-	0.0233	- .0095	.0113	+.067
4"	12	3.35	11.8	.314	19.42	-17.05	24.4	-.002
	13	3.49	8.48	.262	14.57	-12.16	18.62	-.017
	14	3.60	4.96	.244	3.345	- 2.372	8.95	+.0005
	15	3.84	2.72	.244	2.542	- 1.405	4.27	-.0017
	16	4.63	2.20	.192	1.713	- 0.925	3.41	+.050
	17	5.25	1.90	.140	1.488	- 0.699	2.91	+.021
		10.00	1.09	.0175	0.604	- 0.362	.585	+.036
		13.00	0.69	-	0.29	- 0.147	.302	+.036
		15.00	.337	-	.331	- 0.088	.077	+.040
		20.00	.028	-	.041	- .0094	.010	+.042
8"	18	1.35	1.90	.525	.432	- .611	2.36	-.045
	19	1.52	5.20	.489	1.26	- 1.161	3.28	+.075
	20	1.90	11.85	.14	5.20	- 4.76	12.80	+.0475
	21	2.00	19.54	.087	6.09	- 6.59	21.9	+.0725
	22	2.16	24.00	.035	22.0	- 7.86	28.5	+.0775
	23	2.51	12.75	.0175	6.4	- 3.804	17.56	+.12
	24	3.12	4.99	.035	.956	- .467	1.15	+.0378
	25	4.86	2.56	.035	.974	.096	3.55	0
		5.00	1.89	.035	.47	- .057	1.18	-.019
		10.00	.743	.0175	.297	- 0.024	.355	+.021
		15.00	.388	-	.08	- .074	.098	+.0245
		17.50	.11	-	.028	- .0669	.012	+.0012
		20.00	.028	-	.013	- .0087	.003	-.0035
12"	26	0.12	2.24	-	.31	- 0.178	1.93	.025
	27	.73	8.78	-	.14	- .76	10.72	.08
	28	1.12	16.3	.175	5.61	- 5.74	18.36	.142
	29	1.50	25.3	.262	14.23	-14.96	19.9	.123
	30	1.75	30.3	.245	14.28	-15.84	31.2	.102
	31	2.66	6.2	.175	12.80	- 7.62	11.2	.085
	32	7.14	1.42	.07	0.79	- .46	2.0	.008
		10.00	1.04	.035	.23	- .175	.043	.043
		15.00	.38	.0175	.20	- .112	.07	.033
		18.00	.07	-	.086	- .034	.0209	.005
		20.00	.0186	-	.005	- .0085	.0136	0

TABLE II (Continued)

x	pt	y	$\overline{u'^2}$	ε	$\overline{v'^2}$	$\overline{u'v'}$	$\overline{w'^2}$	$\overline{u'w'}$
16"	33	0.12	7.3	-	0.39	- 0.19	8.64	+.101
	34	.28	10.55	-	15.55	- 2.51	15.7	.115
	35	.69	19.0	-	15.05	- 4.06	18.6	.104
	36	.96	17.4	-	16.35	- 7.08	19.5	.061
	37	1.56	16.6	-	17.24	- 6.62	19.5	.037
	38	2.20	12.1	-	19.65	- 7.13	17.2	.026
	39	3.32	4.09	-	5.69	- 1.81	6.6	.021
	40	6.50	1.48	-	.998	- .423	1.5	.047
		10.0	.84	-	.551	- .223	.21	.033
		15.0	.242	-	.186	- .0754	.15	.045
		18.0	.109	-	.102	- .0462	.022	.008
		20.0	.0275	-	.000	- .0031	.019	.003
24"	41	.12	9.12	-	5.33	- .582		
	44	1.06	14.0	-	4.00	- 2.63		
	45	1.20	13.8	-	4.05	- 2.86		
	46	2.73	8.29	-	5.31	- 3.33		
	47	6.16	2.27	-	.70	- .664		
		10.0	.755	-	.565	- .16		
		12.50	.60	-	.55	- .247		
		15.0	.302	-	.433	- .139		
		20.0	.040	-	0	- .0071		
32"	48	.14	5.26	-	2.86	- .935		
	49	.50	7.33	-	2.42	- 1.21		
	50	3.58	6.02	-	5.08	- 3.00		
	51	6.74	2.025	-	.975	- .528		
		10.0	1.221	-	.159	- .268		
		12.5	.735	-	.025	- .0413		
		15.0	.302	-	.236	- .075		
		20.0	.0063	-	.015	- .00136		
40"	52	.10	4.72	-	6.38	- 3.29		
	53	.20	4.94	-	5.51	- 2.29		
	54	4.16	4.88	-	3.67	- 2.03		
	55	6.32	2.40	-	1.76	- .915		
		10.0	1.29	-	.07	- .193		
		12.5	.72	-	.175	- .044		
		15.0	.42	-	.176	- .0615		
		20.0	.057	-	.019	0		

TABLE III

$$\theta = 1/2 \tan^{-1} \frac{2\,\overline{u'v'}}{\overline{u'^2} - \overline{v'^2}}$$

pt	x (in)	z (in)	y (in)	$\bar{U}$	$\overline{u'^2}$	$\overline{v'^2}$	$\overline{u'v'}$	θ (deg)
12	4	4R	3.35	16.2	11.80	19.42	-17.05	38.7
14	4	4R	3.60	27.3	4.96	3.35	- 4.74	35.6
21	8	4R	2.00	10.6	19.54	6.09	- 6.09	21.2
22	8	4R	2.16	13.6	24.00	22.00	- 7.86	41.3
24	8	4R	3.12	22.6	4.99	0.96	- 0.47	2.8
27	12	4R	0.73	5.9	8.78	0.14	- 0.76	5.0
28	12	4R	1.12	8.0	16.30	5.61	- 5.74	23.5
30	12	4R	1.75	14.4	30.30	14.28	-15.84	31.5
31	12	4R	2.66	20.0	6.20	12.80	- 7.62	33.3
33	16	4R	0.12	5.8	7.30	0.39	- 0.19	1.0
36	16	4R	0.96	10.8	17.40	16.35	- 7.03	41.7
37	16	4R	1.56	13.8	12.10	19.65	- 7.15	45.0
38	16	4R	0.96	10.8	16.60	17.24	- 6.02	31.0
44	24	4R	1.06	17.9	12.10	19.65	- 7.13	13.9
48	32	4R	0.14	13.22	5.26	2.86	- 0.94	19.0
49	32	4R	0.50	17.08	7.33	2.42	- 1.24	13.4

REFERENCES

Bendat, J. S. and A. G. Piersol, "Measurement and analysis of random data," John Wiley and Sons, Inc., New York, 1966.

Dool, J. L., "Stochastic processes," John Wiley and Sons, Inc., New York, 1953.

Hinze, J. O., "Turbulence" McGraw-Hill, New York, 1959.

Lumley, J. L. and H. A. Panofsky, "The structure of atmospheric turbulence," John Wiley and Sons, New York, 1964.

Margolis, D. P. and J. L. Lumley, "Curved turbulent mixing layer" Physics of Fluids, Vol. 8, pp. 1775-1784, 1965.

Parzen, E. "Modern probability theory and its application," John Wiley and Sons, Inc., New York, 1960.

Pasquil, F. "Atmospheric Diffusion" D. Van Nostrand Co., Ltd. London 1962.

Plate, E. J., P. Baer, and F. F. Yeh, "Wind speed statistics along a hypothetical missile trajectory down wind of a sinusoidal model hill," presented at Unguided Rocket Ballistics Conference, White Sands Missile Range, New Mexico. Oct. 1967, CER67-68EJP-PB-FFY6.

Plate, E. J. and C. W. Lin, "The velocity field downstream from a two-dimensional model hill, part I of final report," CSU 1965, CER65EJP14.

Plate, E. J. and C. W. Lin, "The velocity field downstream from a two-dimensional model hill, part II of final report," CSU August 1965, CER65EJP-CWL41.

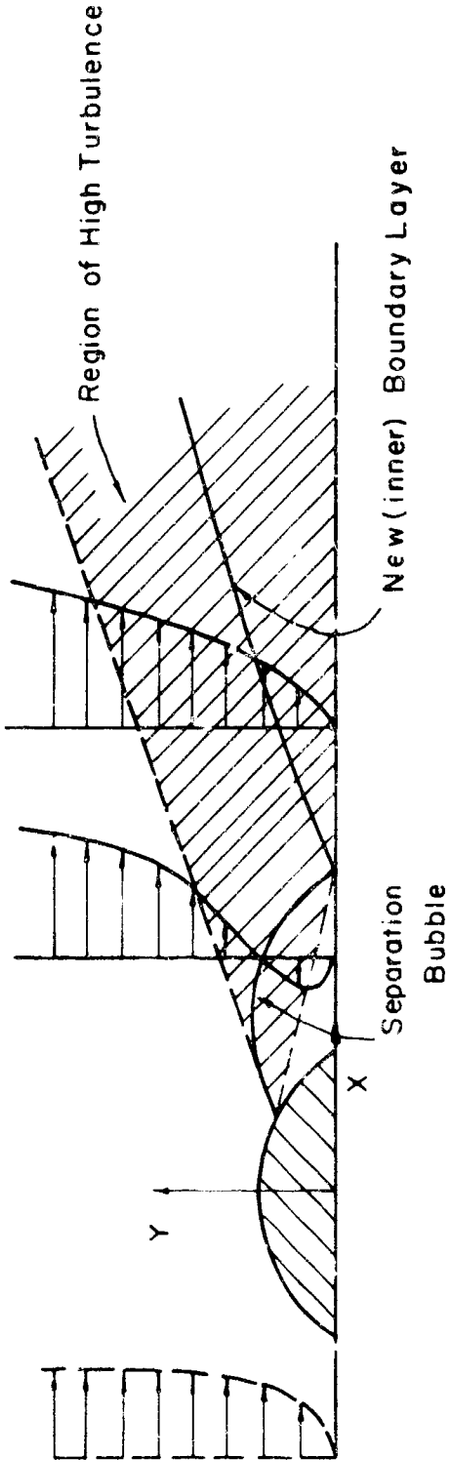

Fig. 1. Sketch of flow zones.

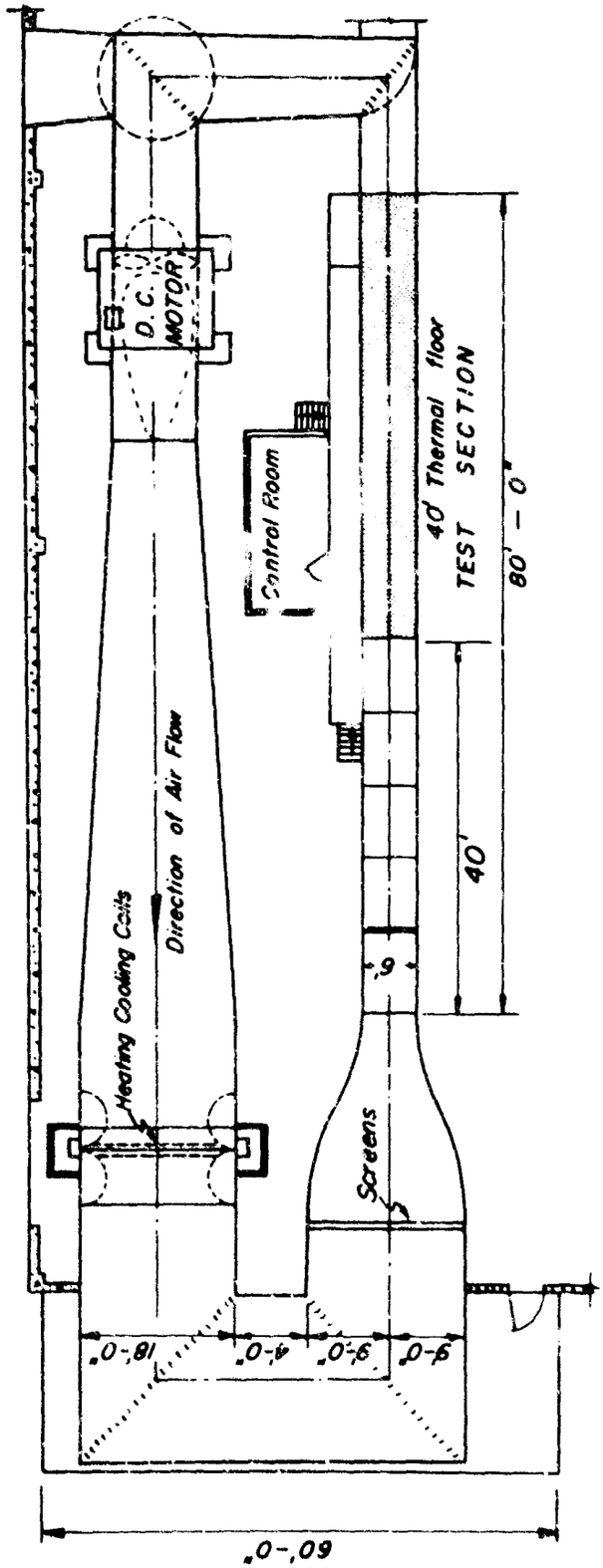

Fig. 3. Large wind tunnel.

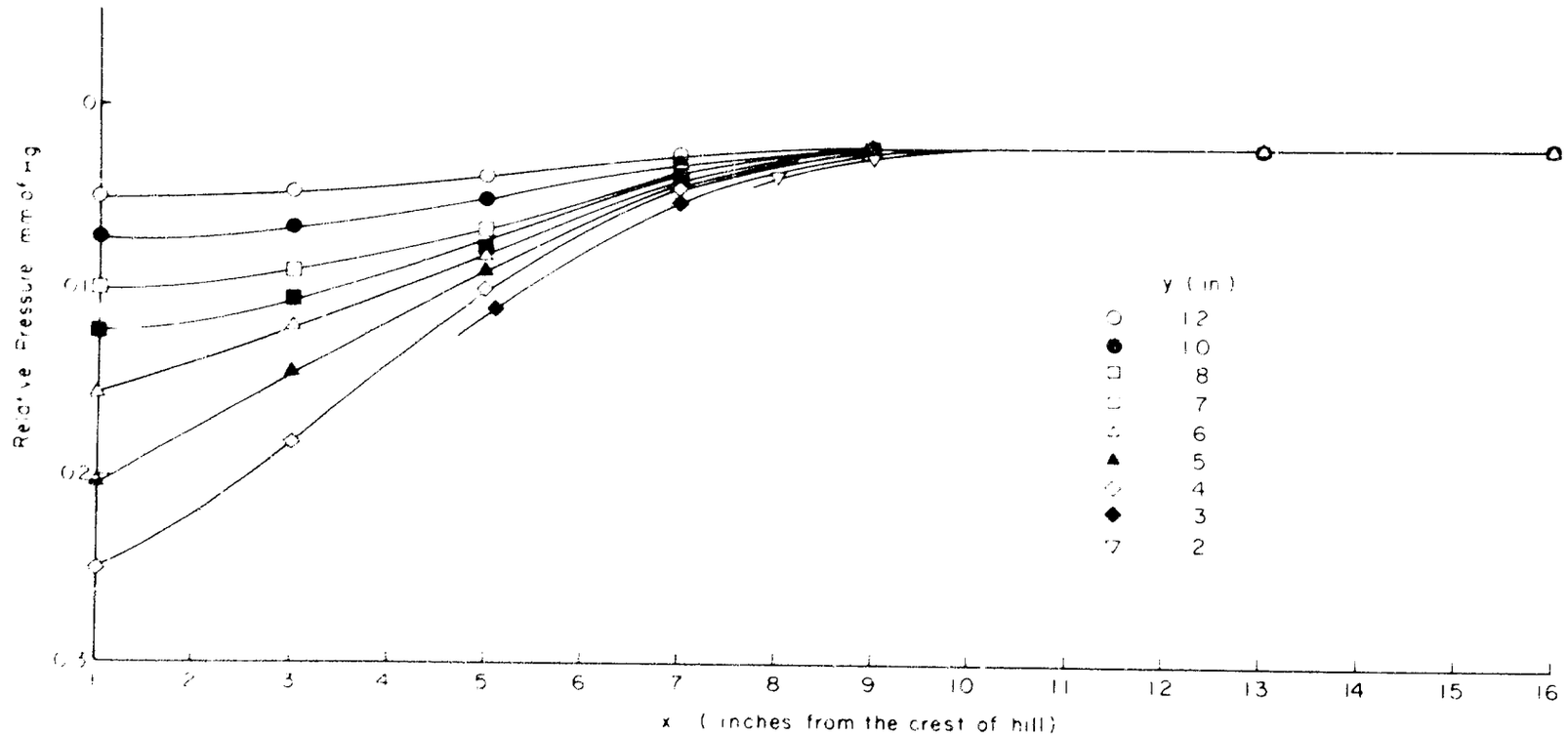

Fig. 3. Pressure distribution curves.

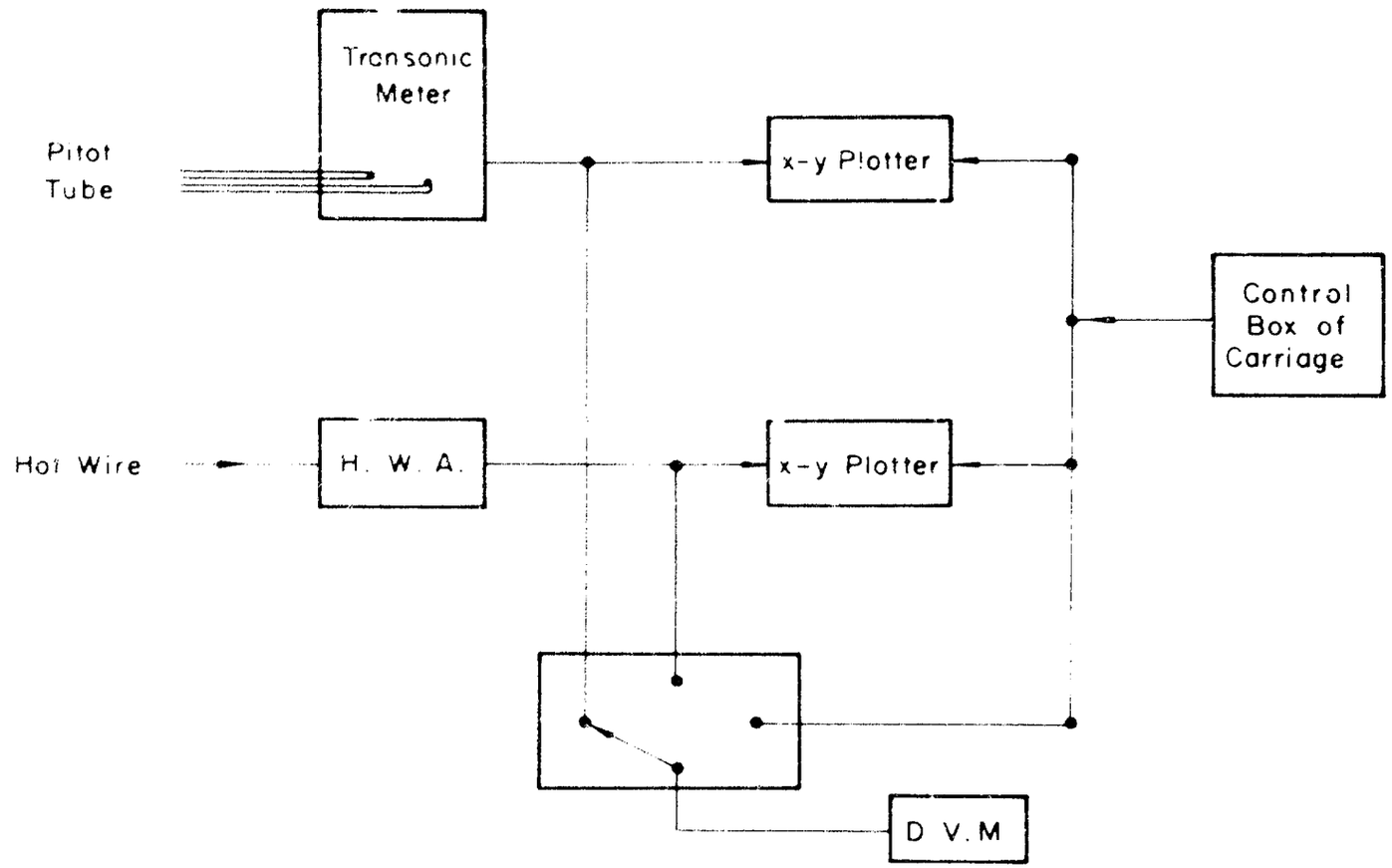

Fig. 1. Block diagram for setup of mean velocity measurements.

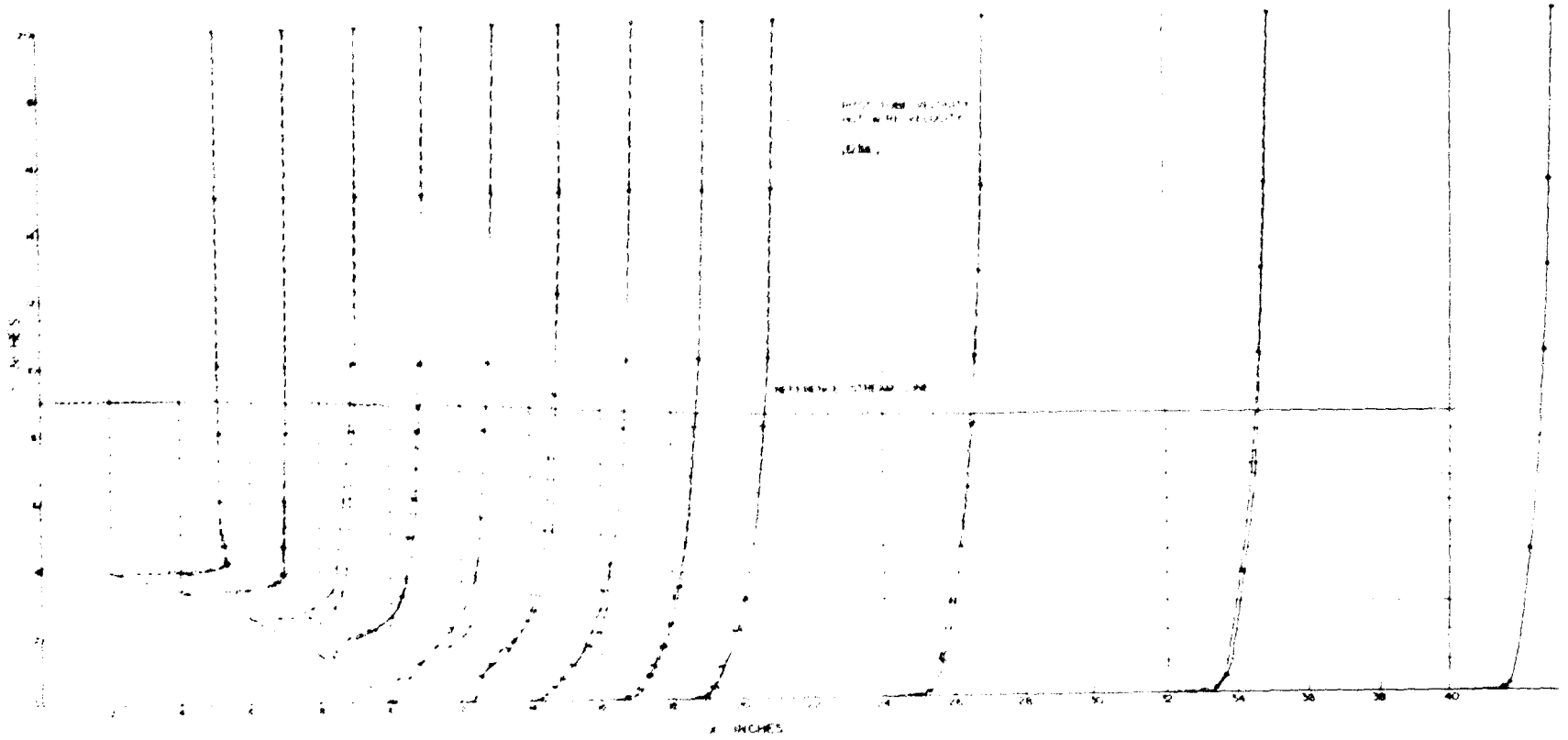

Fig. 5. Mean velocity distribution and stream line pattern.

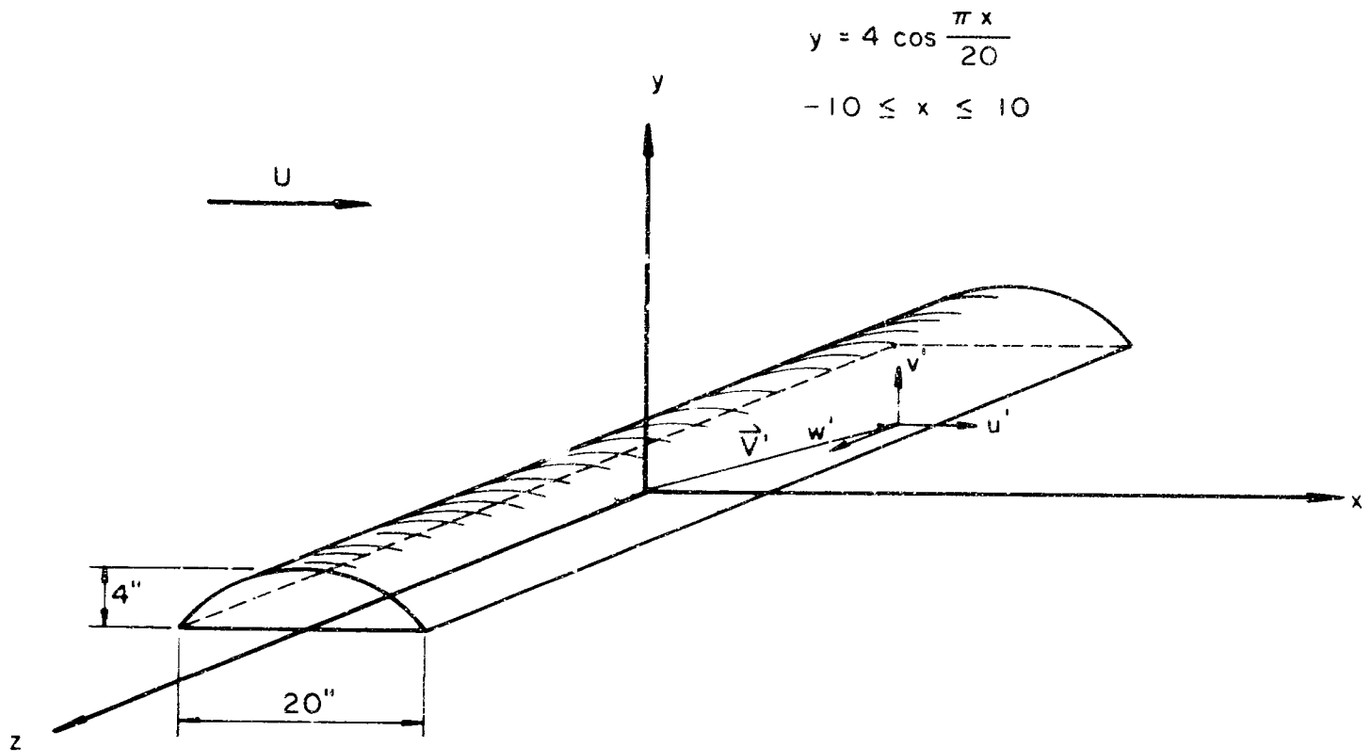

Fig. 6. Hill model dimensions and the coordinates of the flow field.

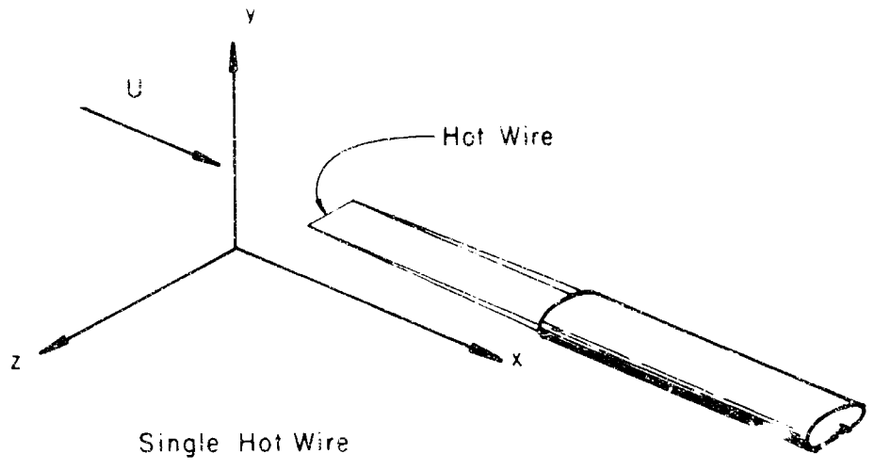

Single Hot Wire

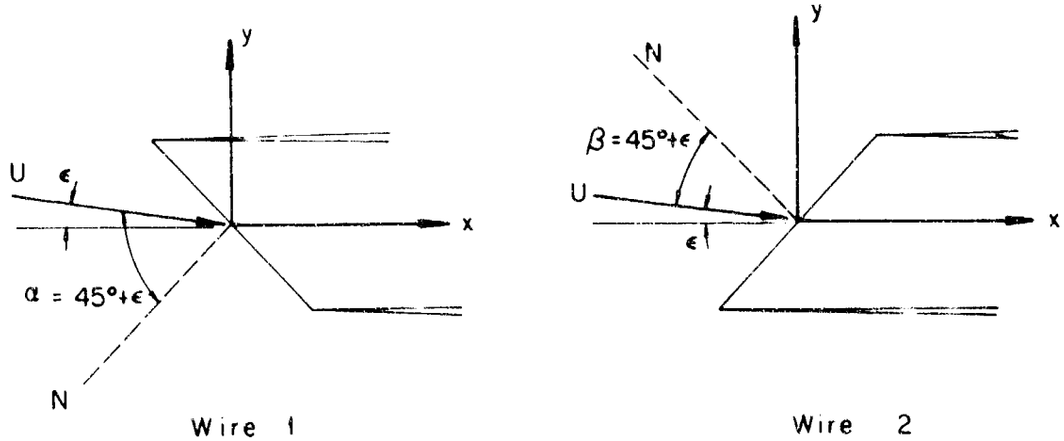

Wire 1 Wire 2

Crossed Wire

Fig. 7. Coordinates of the single and the crossed hot wires.

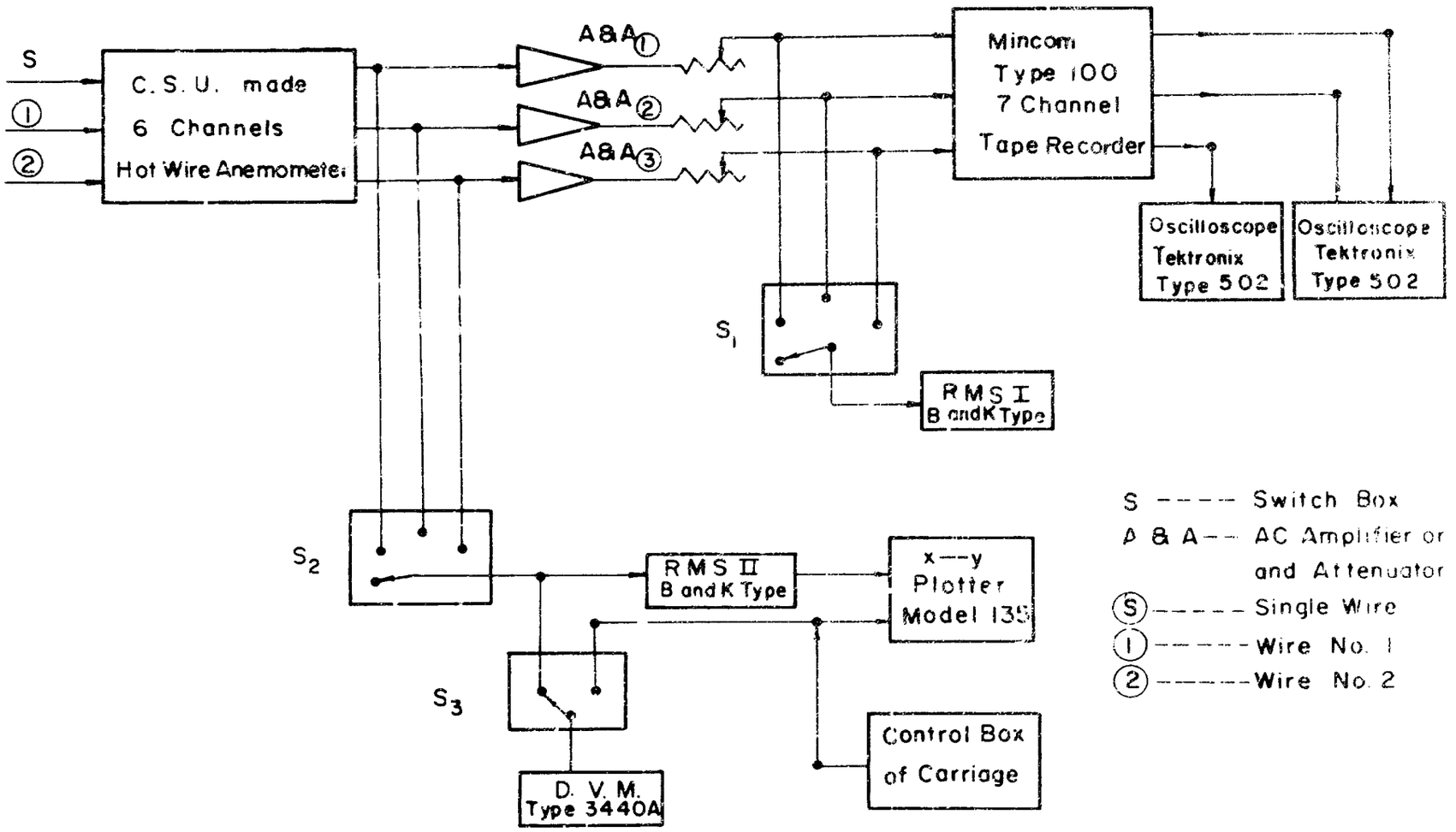

Fig. 8. Block diagram for setup of turbulent measurements.

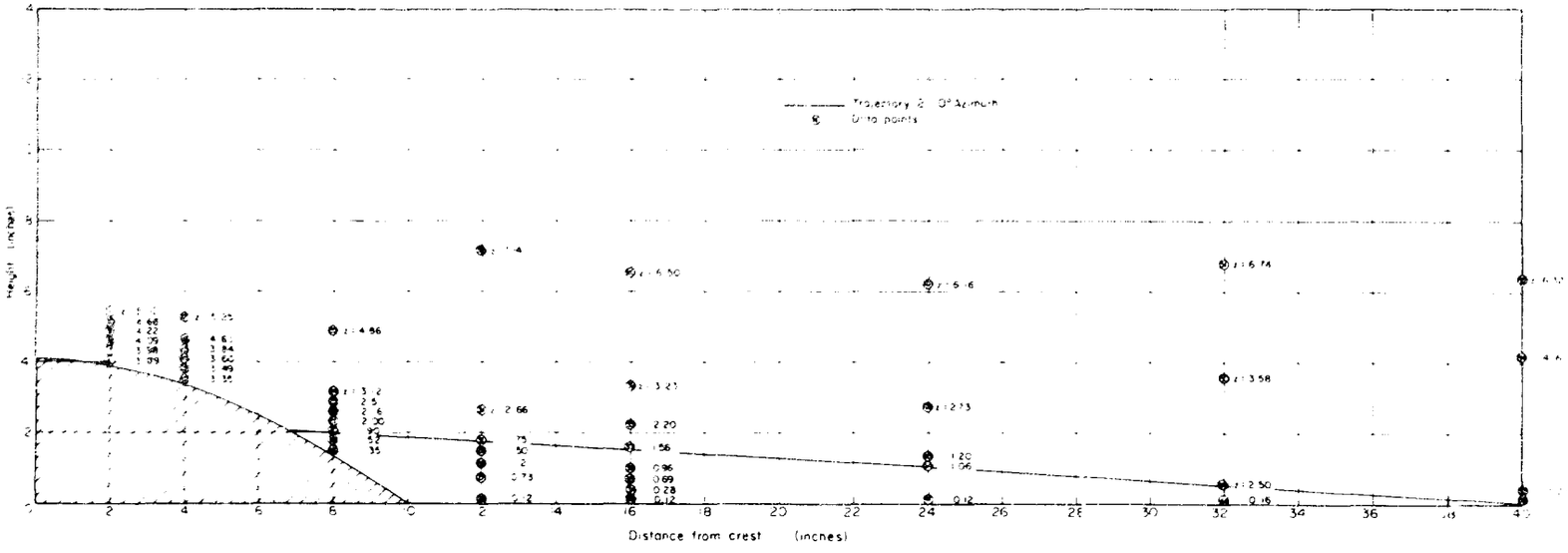

Fig. 9. Location of test points.

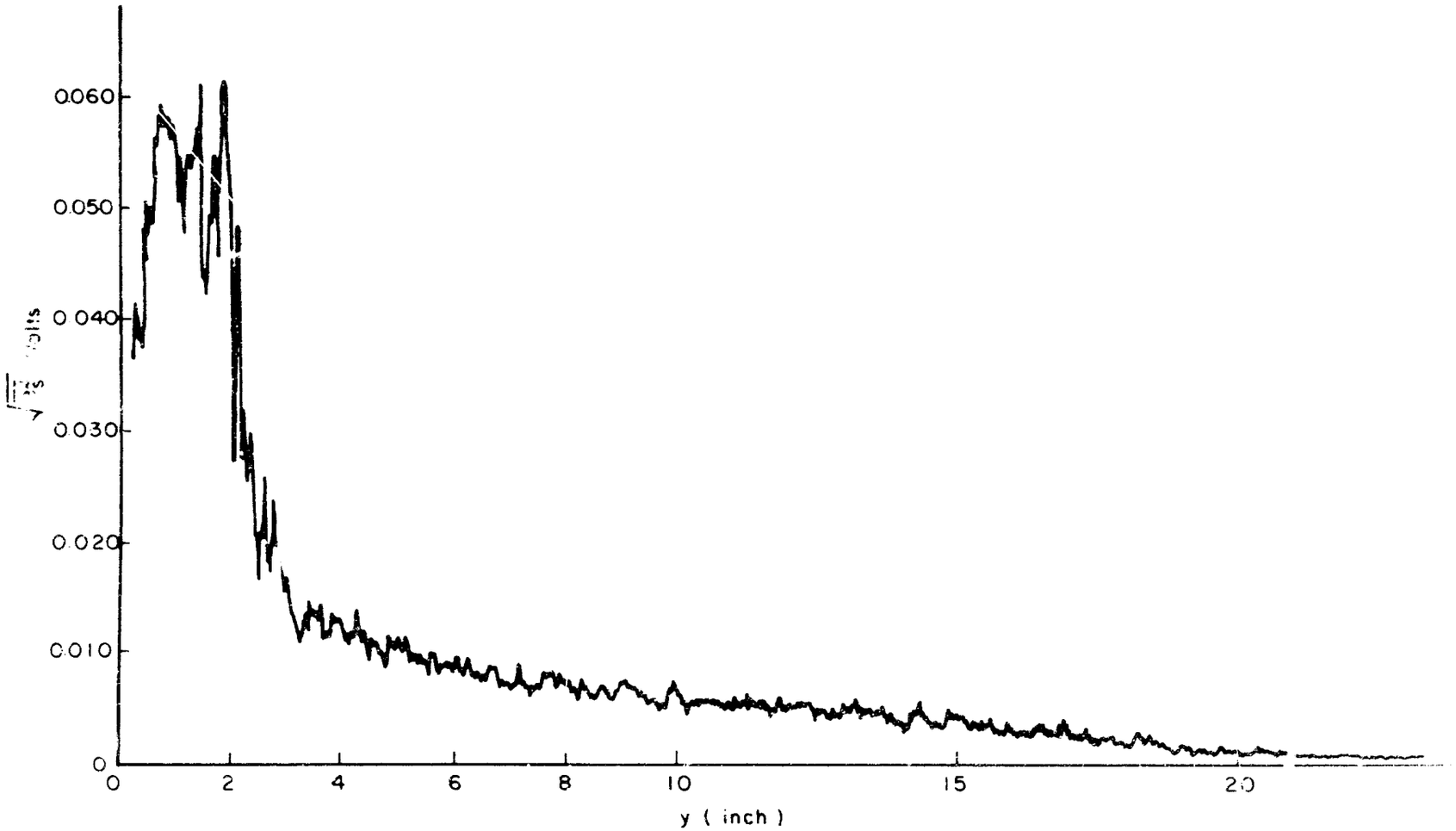

Fig. 10. A typical continuous RMS profile for single wire.

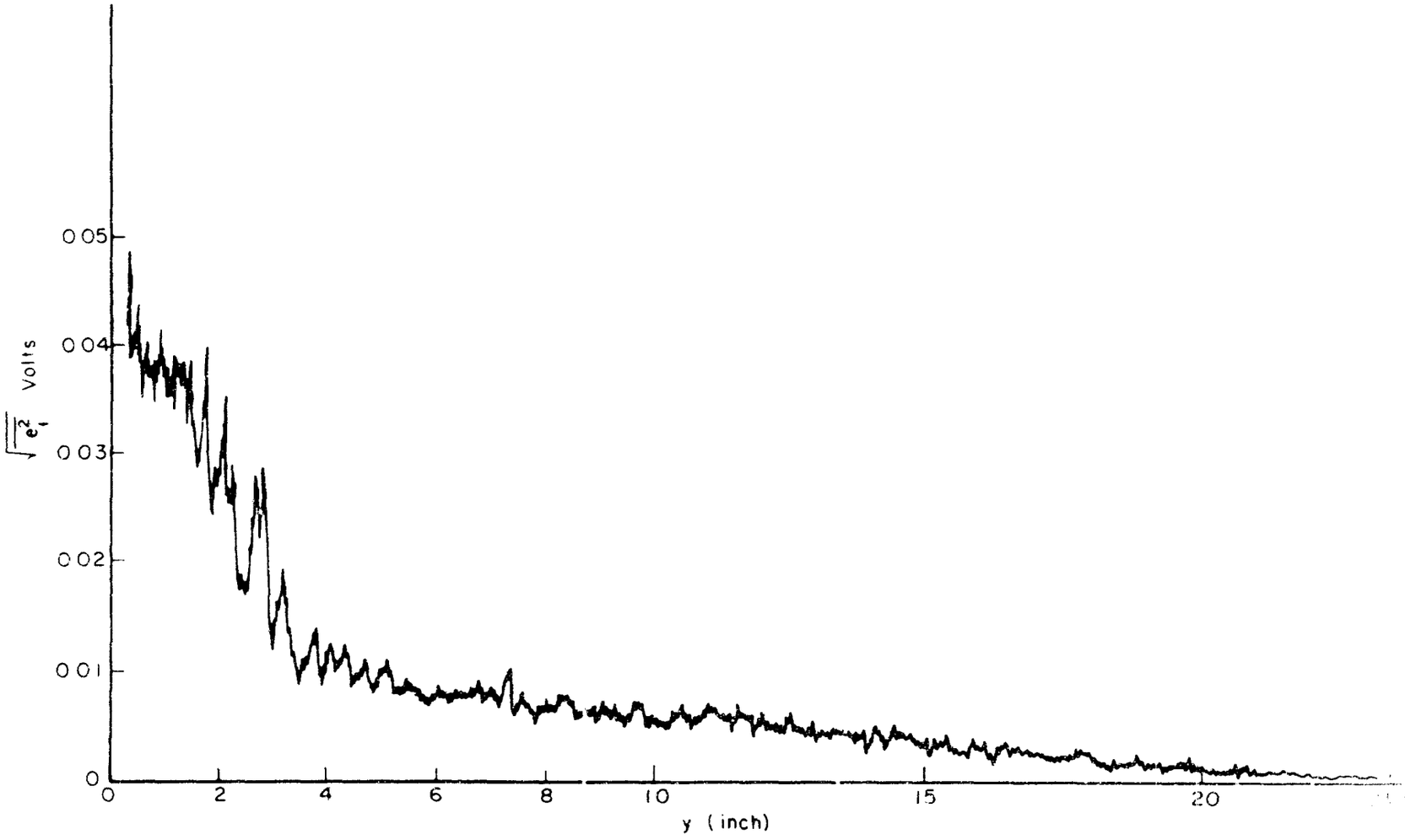

Fig. 11. A typical continuous RMS profile for wire 1 of the crossed hot wire.

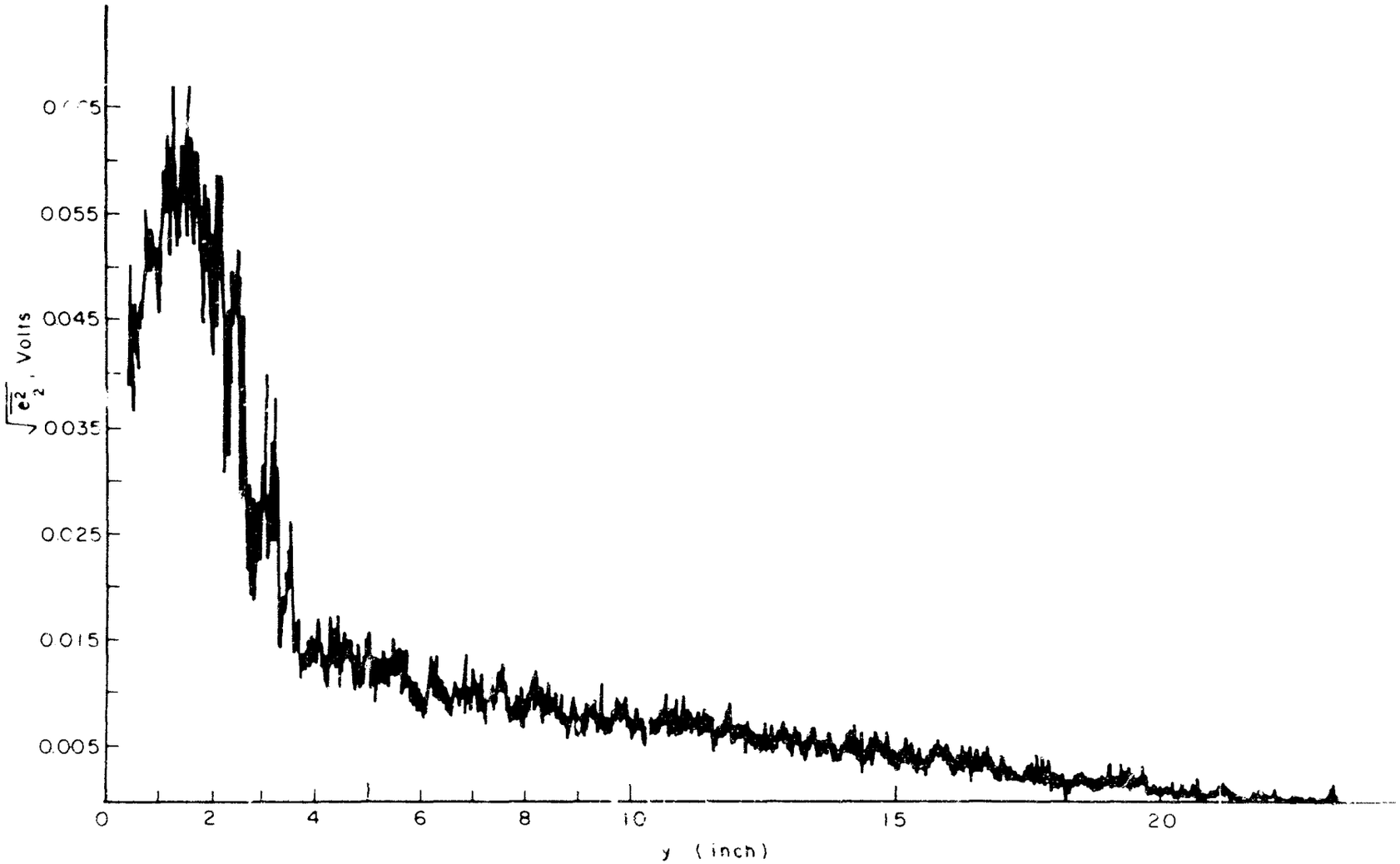

Fig. 12. A typical continuous RMS profile for wire 2 of the crossed hot wire.

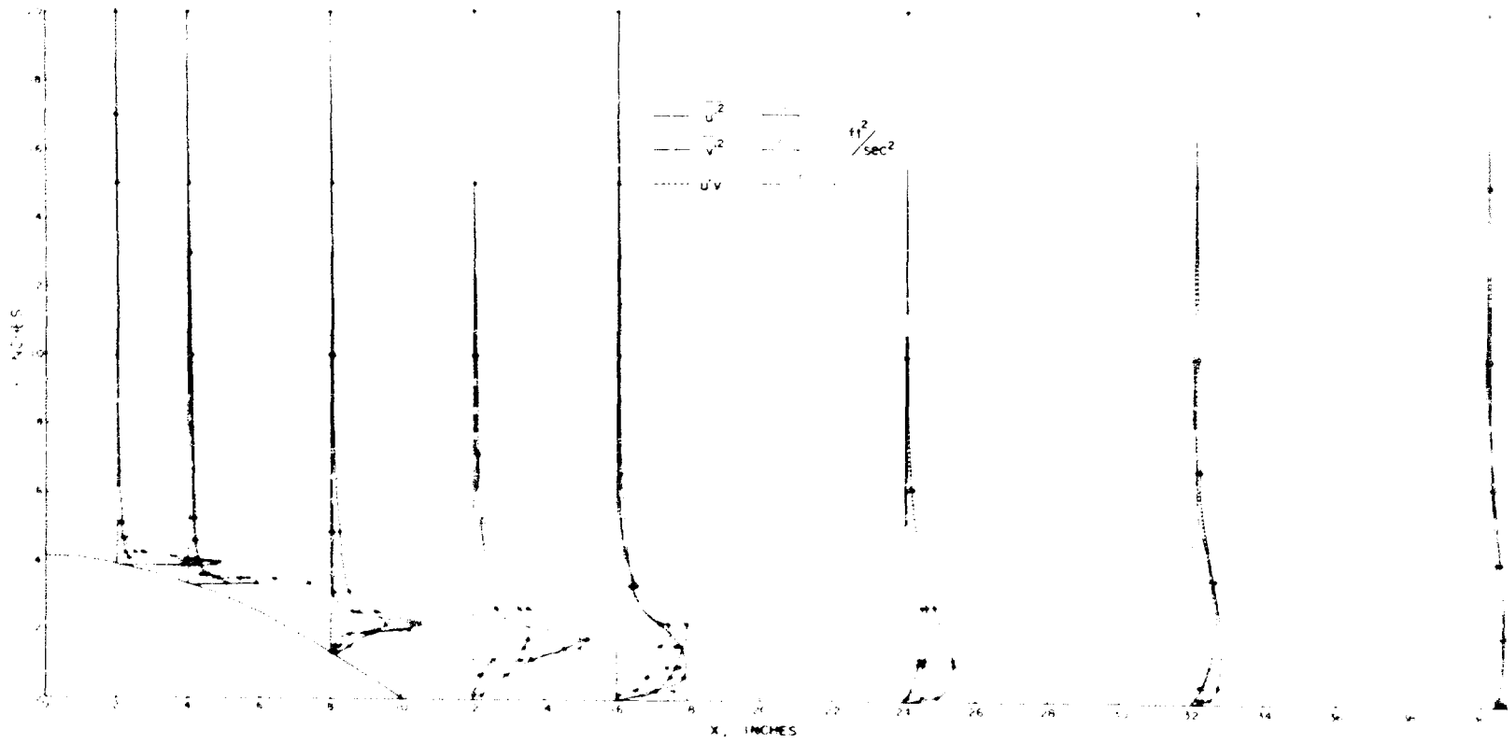

Fig. 13. $\overline{u'^2}$ $\overline{v'^2}$ and $\overline{u'v'}$ profiles at selected sections.

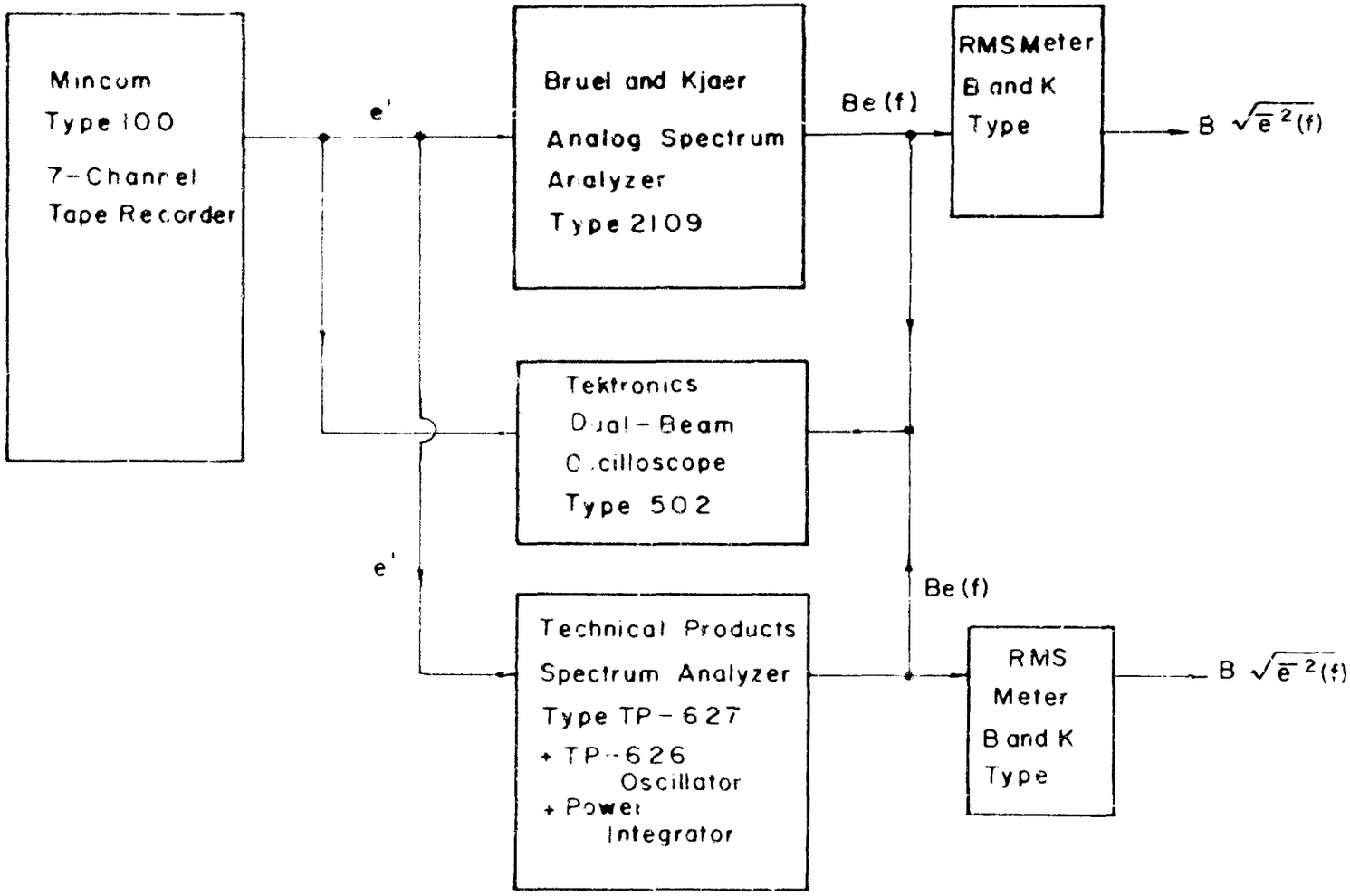

Fig. 14. Block diagram for setup of measurement of turbulent spectra.

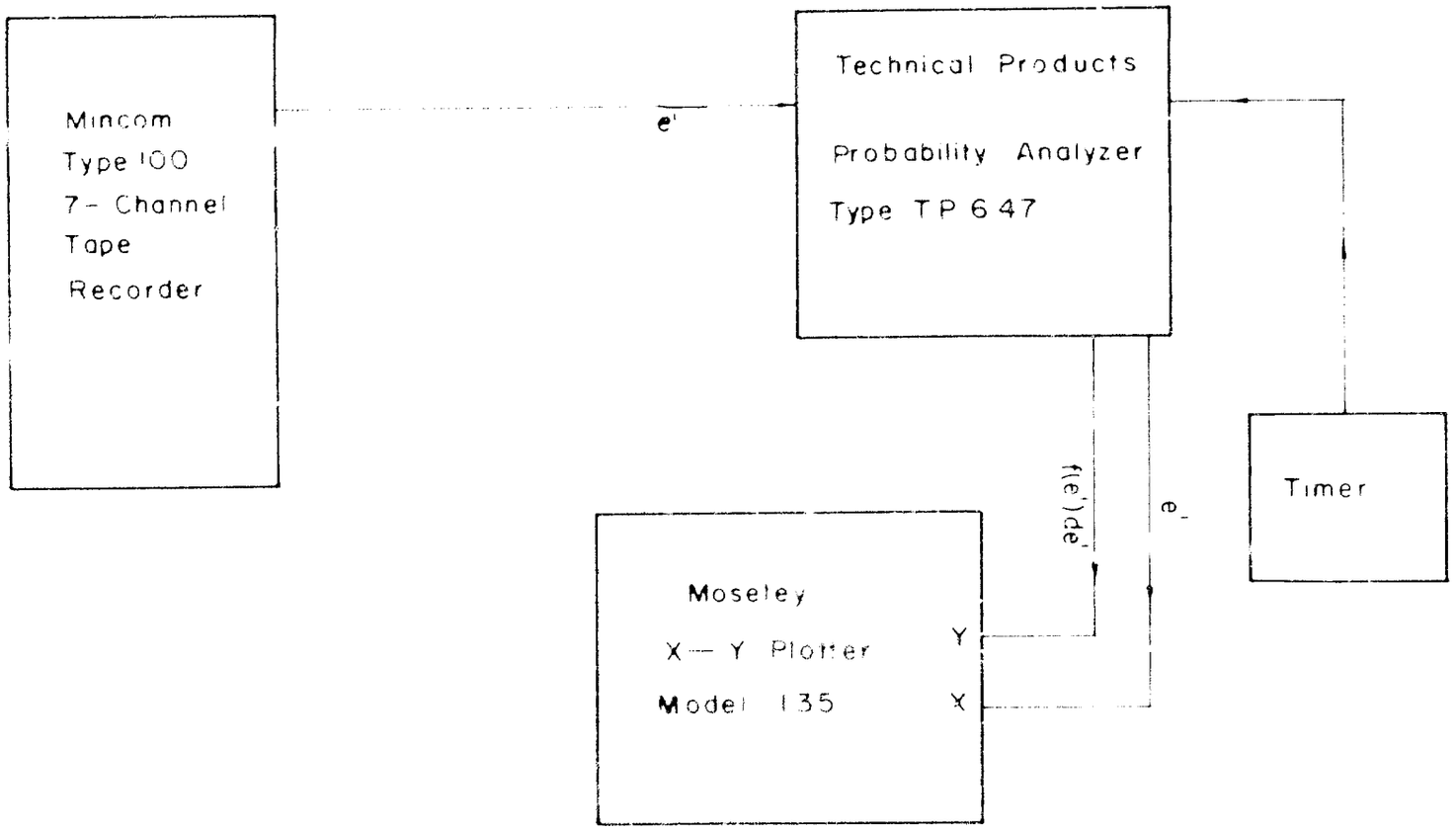

Fig. 13. Setup for measuring the probability density of a single turbulent component.

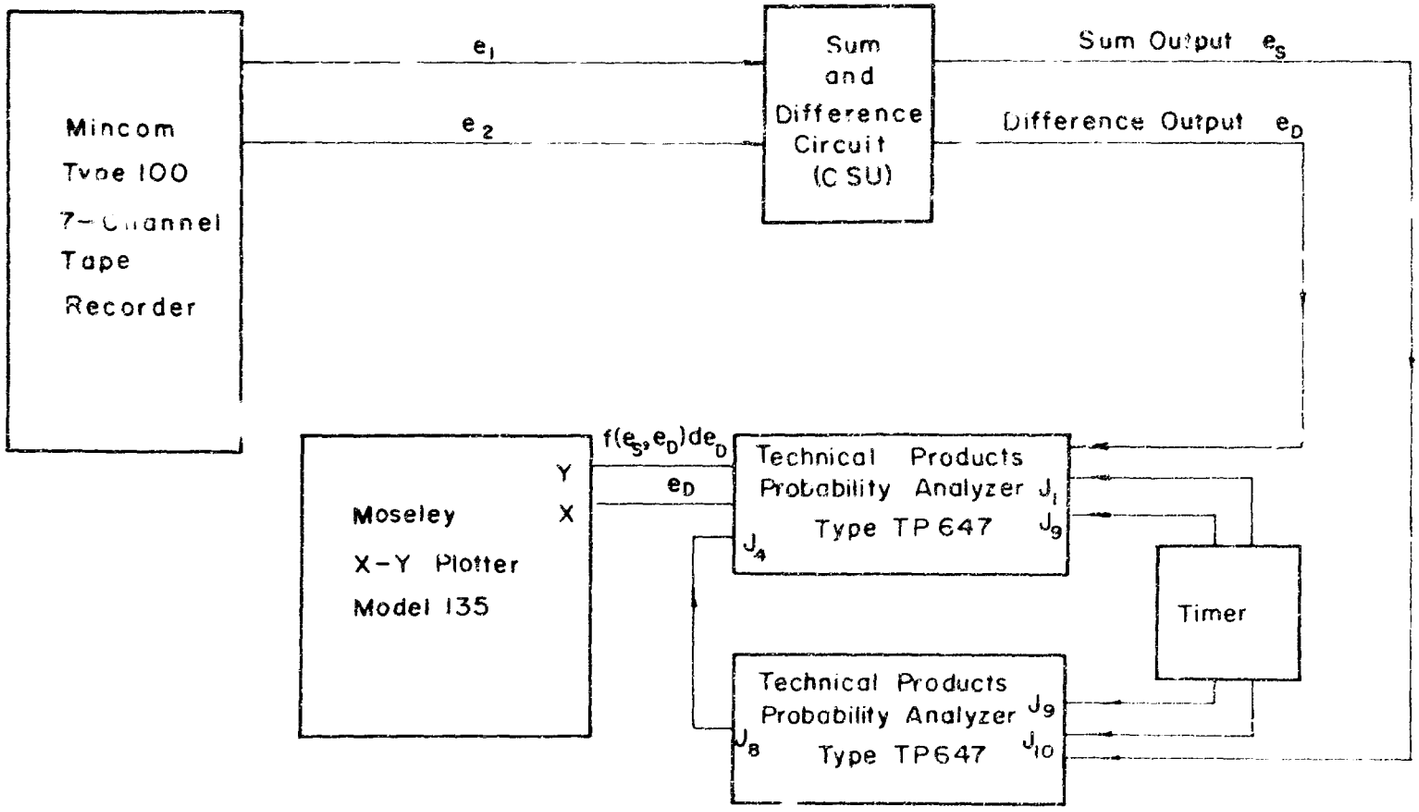

Fig. 16. Setup for measuring the joint probability density of two turbulent components.

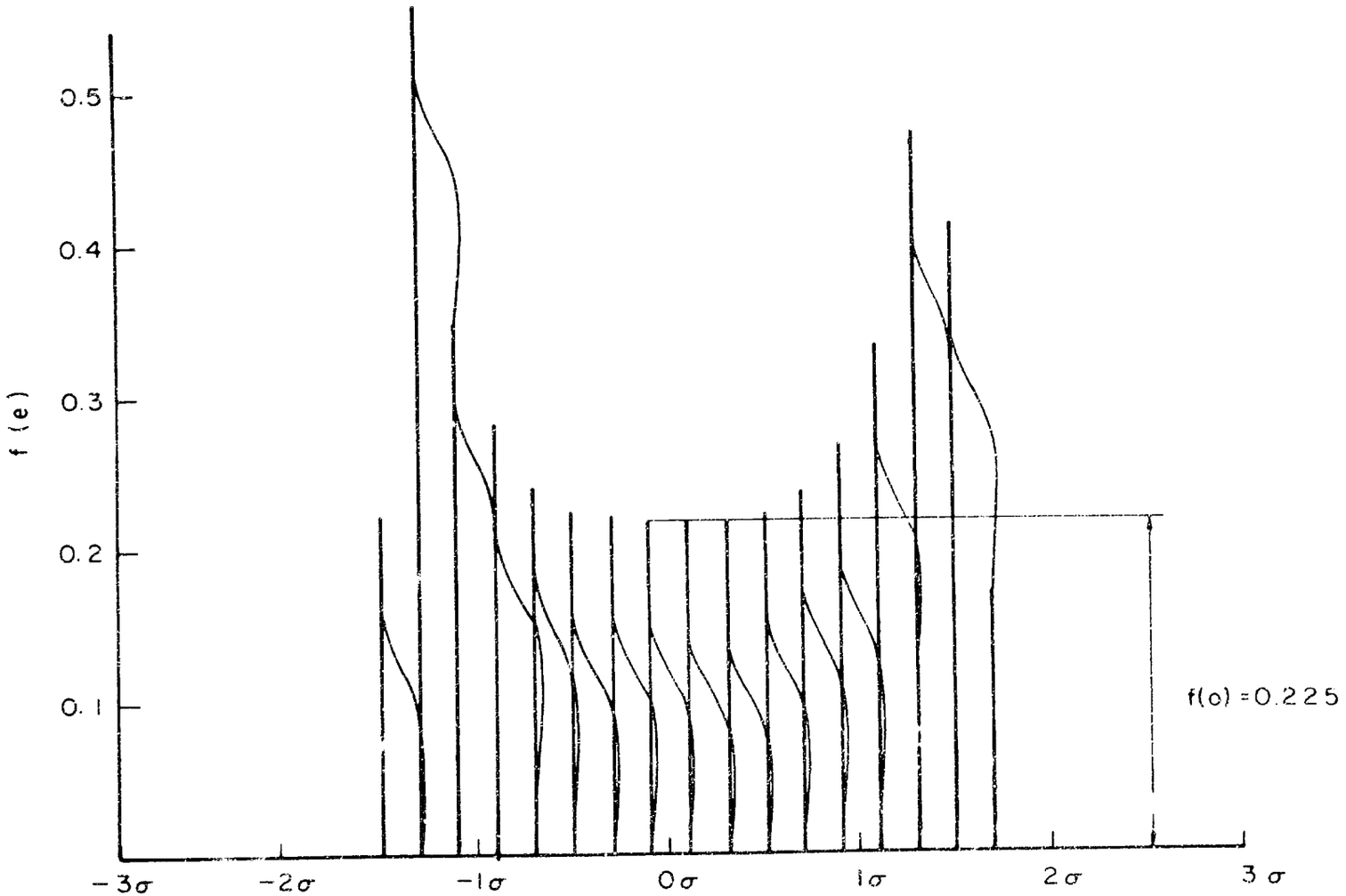

Fig. 17. Probability density of a calibrated sine wave.

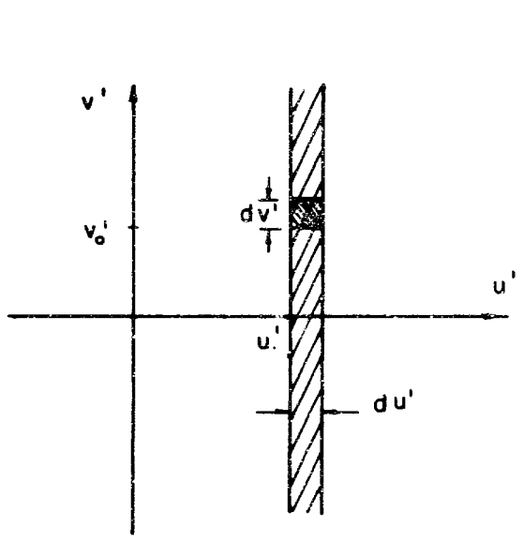

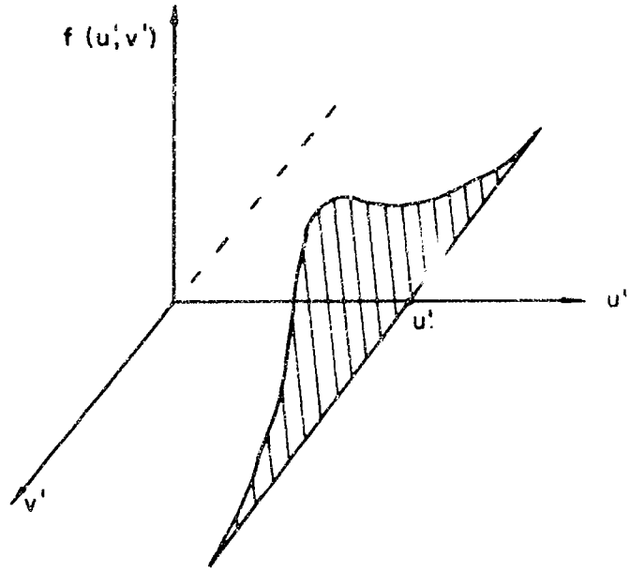

$$f(v'/u' = u_o').\,dv' = \frac{p[u_o' < u' \le u_o' + du',\ v_o' < v' \le v_o' + dv']}{p[u_o' < u' \le u_o' + du']}$$

Fig. 18. Sketch for evaluating the conditional probability density.

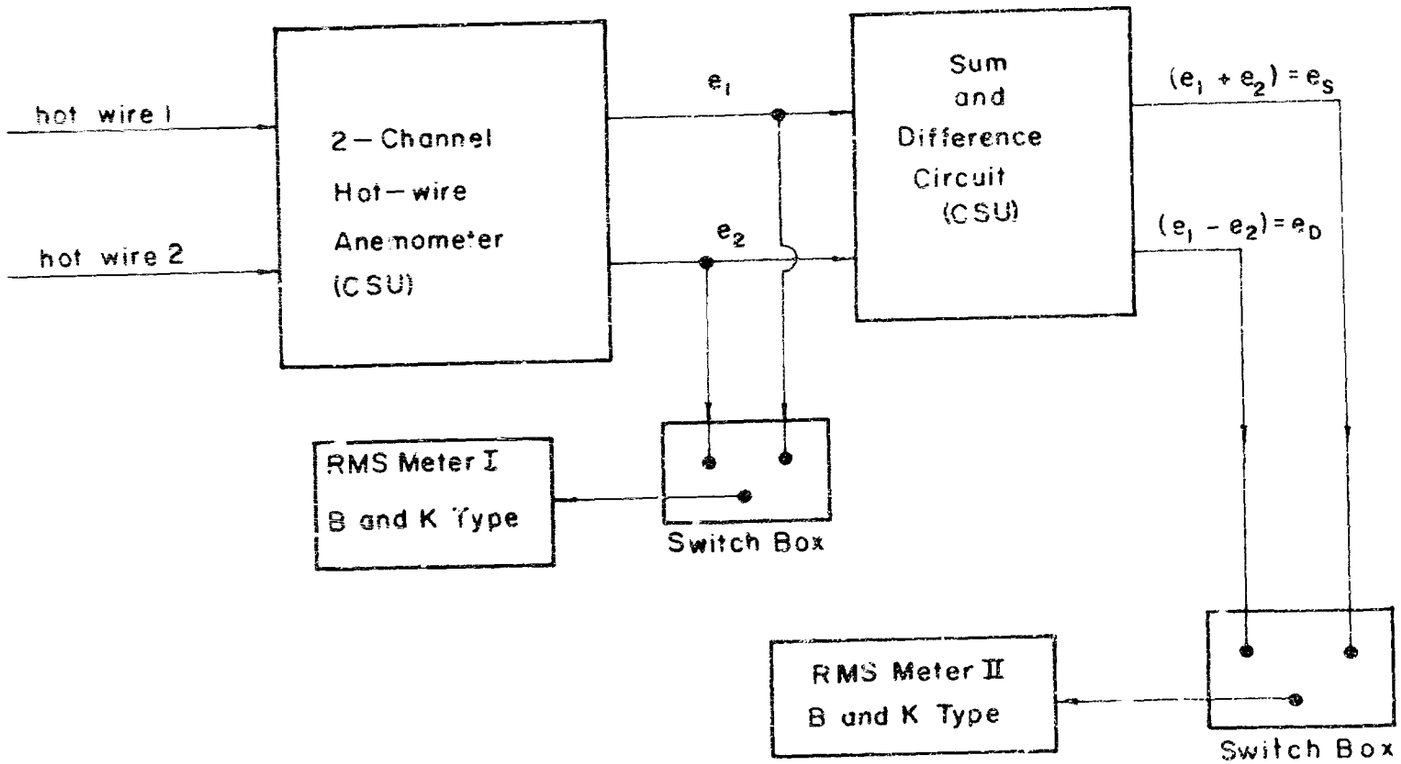

Fig. 19. Setup for measuring the space correlation coefficients along the trajectories.

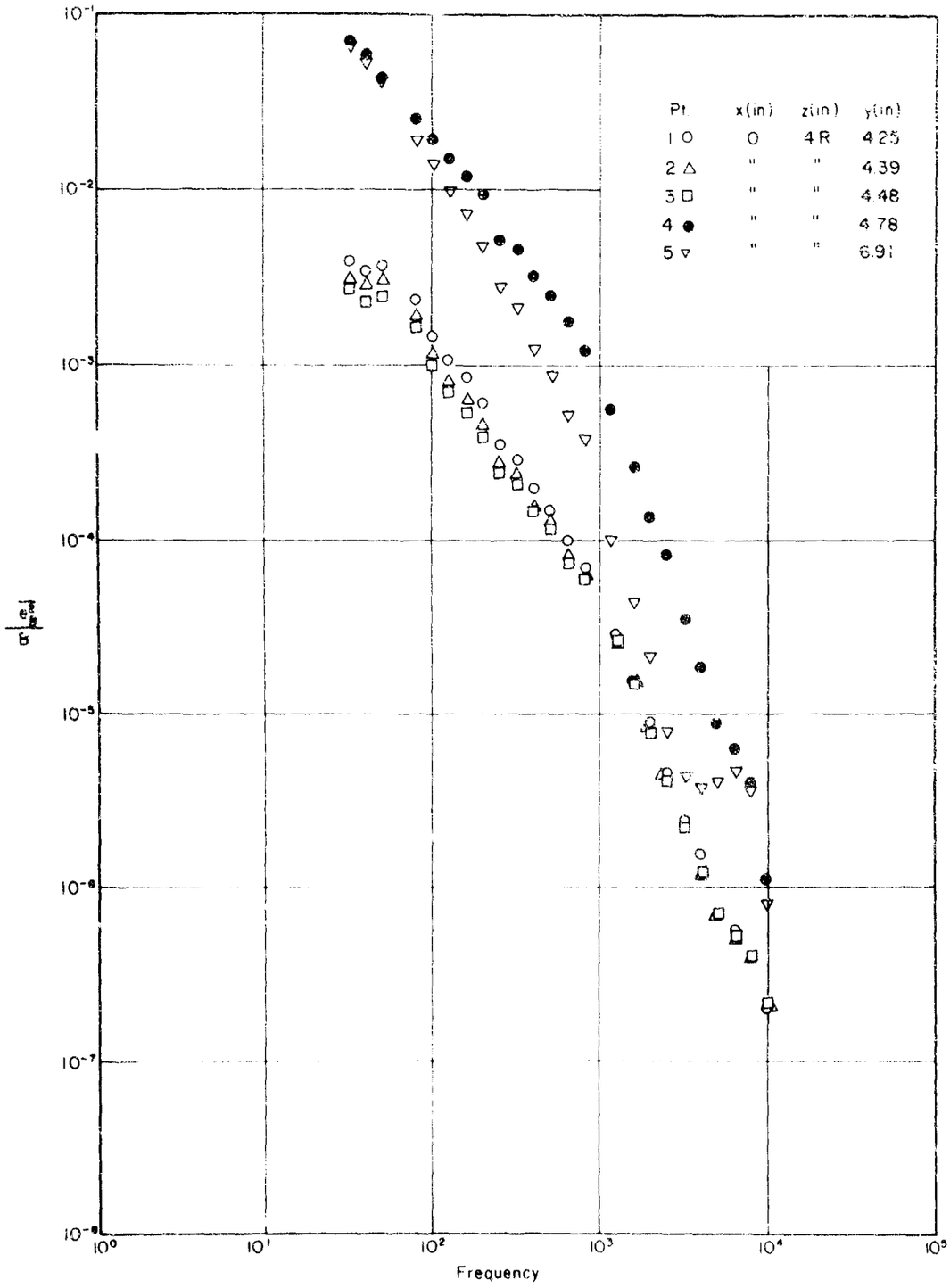

Fig. 20. Dimensional turbulent spectra of u'-component for test points at x = 0 inch.

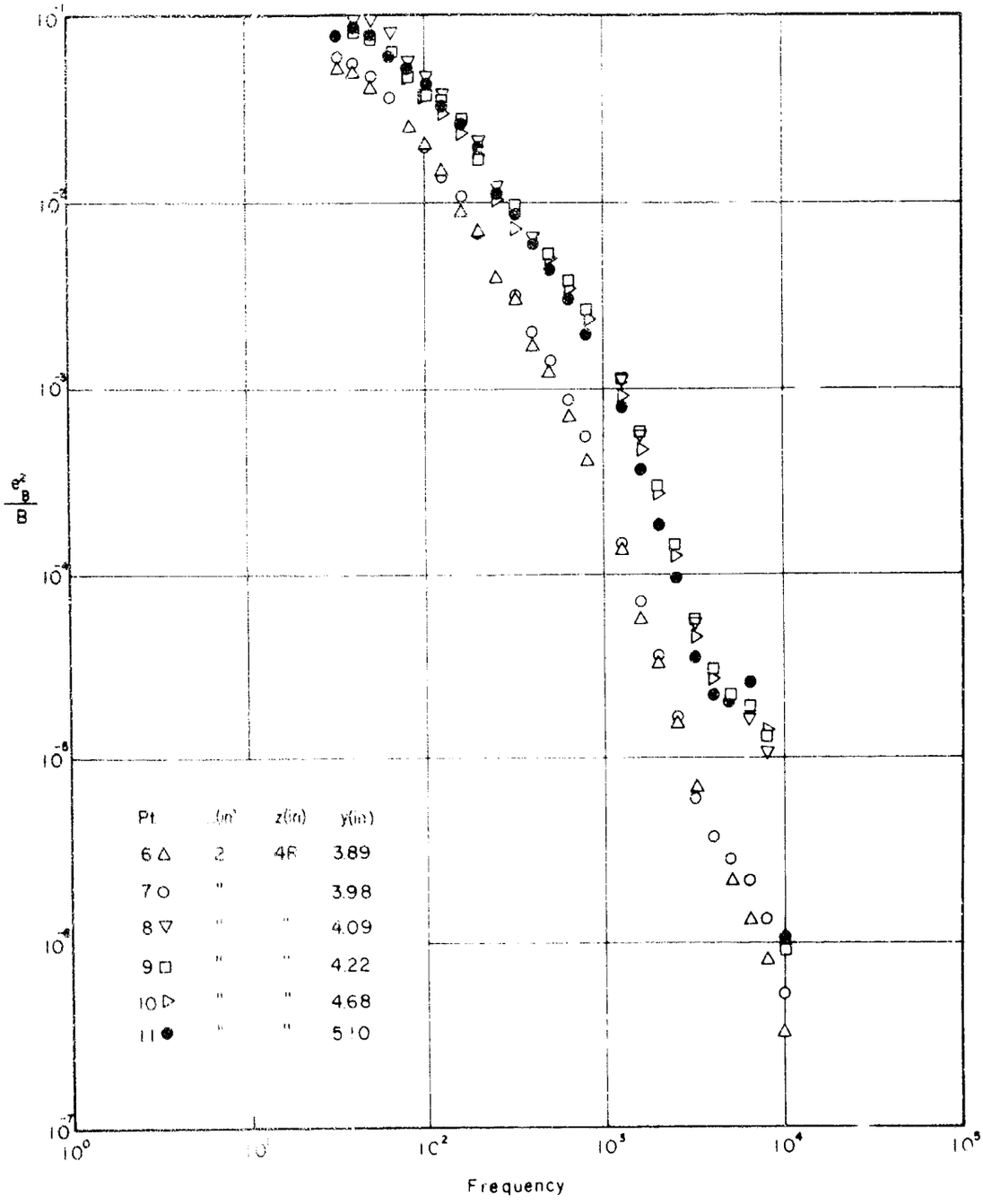

Fig. 21. Dimensional turbulent spectra of u'- omponent for test points at x = 2 inches.

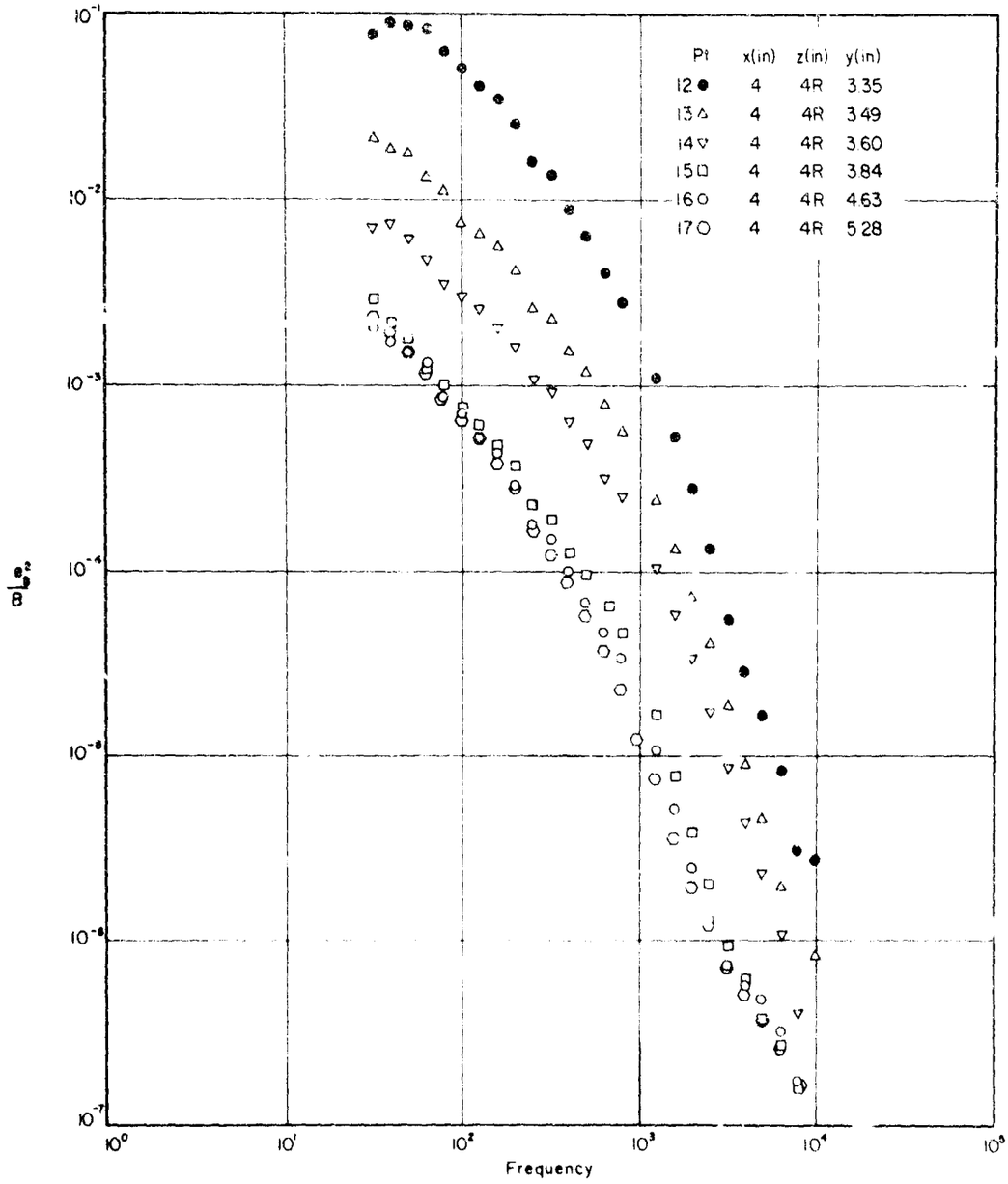

Fig. 22. Dimensional turbulent spectra of u'-component for test points at x = 4 inches.

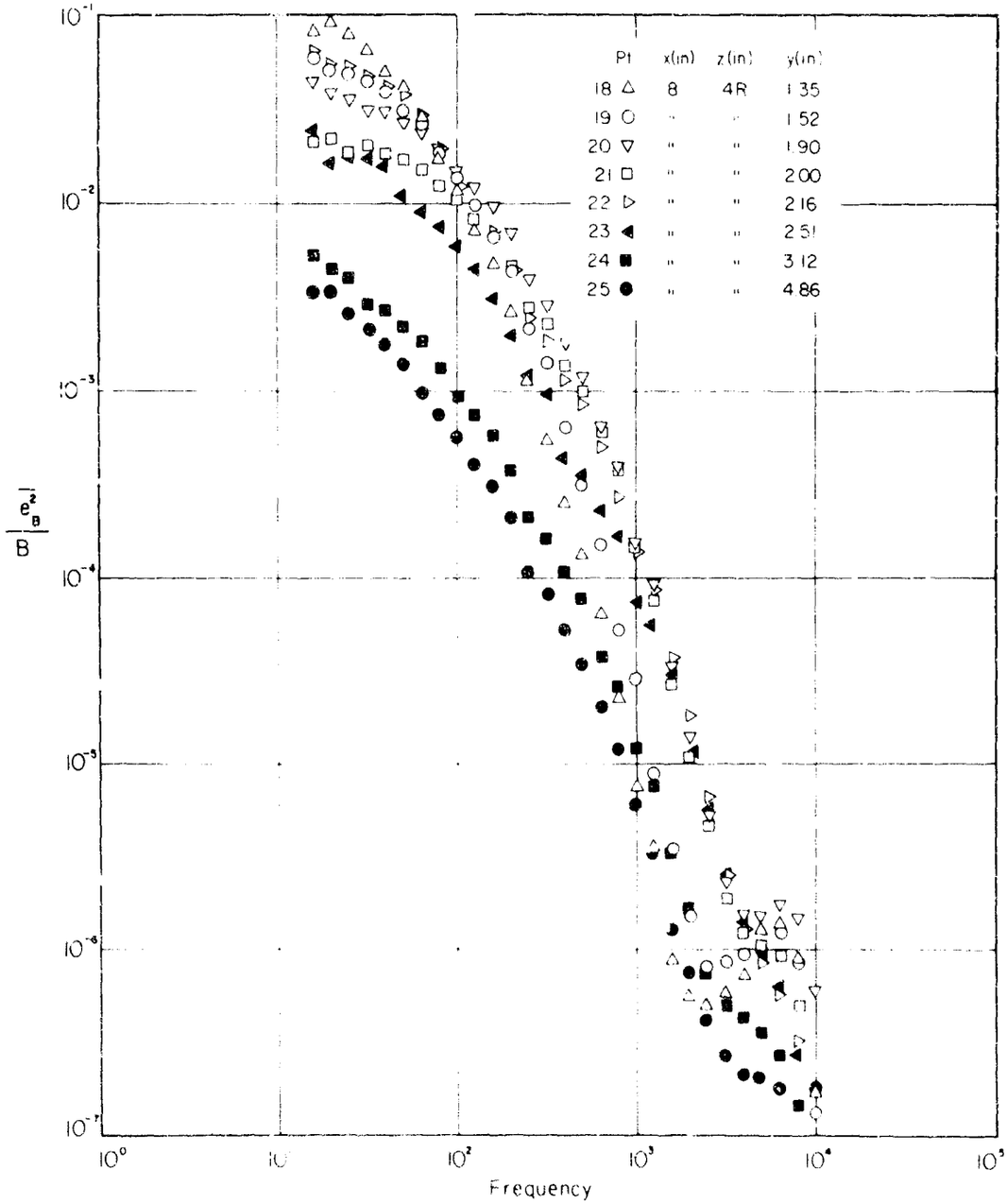

Fig. 23. Dimensional turbulent spectra of u'-component for test points at x = 8 inch.

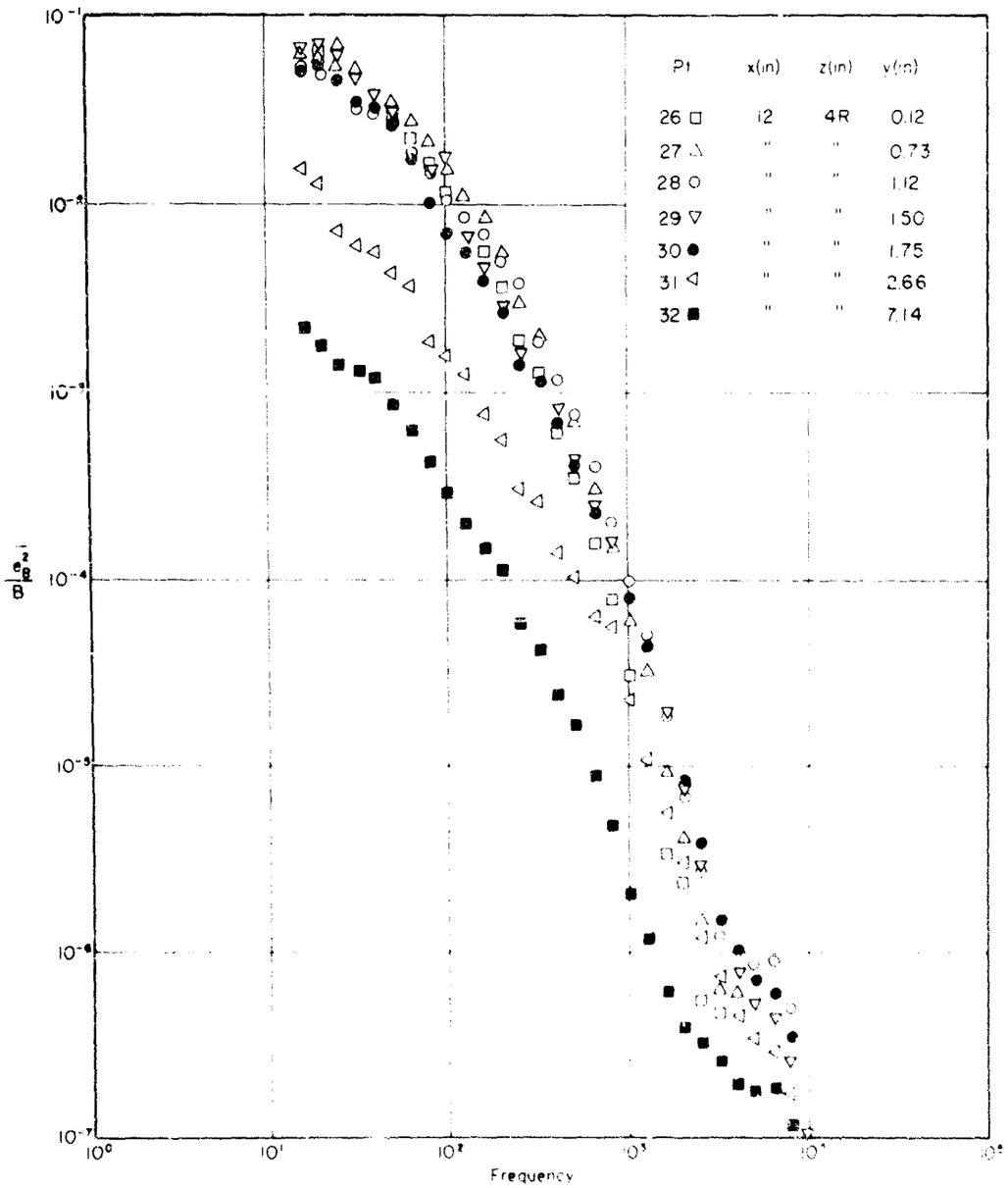

Fig. 24. Dimensional turbulent spectra of '-component for test points at x = 12 inch.

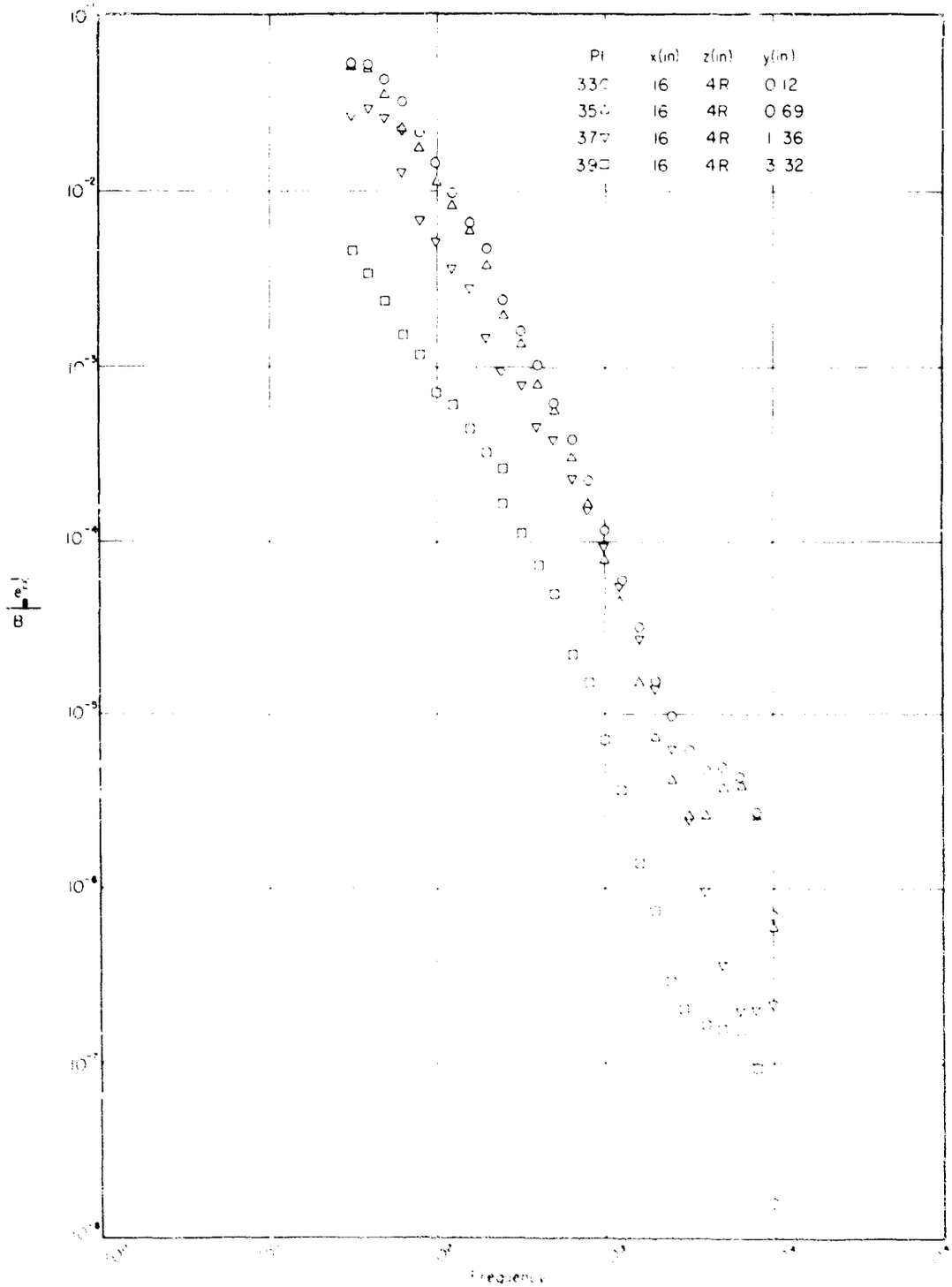

Fig. 25. Dimensional turbulent spectra of u'-component for test points at x = 16 inch.

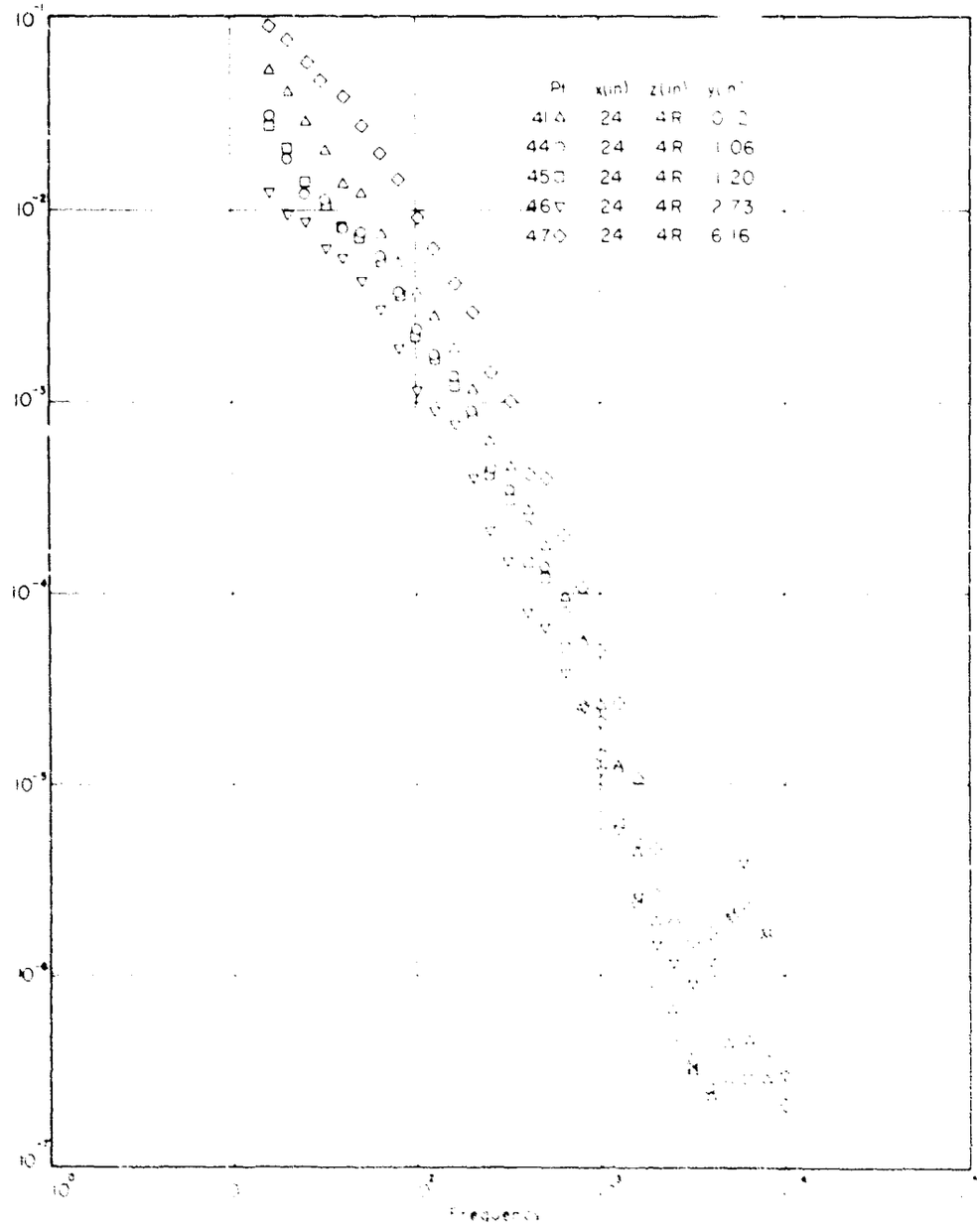

Fig. 26. Dimensional turbulent spectra of u'-component for test points at x = 24 inch.

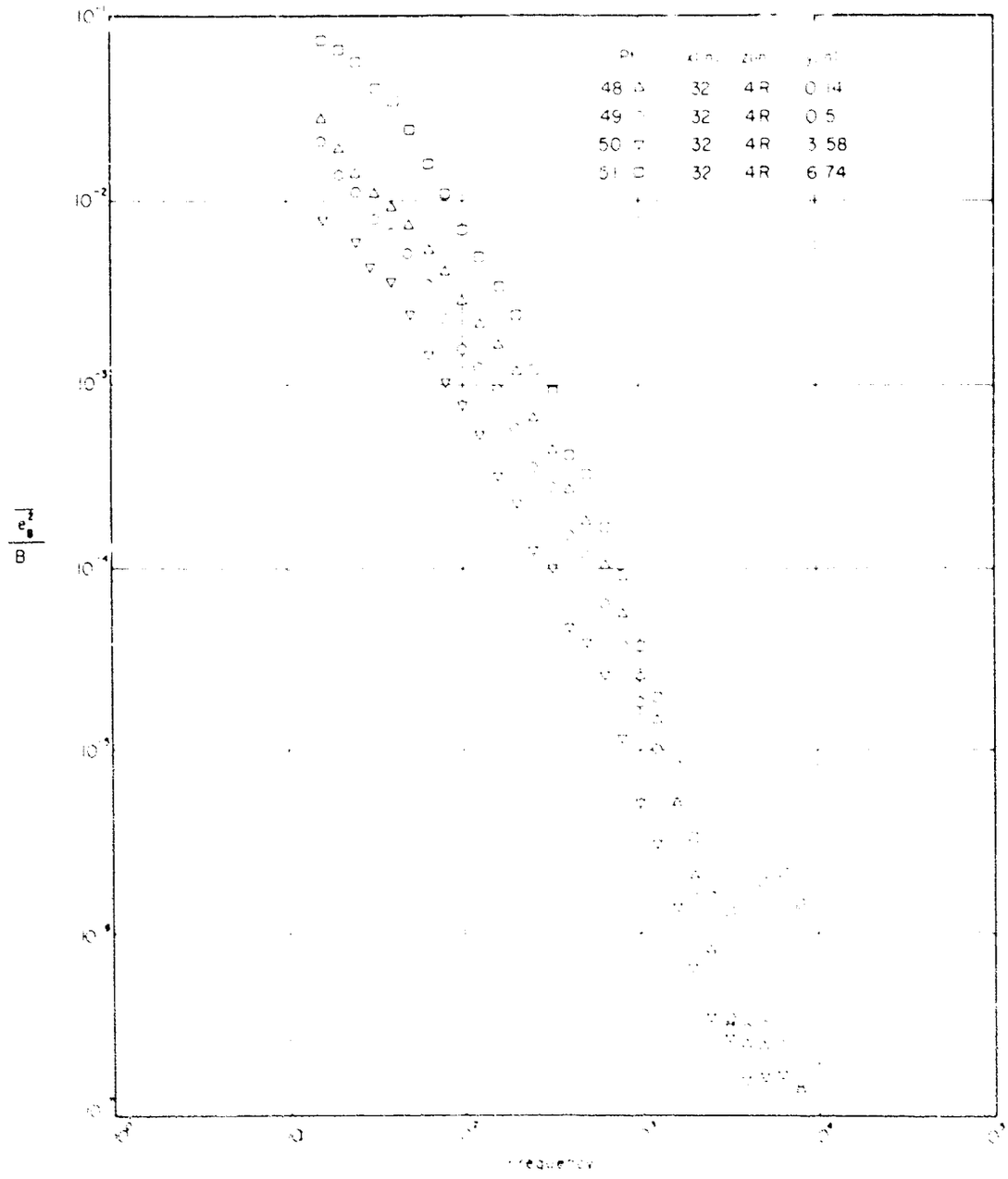

Fig. 27. Dimensional turbulent spectra of u'-component for test points at x = 32 inch.

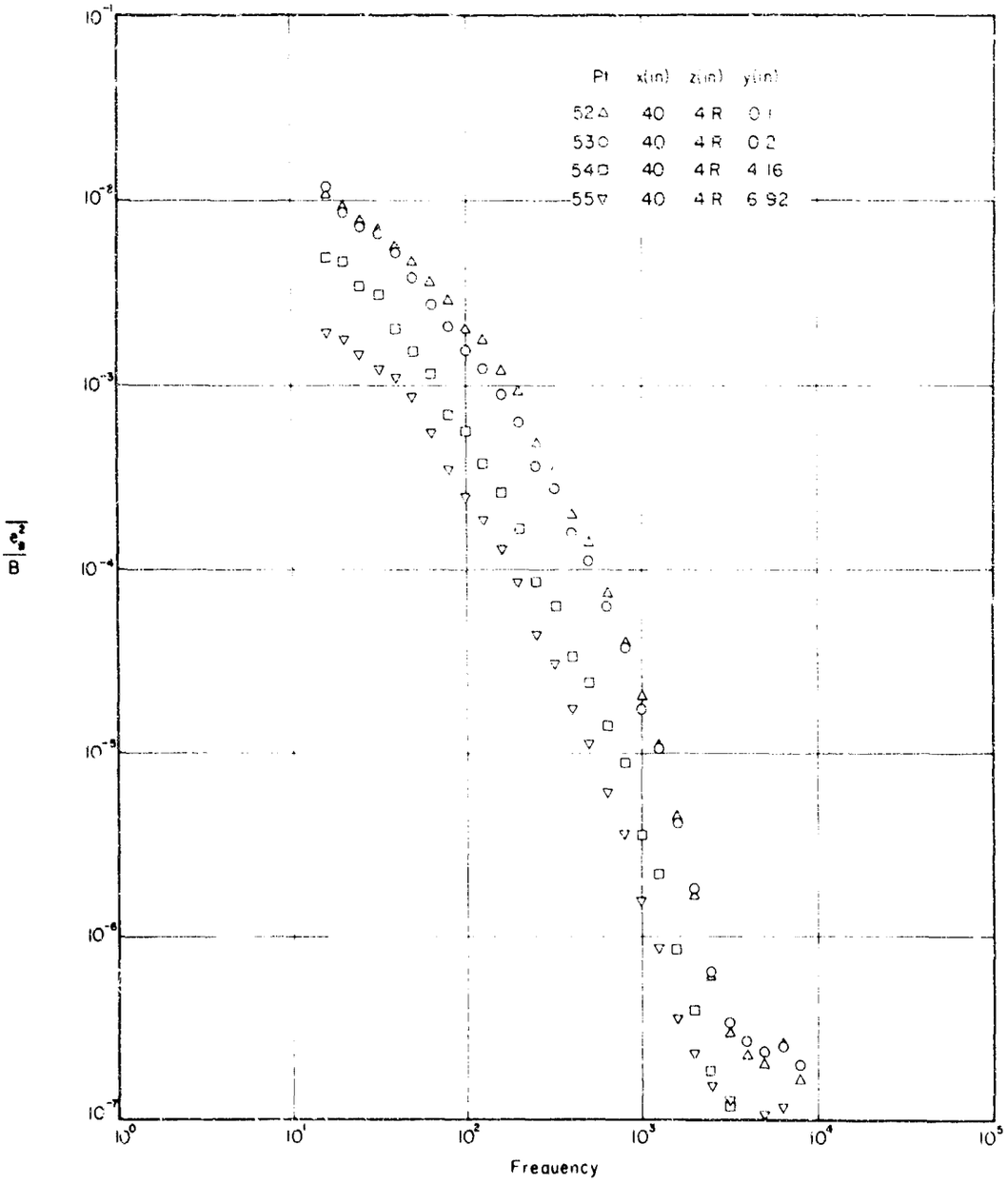

Fig. 28. Dimensional turbulent spectra of u'-component for test points at x = 60 inch.

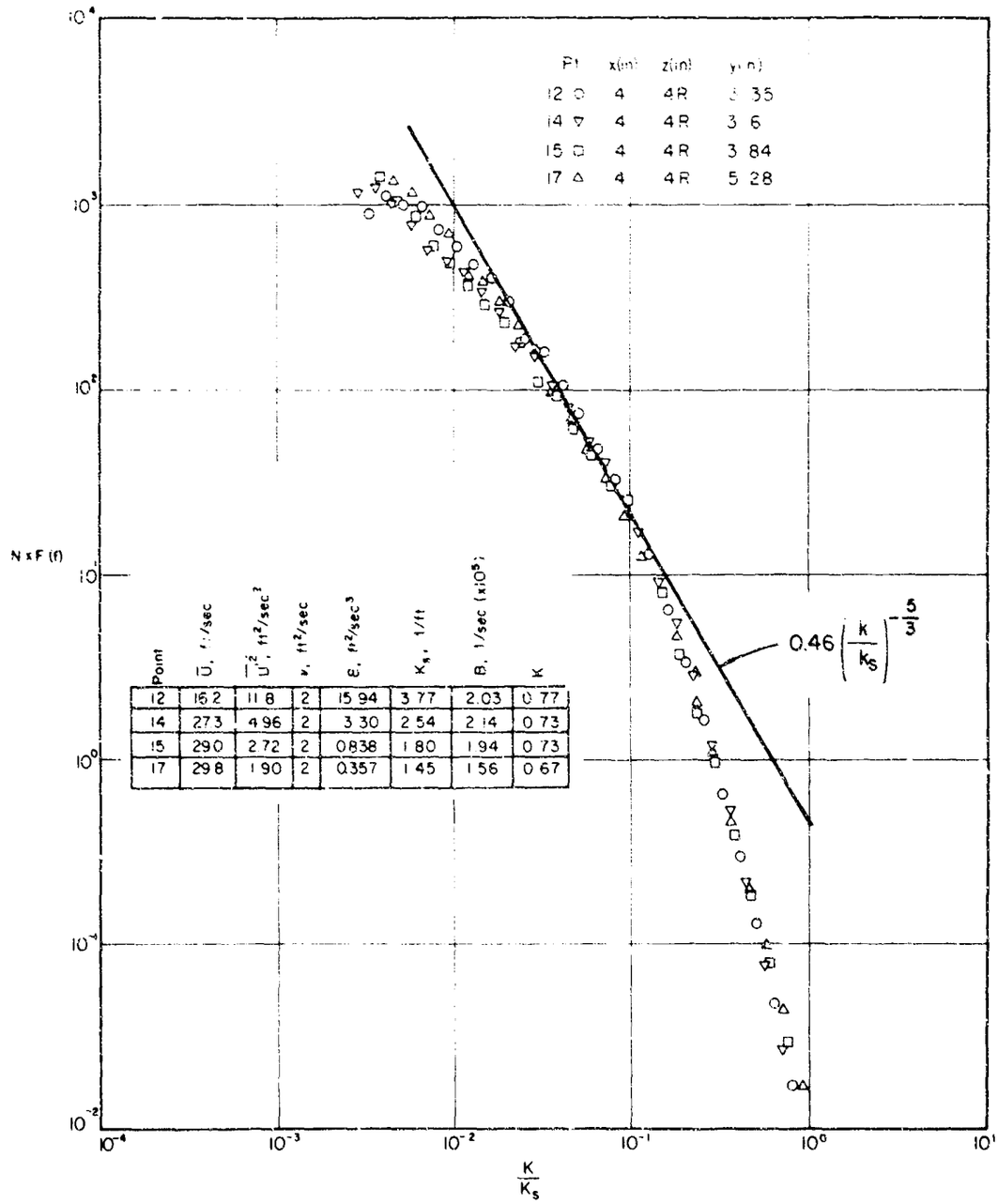

Fig. 29. Non-dimensional turbulent spectra of u'-component for test points at x = 4 inches.

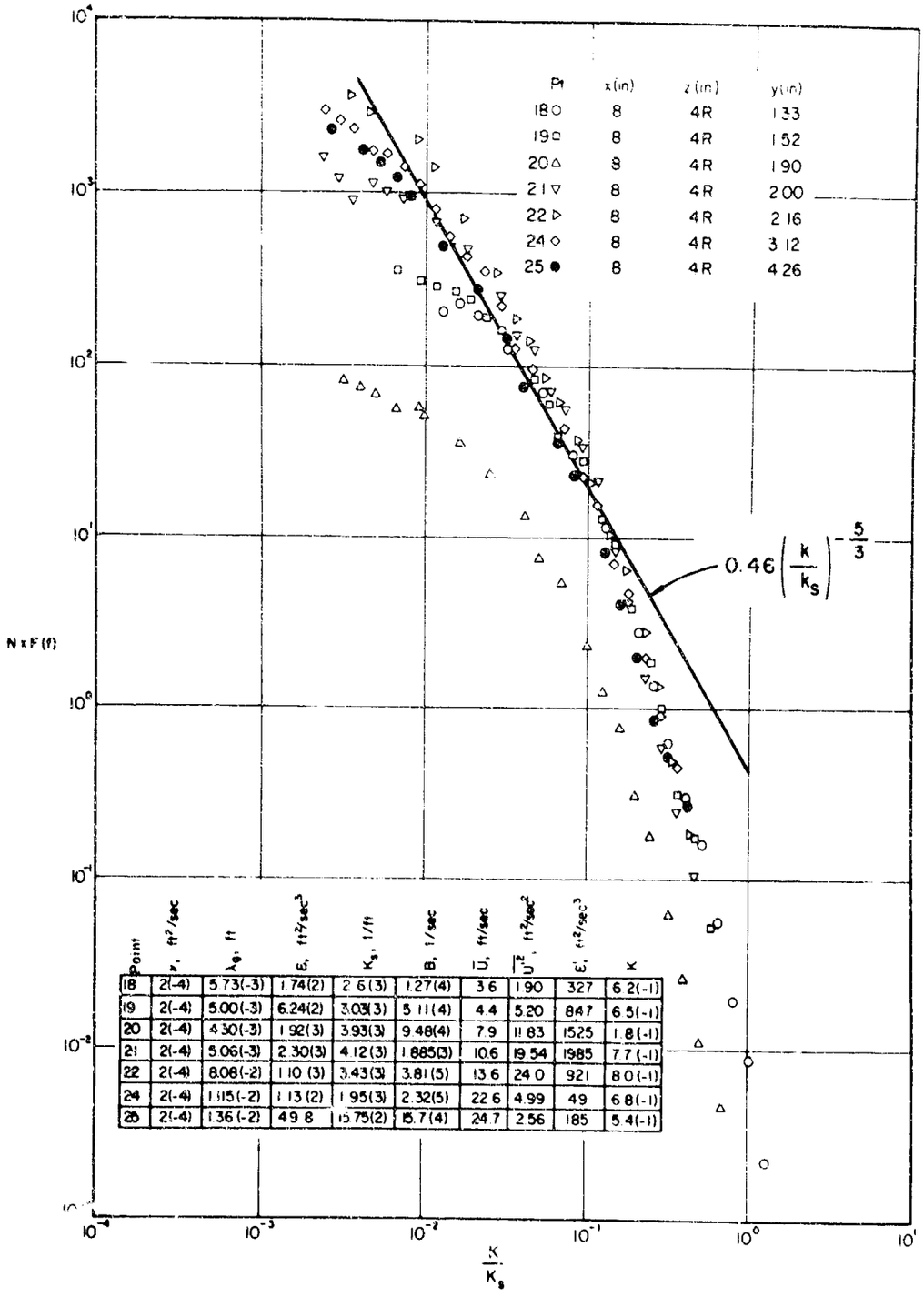

Fig. 30. Non-dimensional turbulent spectra of u'-component for test points at x = 8 inches.

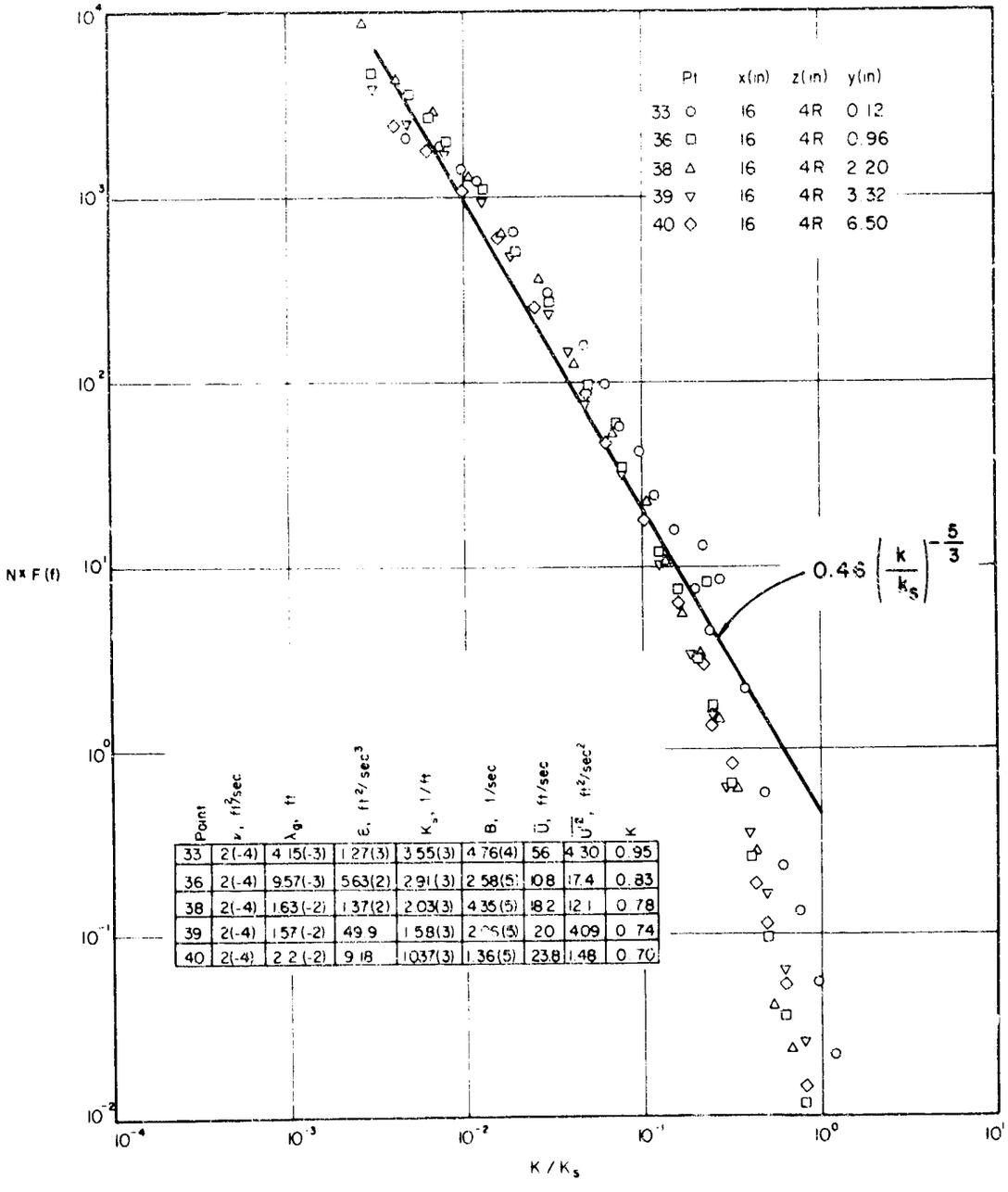

Point	ν, ft²/sec	λ_g, ft	ε, ft²/sec³	K_s, 1/ft	B, 1/sec	Ū, ft/sec	$\overline{U'^2}$, ft²/sec²	K
33	2(-4)	4.15(-3)	1.27(3)	3.55(3)	4.76(4)	56	4.30	0.95
36	2(-4)	9.57(-3)	563(2)	2.91(3)	2.58(5)	10.8	17.4	0.83
38	2(-4)	1.63(-2)	1.37(2)	2.03(3)	4.35(5)	18.2	12.1	0.78
39	2(-4)	1.57(-2)	49.9	1.58(3)	2.06(5)	20	4.09	0.74
40	2(-4)	2.2(-2)	9.18	1.037(3)	1.36(5)	23.8	1.48	0.70

Fig. 31. Non-dimensional turbulent spectra of u'-component for test points at x = 16 inches.

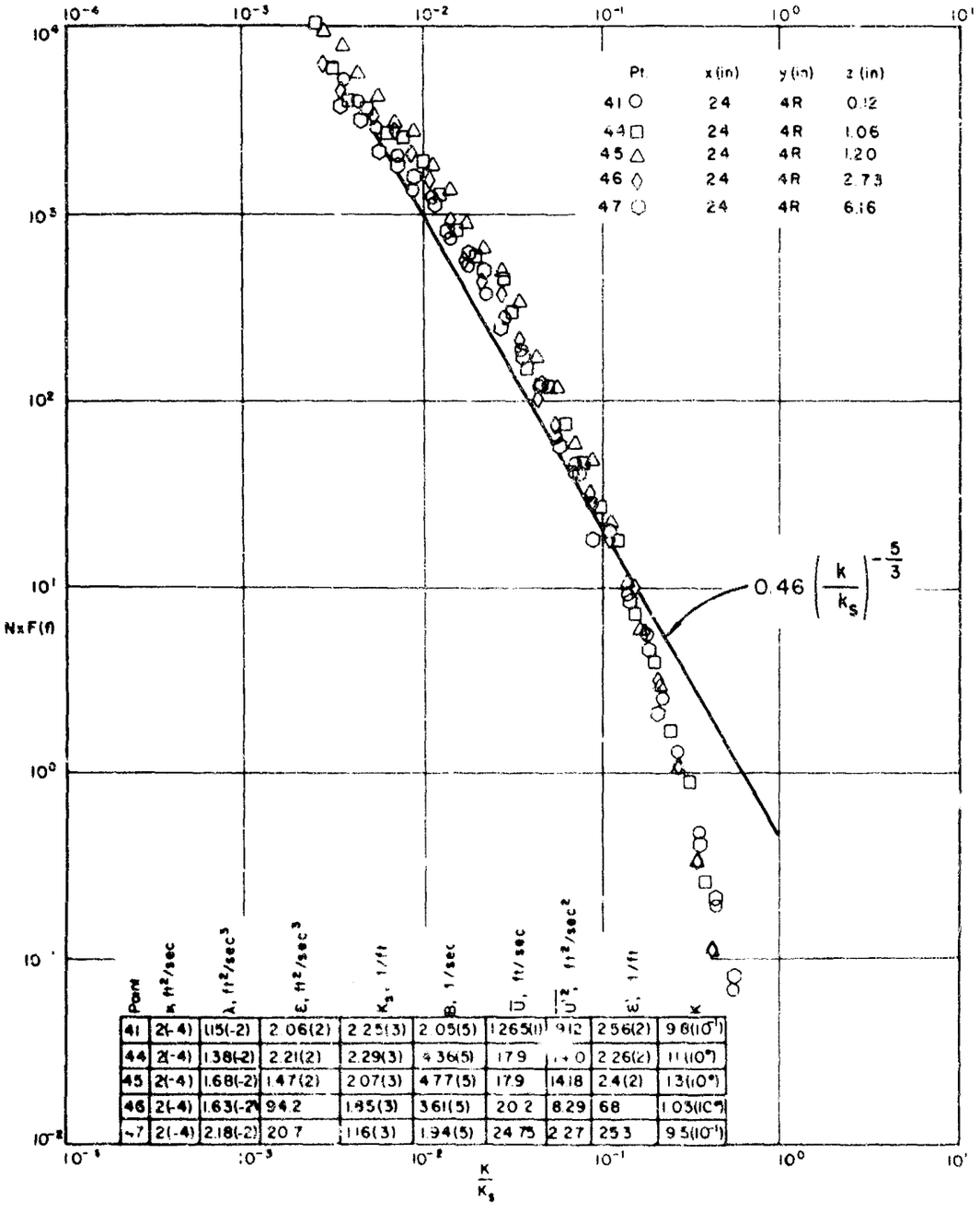

Pont	ν, ft²/sec	λ, ft²/sec³	ε, ft²/sec³	K_s, 1/ft	β, 1/sec	$\bar{U}$, ft/sec	$\overline{u'^2}$, ft²/sec²	ω', 1/ft	κ
41	2(-4)	1.15(-2)	2.06(2)	2.25(3)	2.05(5)	1265(1)	912	2.56(2)	9.8(10⁻¹)
44	2(-4)	1.38(-2)	2.21(2)	2.29(3)	4.36(5)	17.9	14.0	2.26(2)	1.1(10⁰)
45	2(-4)	1.68(-2)	1.47(2)	2.07(3)	4.77(5)	17.9	14.18	2.4(2)	1.3(10⁰)
46	2(-4)	1.63(-2)	94.2	1.85(3)	3.61(5)	20.2	8.29	68	1.05(10⁰)
~7	2(-4)	2.18(-2)	20.7	1.16(3)	1.94(5)	24.75	2.27	25.3	9.5(10⁻¹)

Fig. 32. Non-dimensional turbulent spectra of u'-component for test points at x = 24 inches.

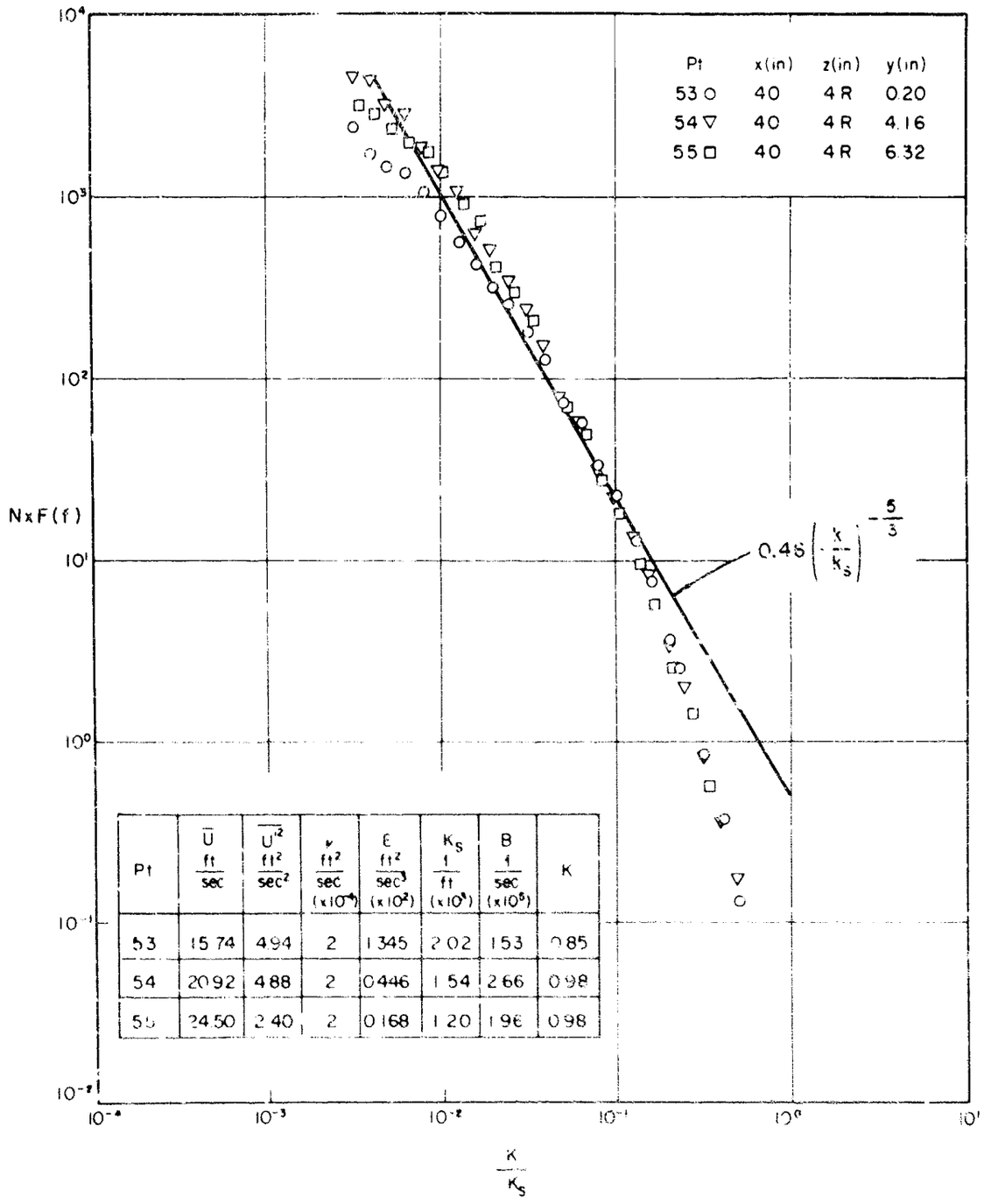

Pt	$\bar{U}$ ft/sec	$\overline{u'^2}$ ft²/sec²	ν ft²/sec (x10⁻⁵)	ϵ ft²/sec³ (x10²)	K_s 1/ft (x10⁵)	B 1/sec (x10⁵)	K
53	15.74	4.94	2	1.345	2.02	1.53	0.85
54	20.92	4.88	2	0.446	1.54	2.66	0.98
55	24.50	2.40	2	0.168	1.20	1.96	0.98

Fig. 33. Non-dimensional turbulent spectra of u'-component for test points at x = 40 inches.

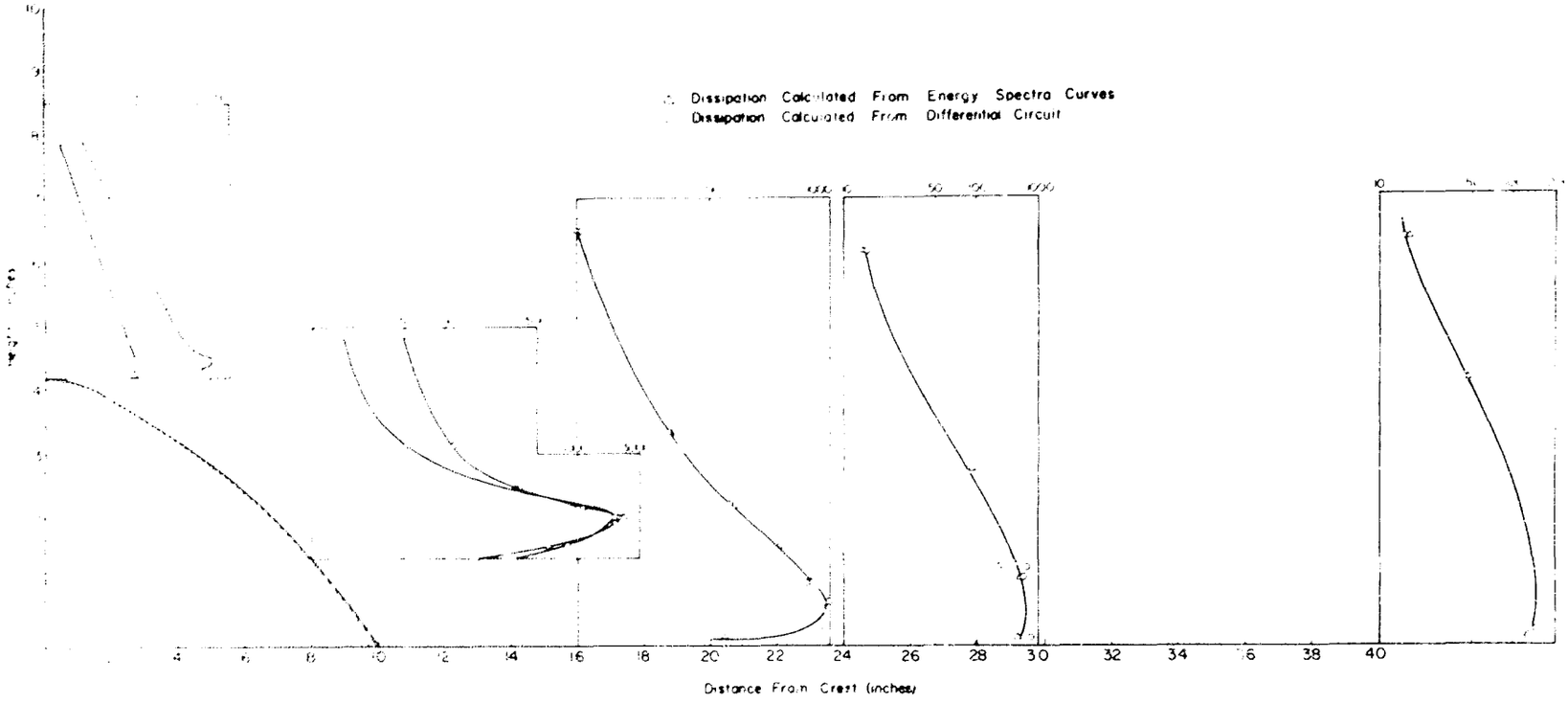

Fig. 34. Turbulent energy dissipation profiles at various sections.

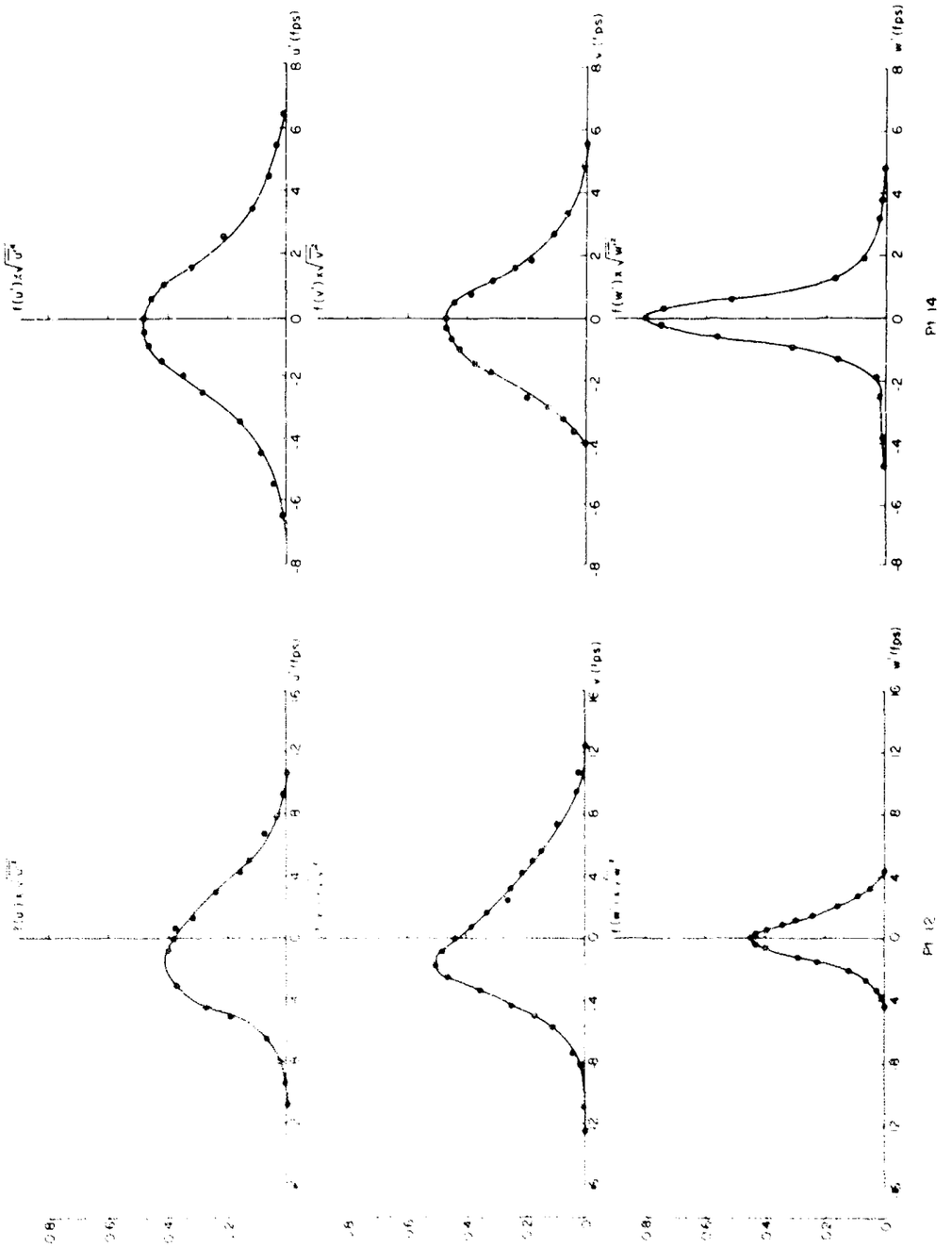

Fig. 35. Probability densities of the single turbulent components at test points No. 12 and 11.

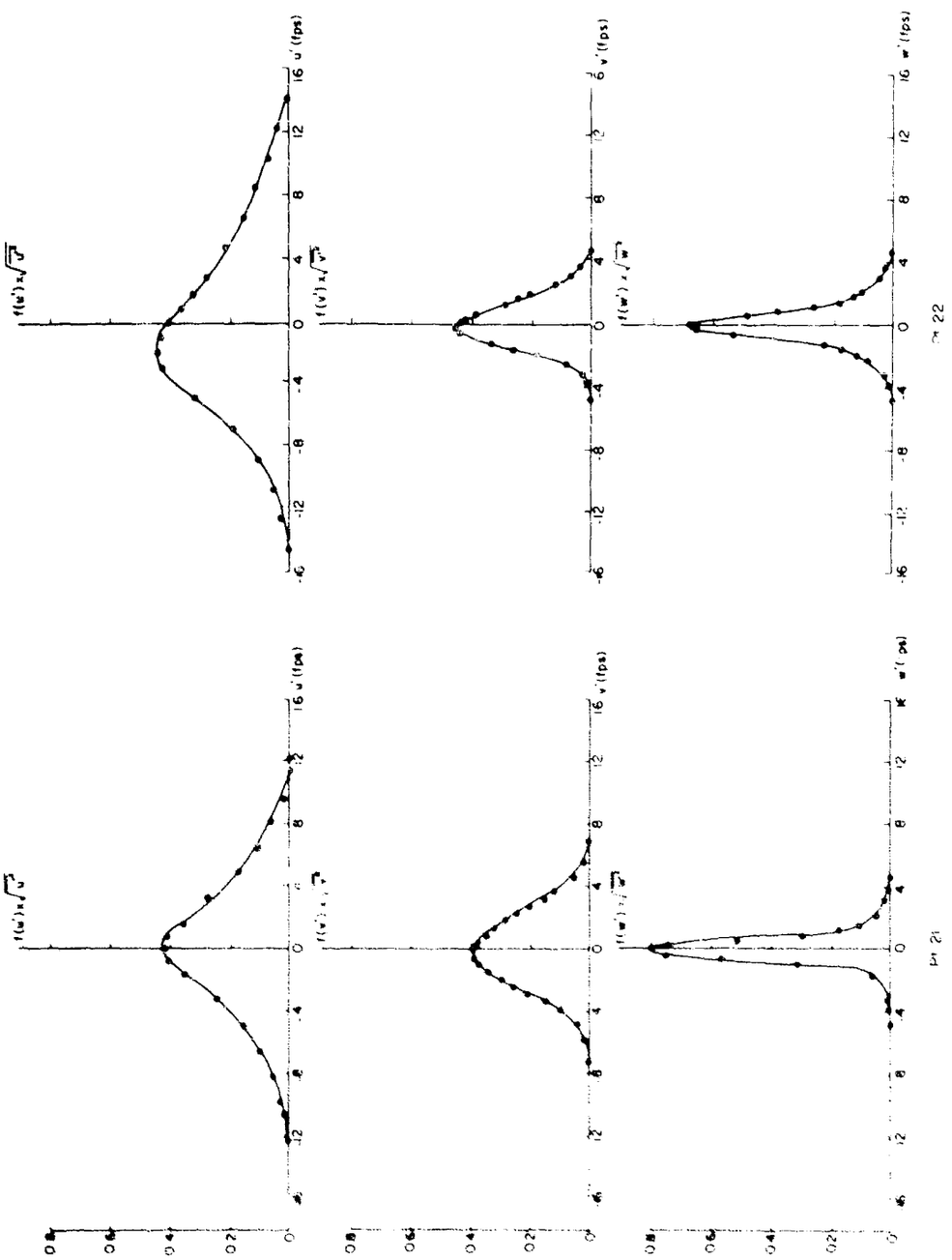

Fig. 36. Probability densities of the single turbulent components at test points No. 21 and 22.

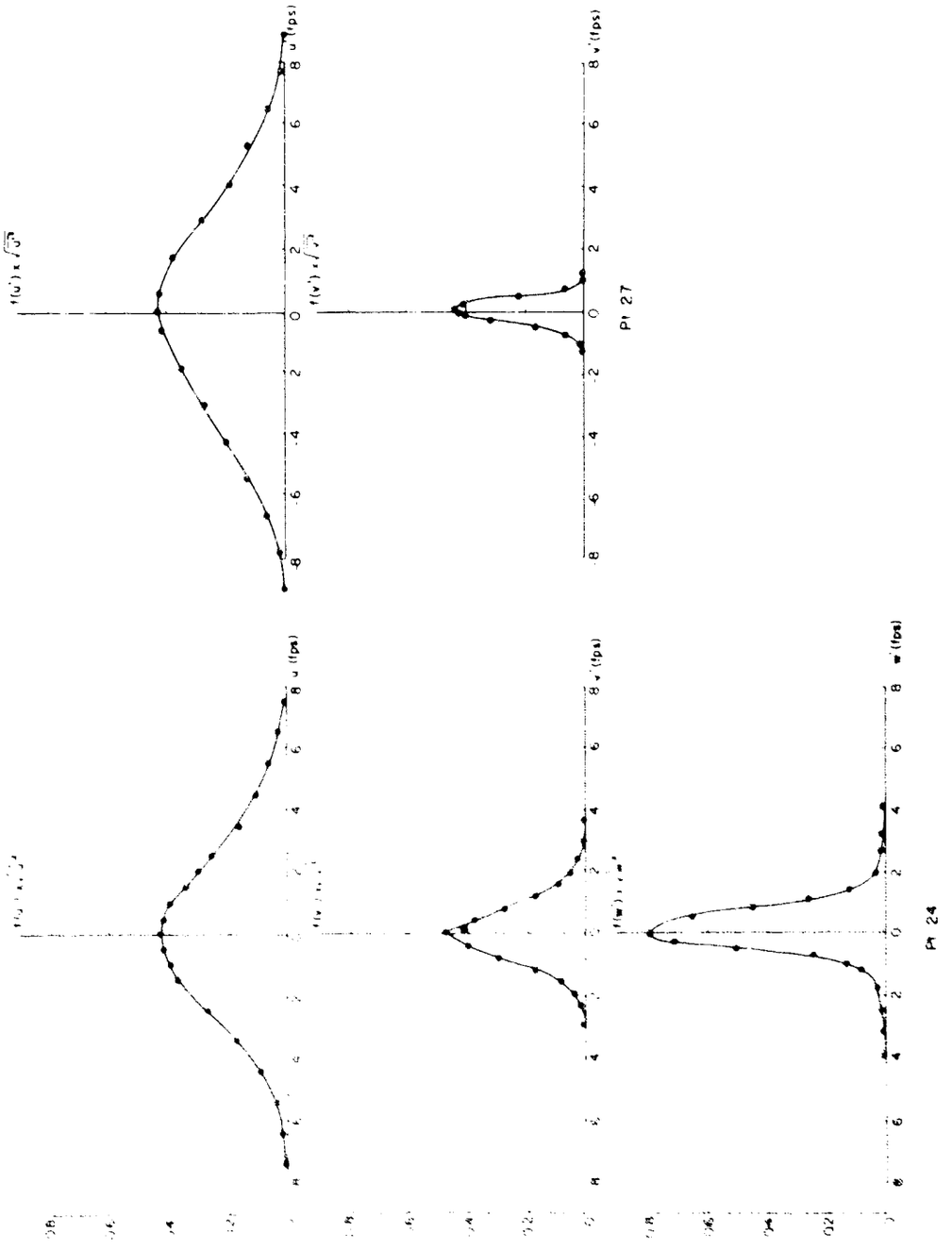

Fig. 37. Probability densities of the single turbulent components at test points No. 24 and 27.

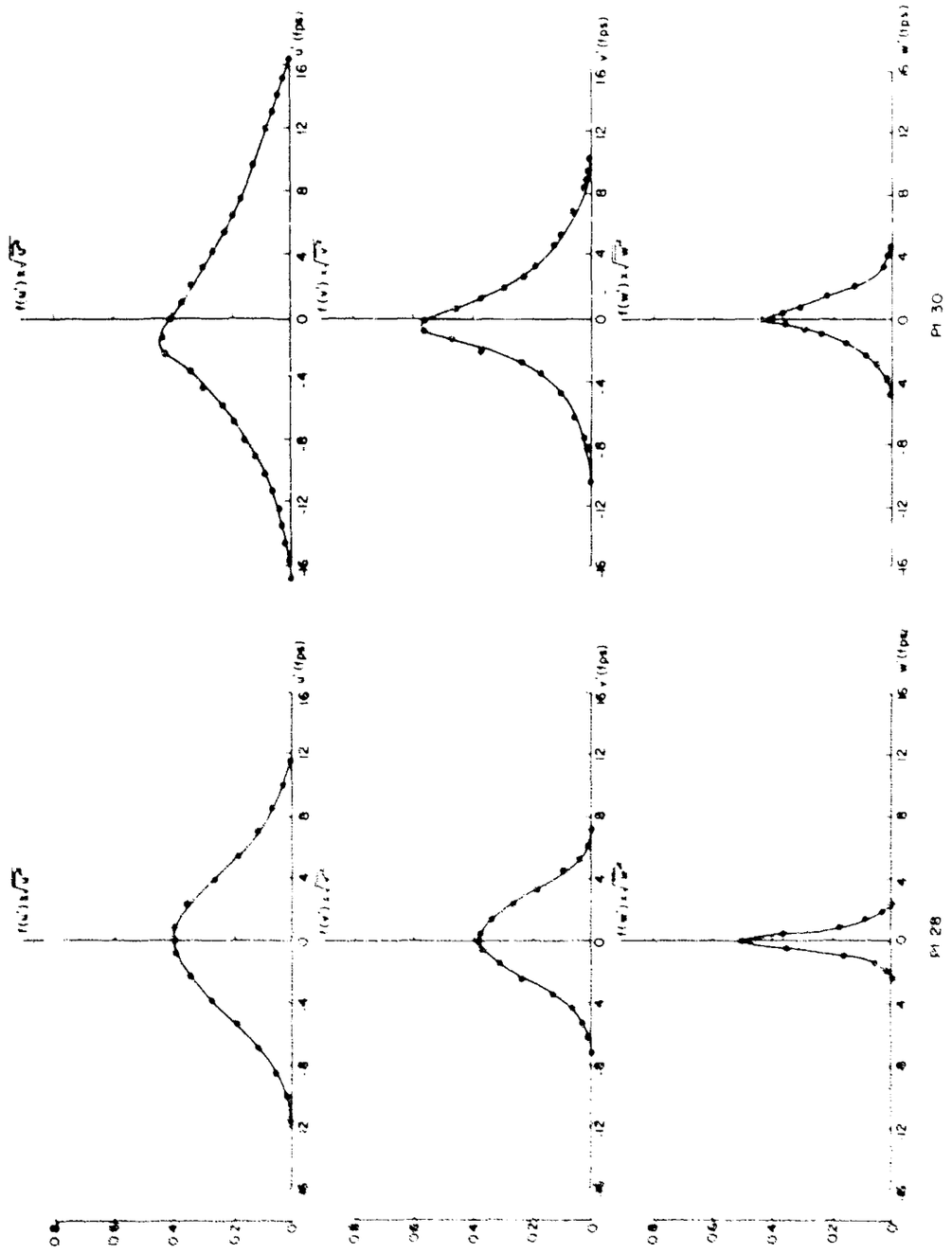

Fig. 38. Probability densities of the single turbulent components at test points No. 28 and 30.

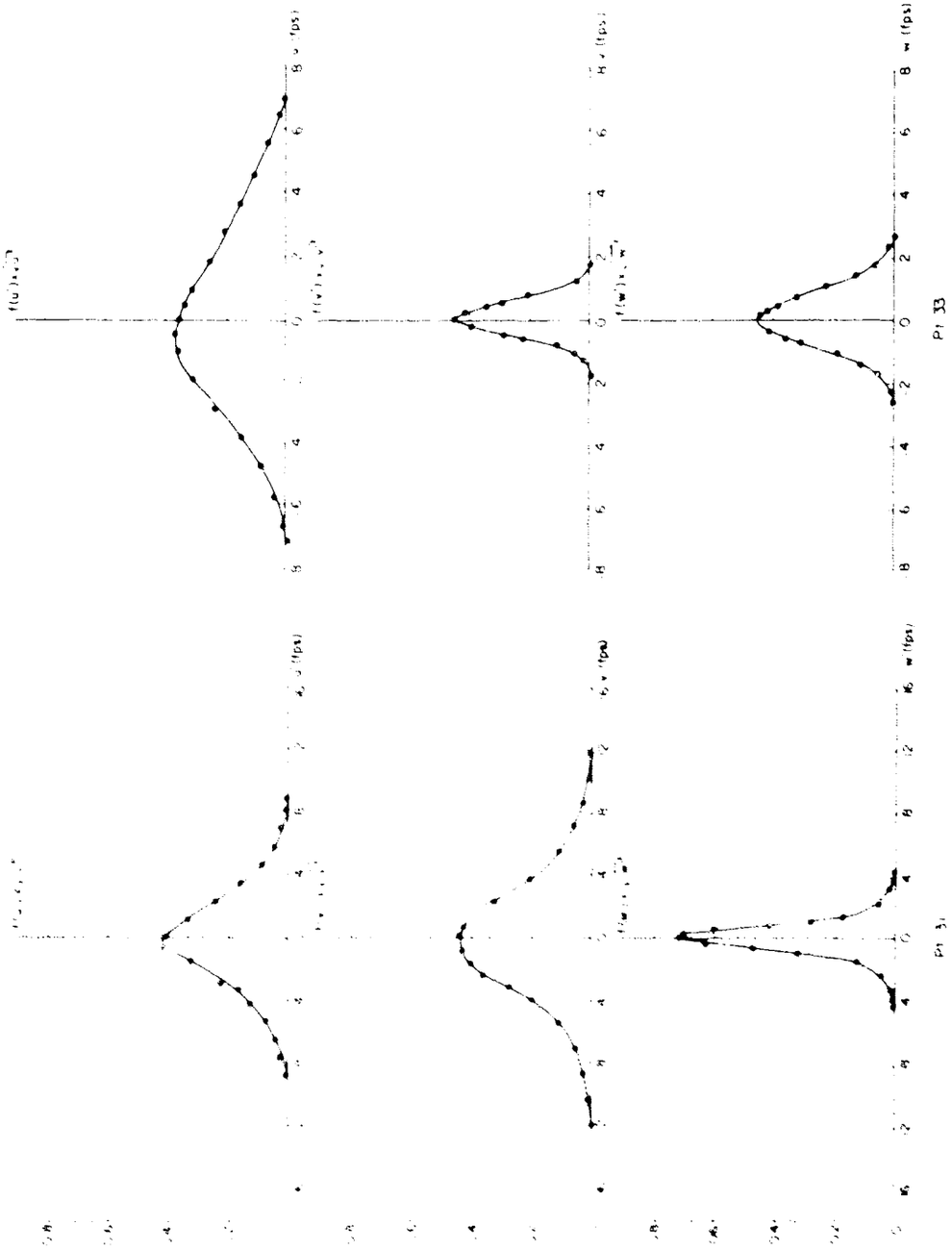

Fig. 39 Probability densities of the single turbulent components at test points No. 31 and 33.

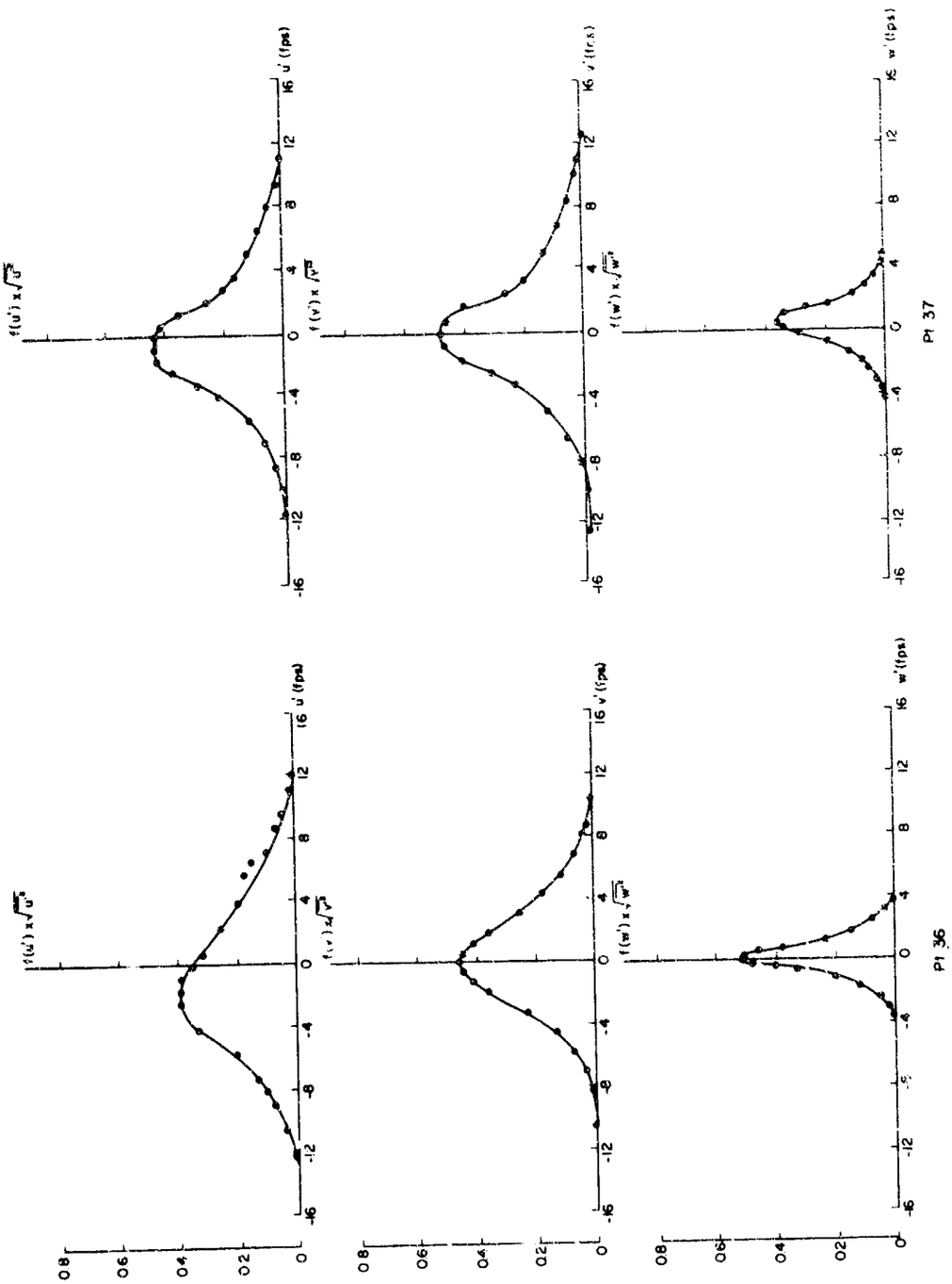

Fig. 40. Probability densities of the single turbulent components at test points No. 36 and 37.

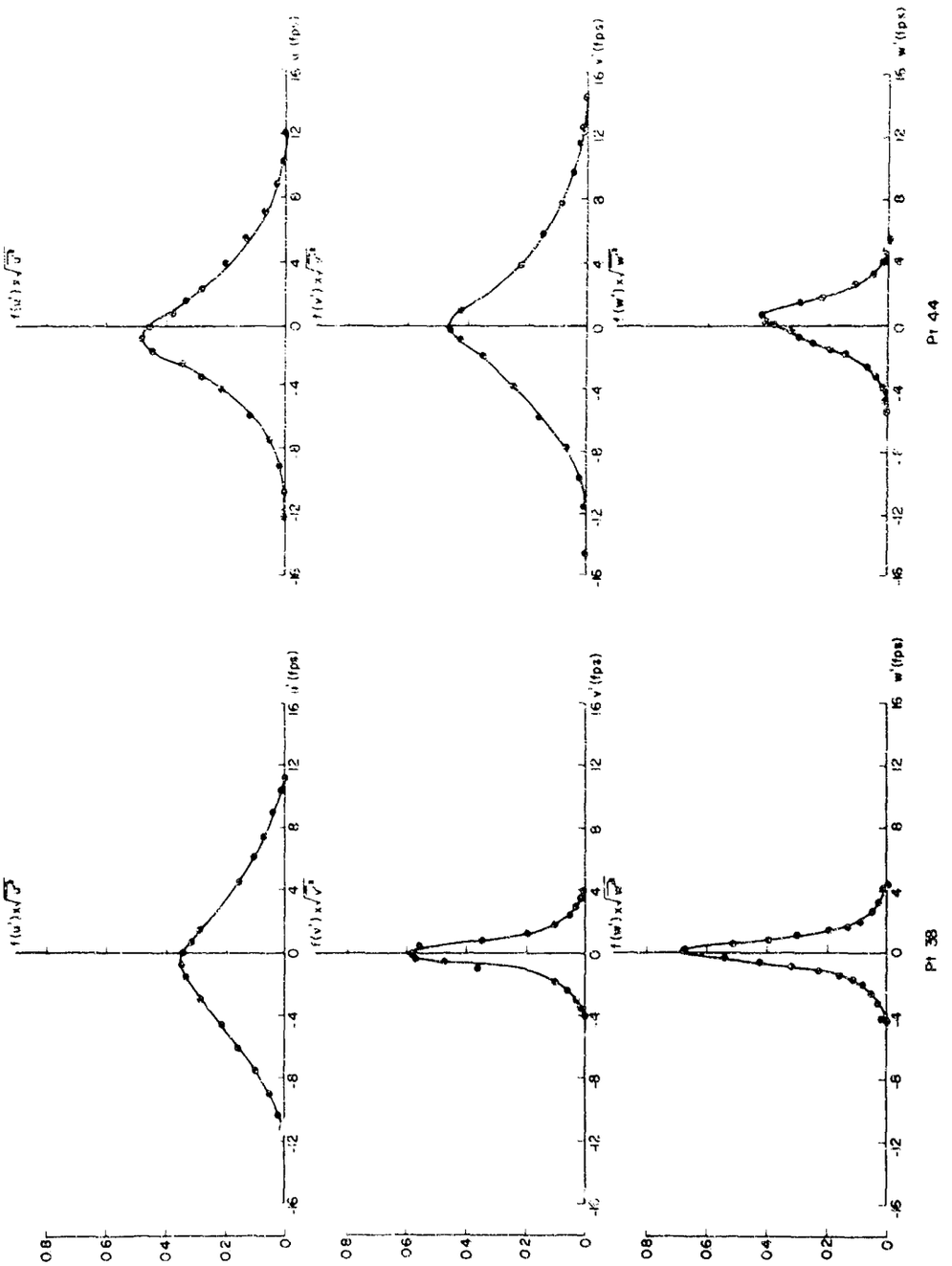

Fig. 41. Probability densities of the single turbulent components at test points No. 38 and 44.

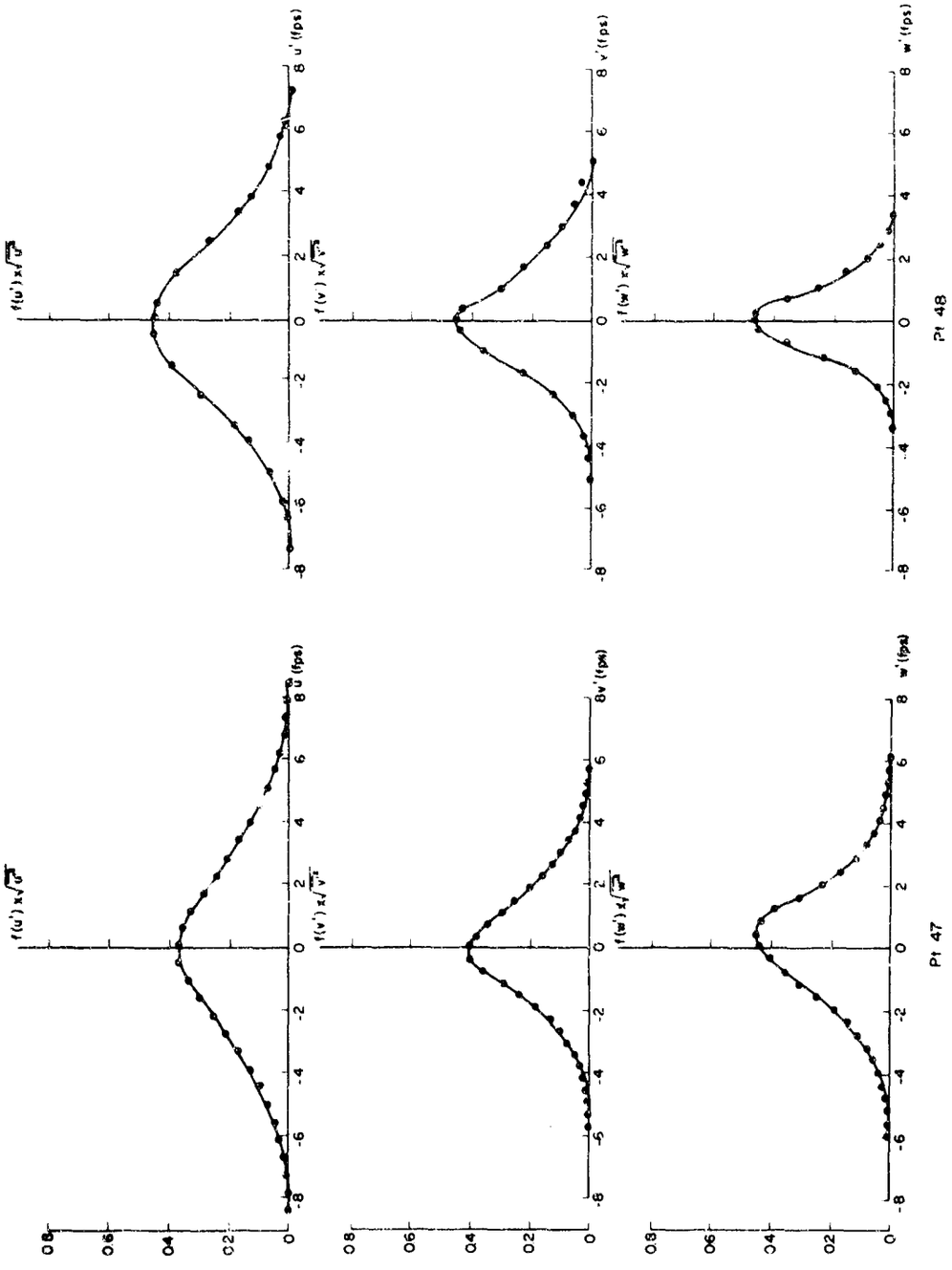

Fig. 42. Probability densities of the single turbulent components at test points No. 47 and 48.

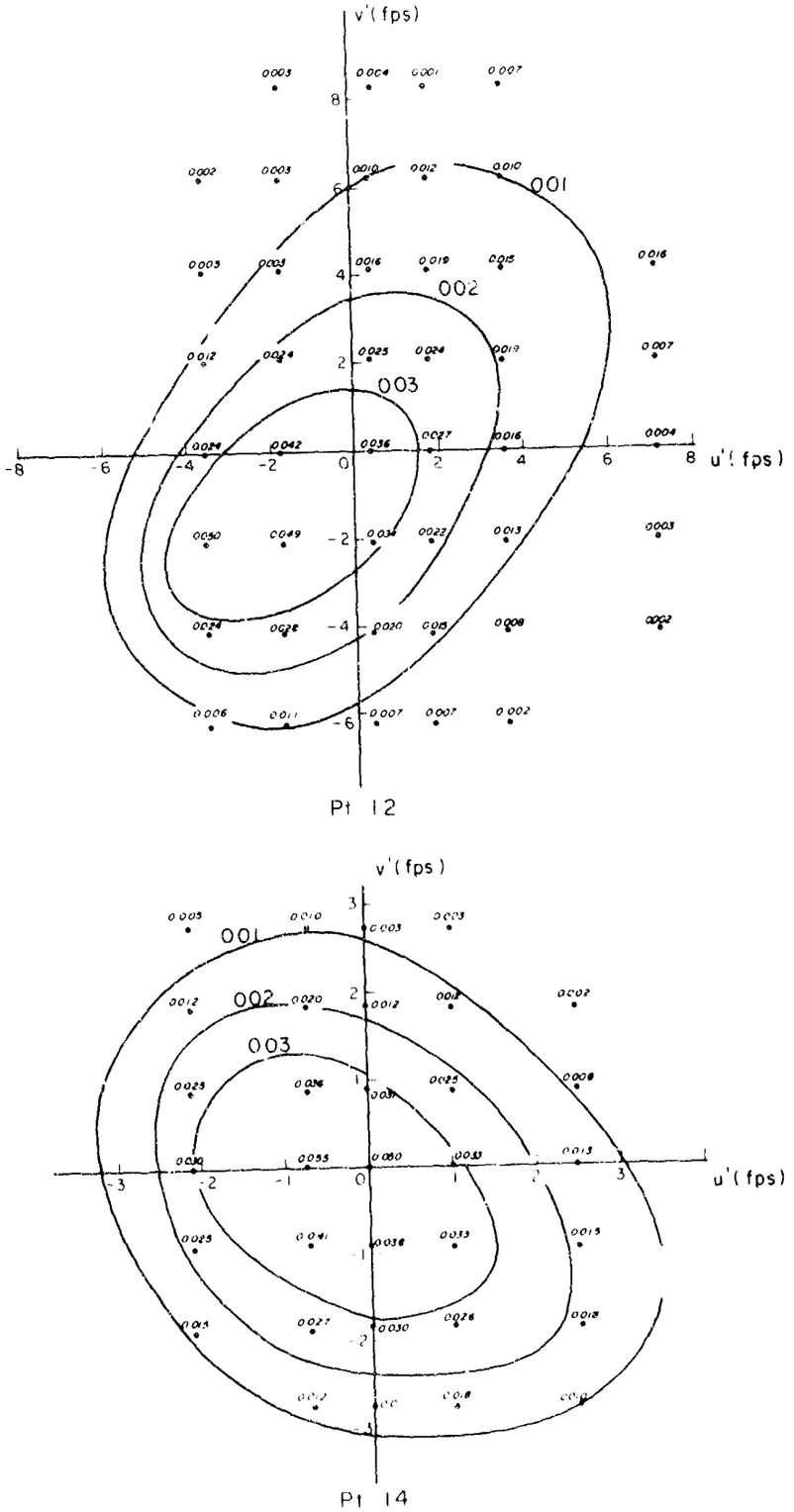

Fig. 43. Joint probability densities of u'- and v'- components at test points No. 12 and 14. (Numerical values on the contours = $f(u',v')$ $\sqrt{\overline{u'^2}}$ $\sqrt{\overline{v'^2}}$).

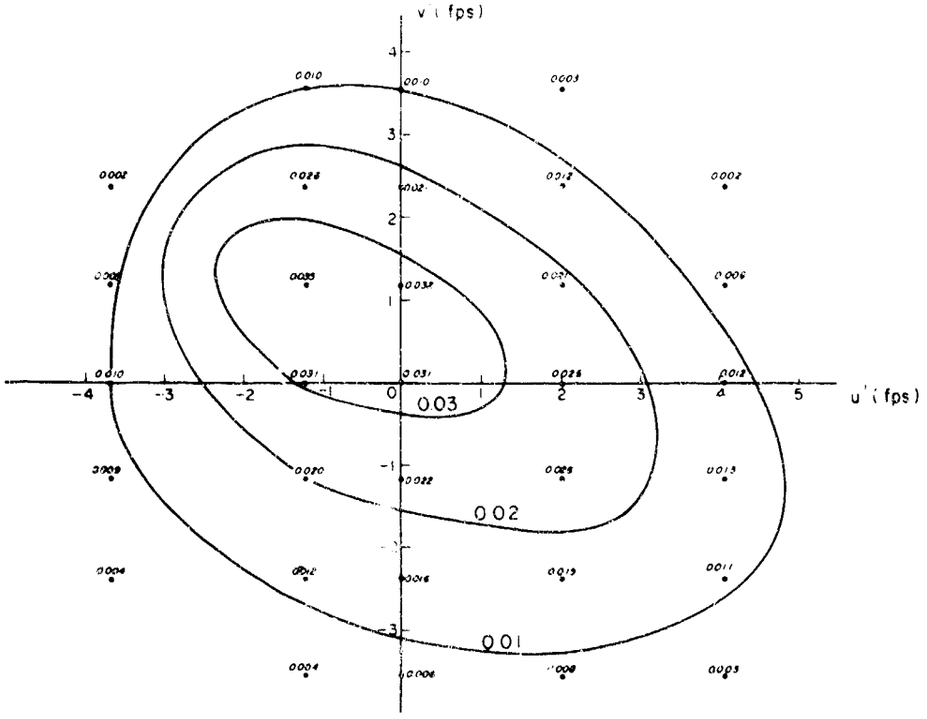

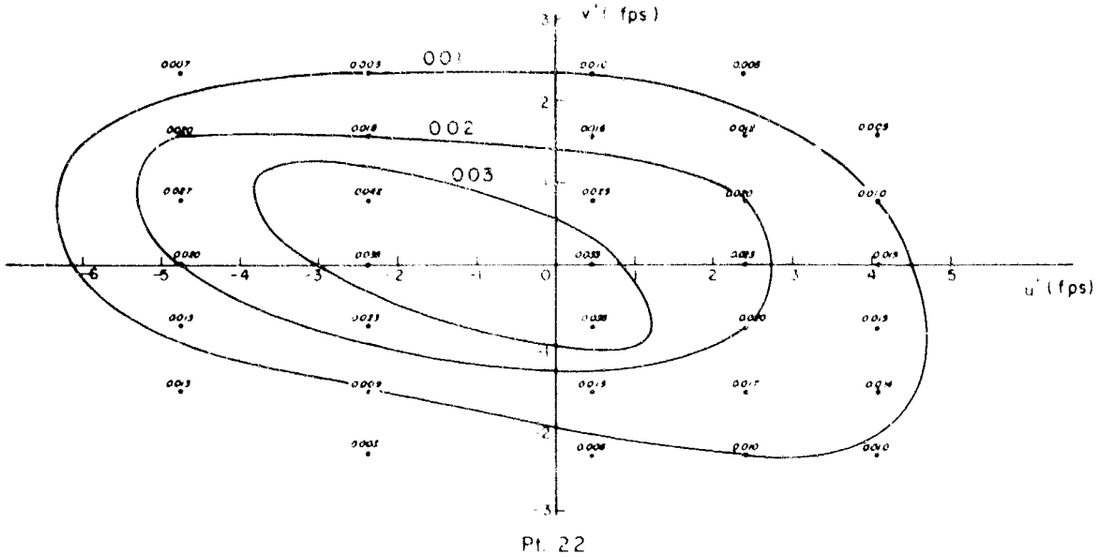

Fig. 44. Joint probability densities of u'- and v'- components at test points No. 21 and 22. (Numerical values on the contours = $f(u',v')$ $\sqrt{\overline{u'^2}}$ $\sqrt{\overline{v'^2}}$).

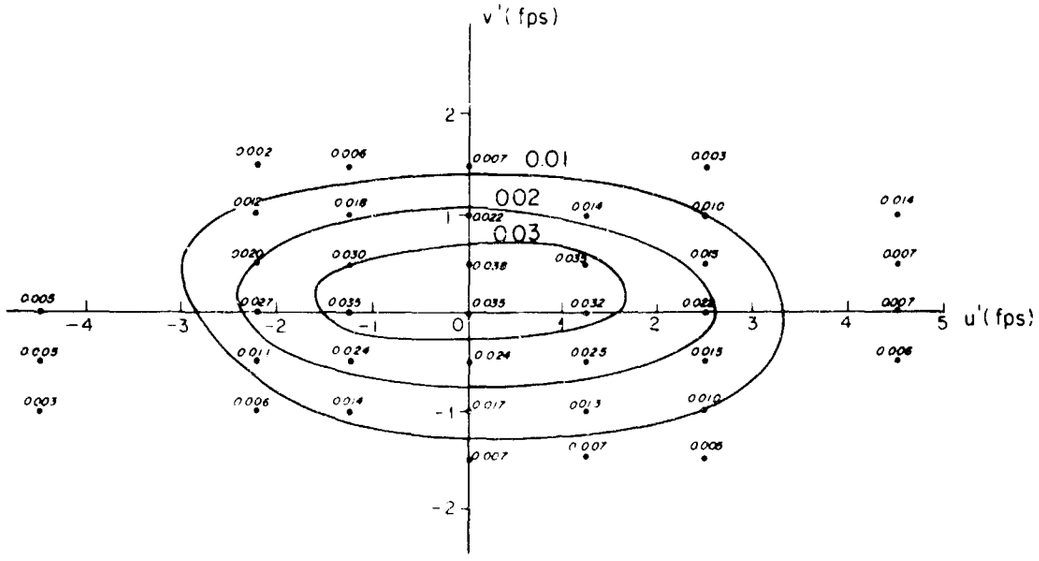

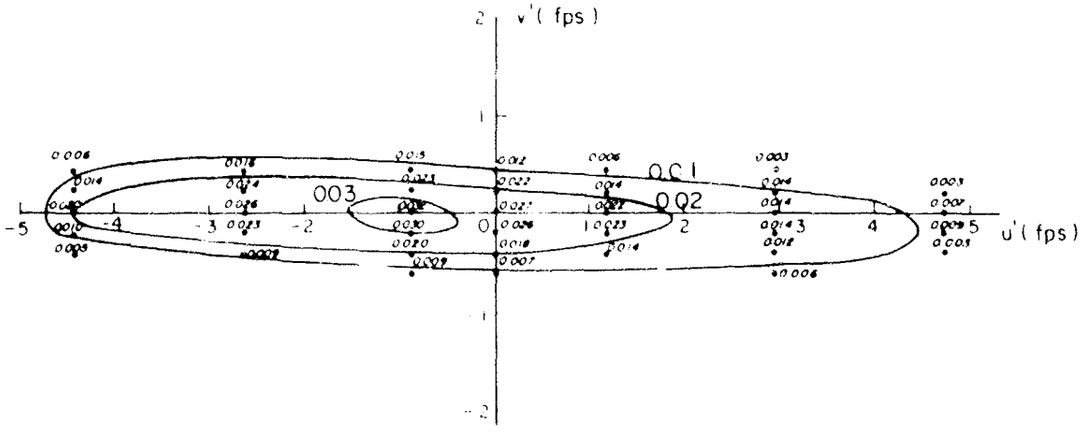

Fig. 45. Joint probability densities of u'- and v'- components at test points No. 24 and 27. (Numerical values on the contours = $f(u',v')$ $\sqrt{\overline{u'^2}}$ $\sqrt{\overline{v'^2}}$).

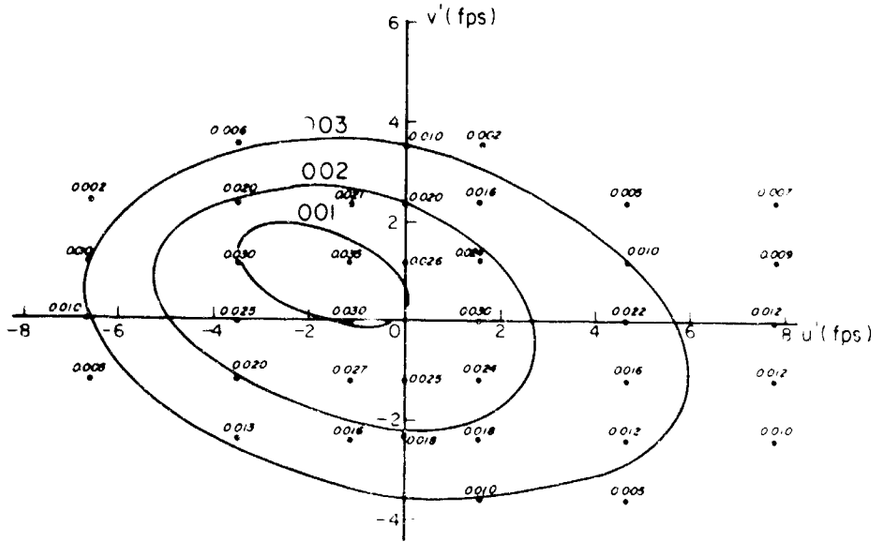

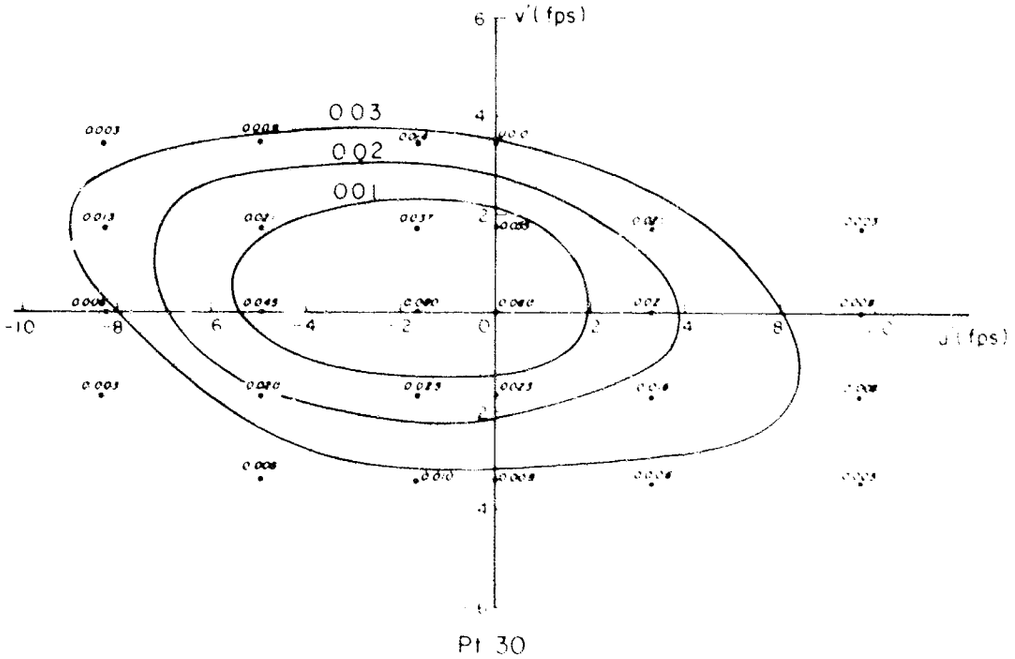

Fig. 46. Joint probability densities of u'- and v'- components at test points No. 28 and 30. (Numerical values on the contours = f(u',v') $\sqrt{\overline{u'^2}}$ $\sqrt{\overline{v'^2}}$).

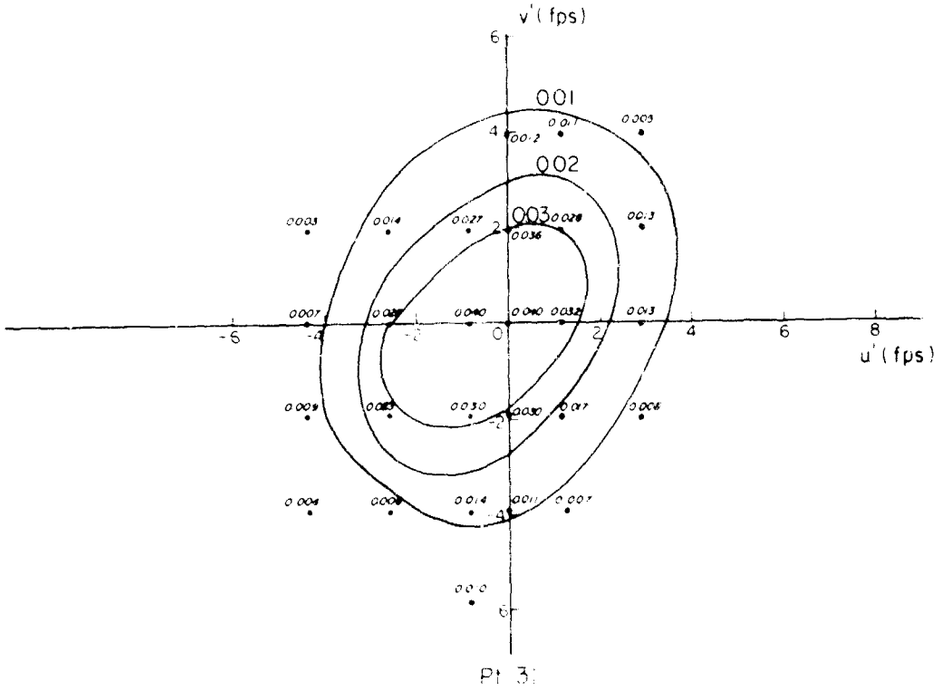

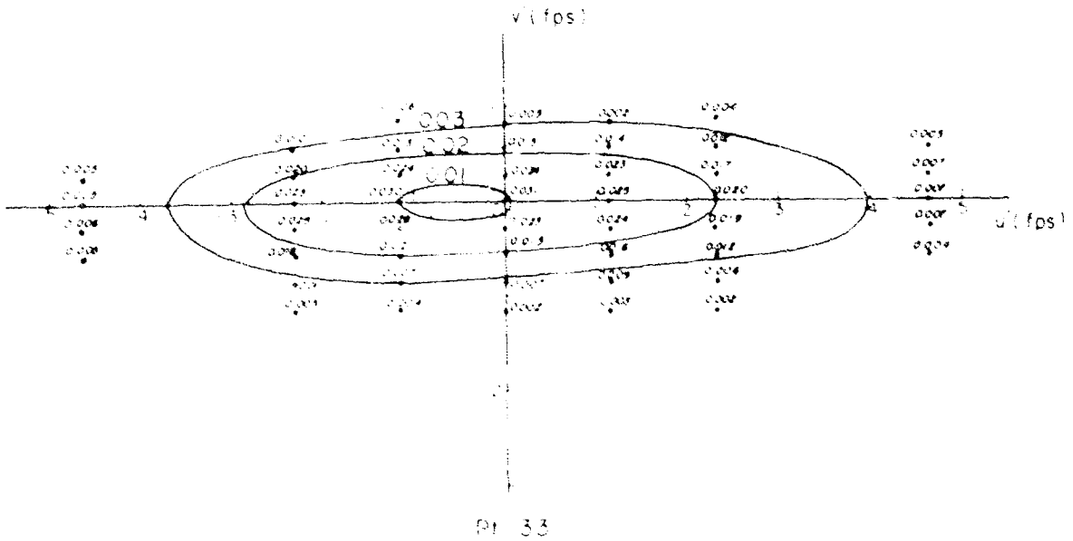

Fig. 47. Joint probability densities of u'- and v'- components at test points No. 31 and 33. (Numerical values on the contours = $f(u',v')\sqrt{\overline{u'^2}}\sqrt{\overline{v'^2}}$)

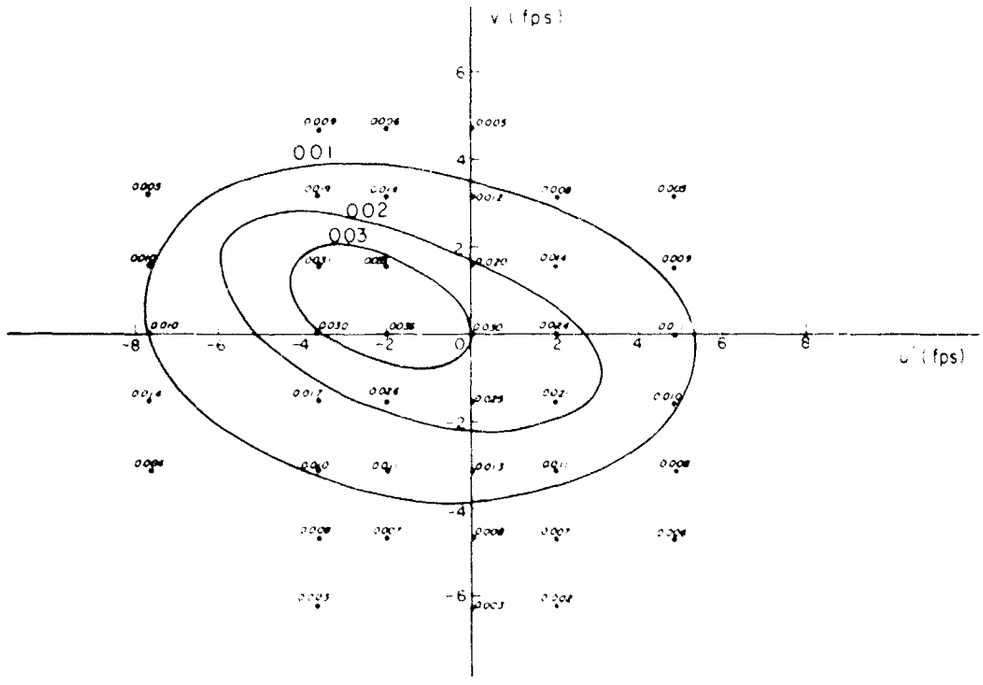

Pt 36

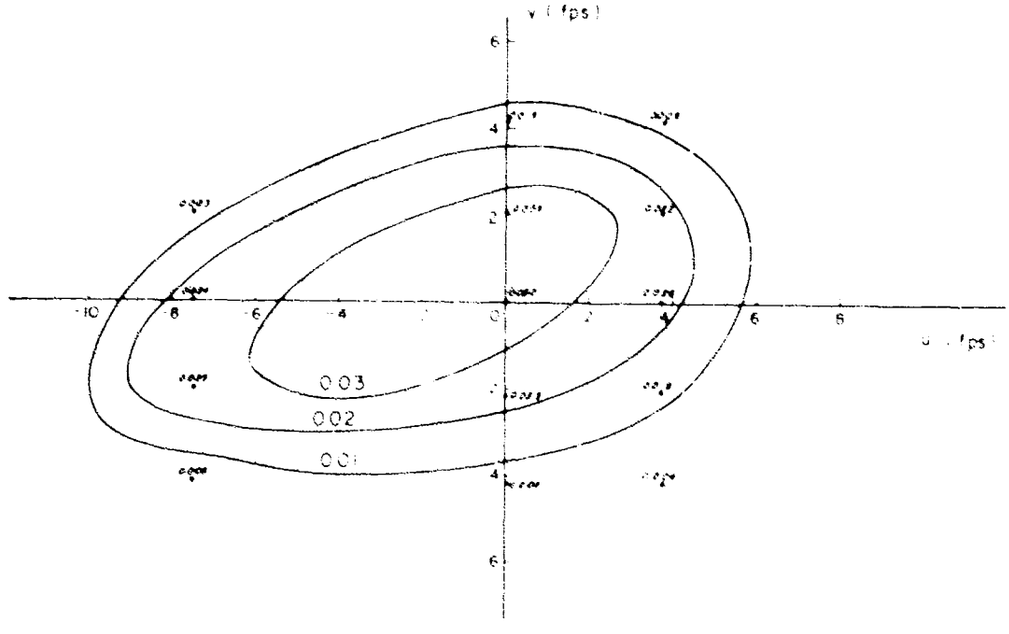

Pt 37

Fig 48. Joint probability densities of u'- and v'- components at test points No. 36 and 37. (Numerical values on the contours = $f(u',v') \sqrt{\overline{u'^2}} \sqrt{\overline{v'^2}}$).

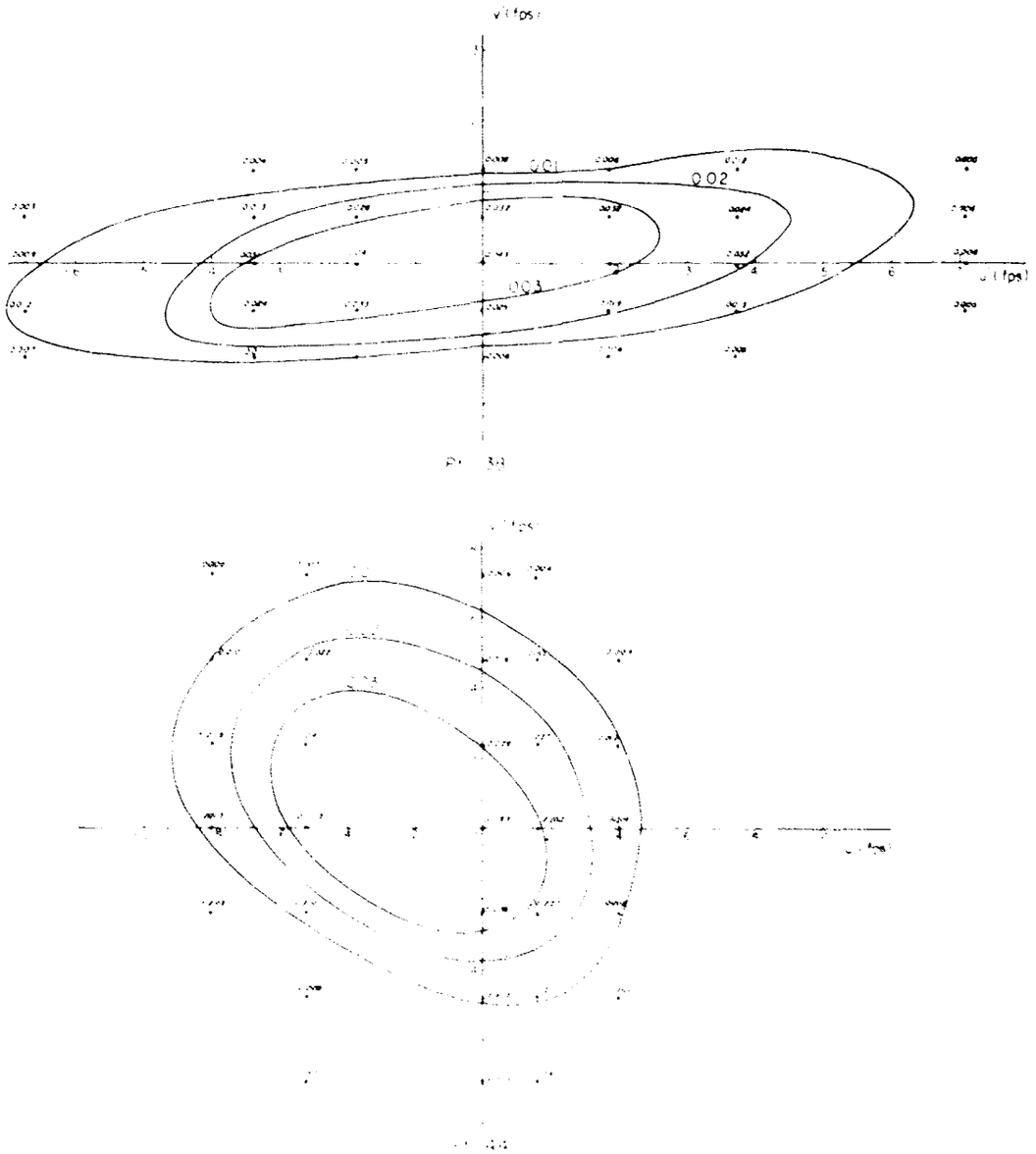

Fig. 49. Joint probability densities of u'- and v'- components at test points No. 38 and 40. (Numerical values on the contours = f(u',v') $\sqrt{\overline{u'^2}}$ $\sqrt{\overline{v'^2}}$.)

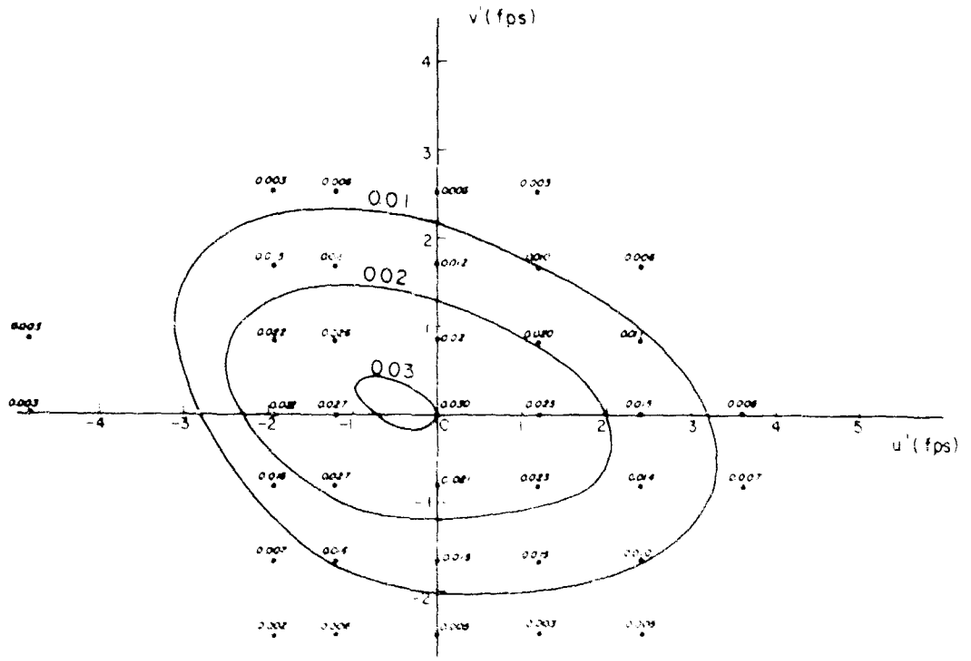

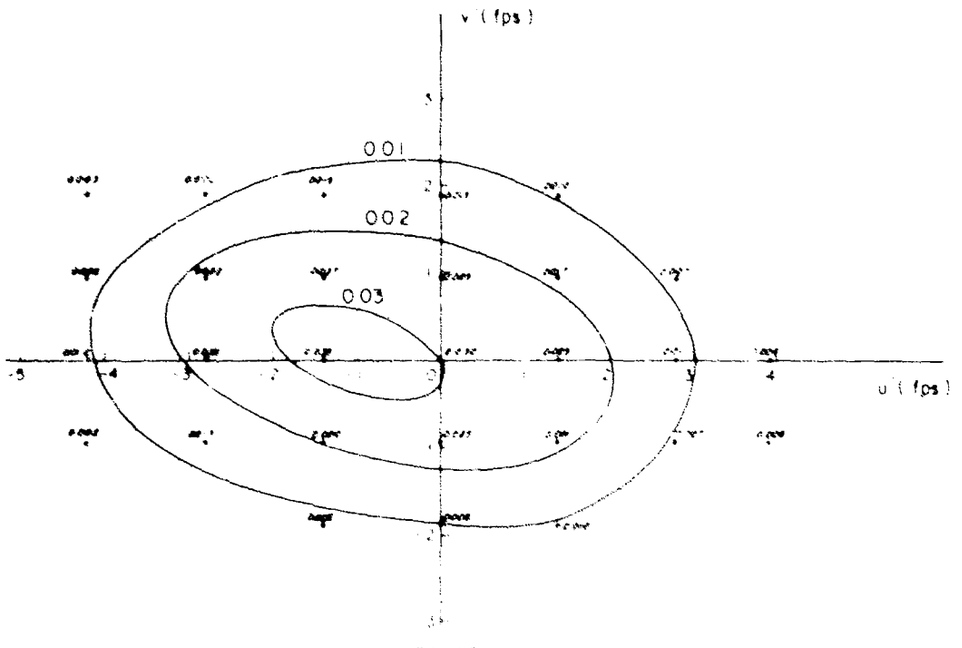

Fig. 50. Joint probability densities of u'- and v'- components at test points No. 48 and 49. (Numerical values on the contours = $f(u',v') \sqrt{\overline{u'^2}} \sqrt{\overline{v'^2}}$).

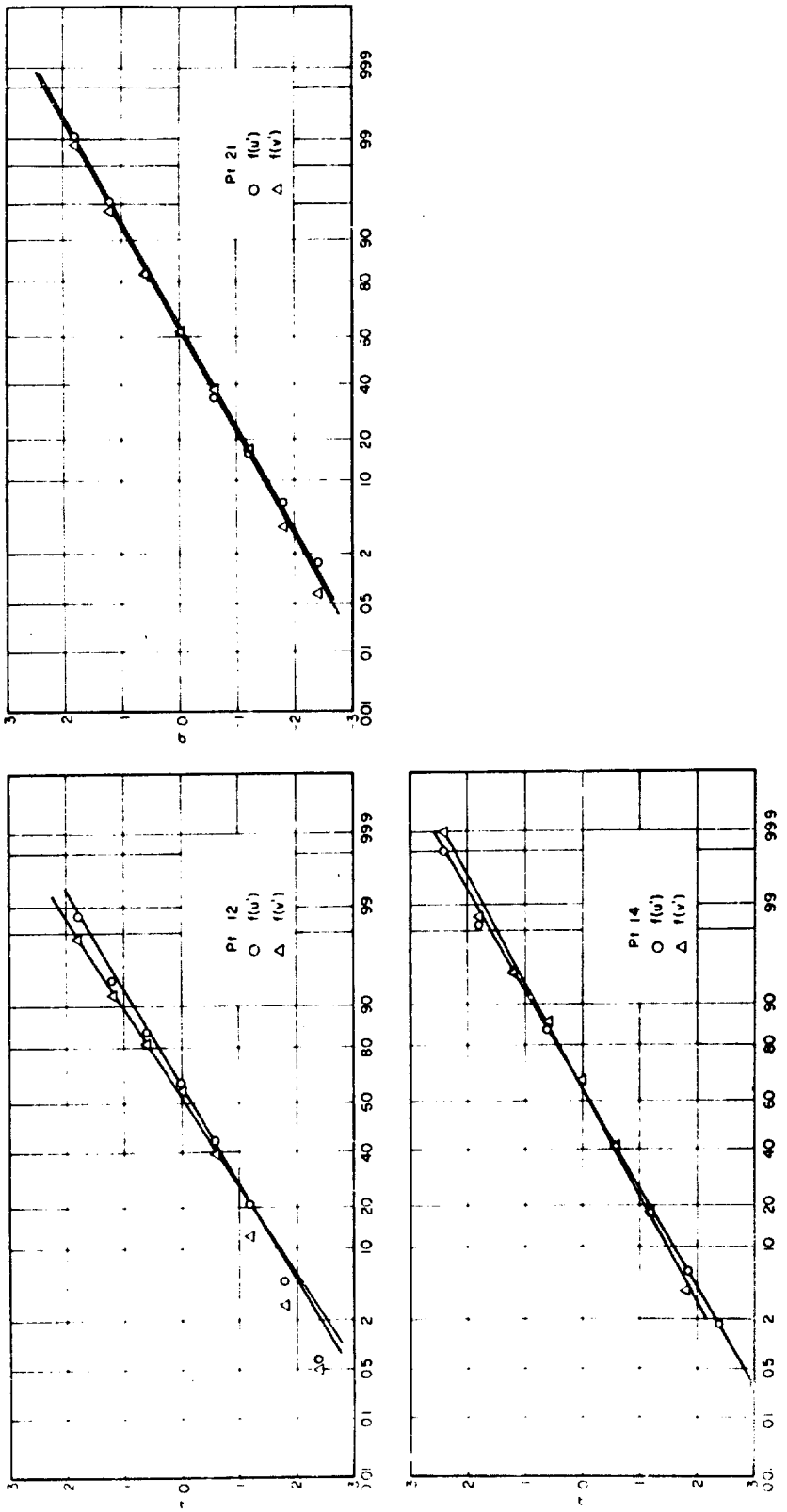

Fig. 51. Plots of the measured cumulative probability densities on the probability papers for test points No. 12, 14, and 21.

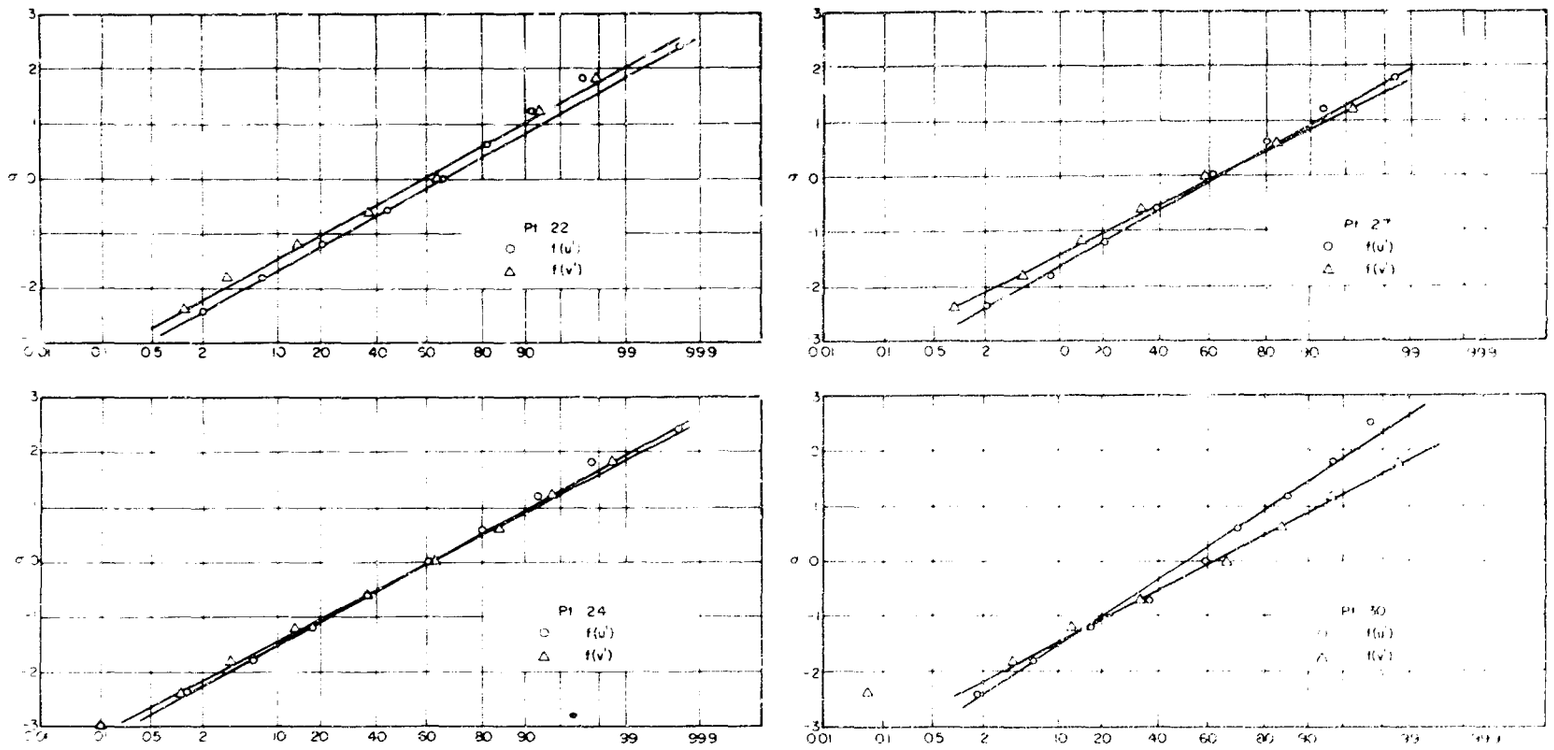

Fig. 52. Plots of the measured cumulative probability densities on the probability papers for test points No. 22, 24, 27 and 30.

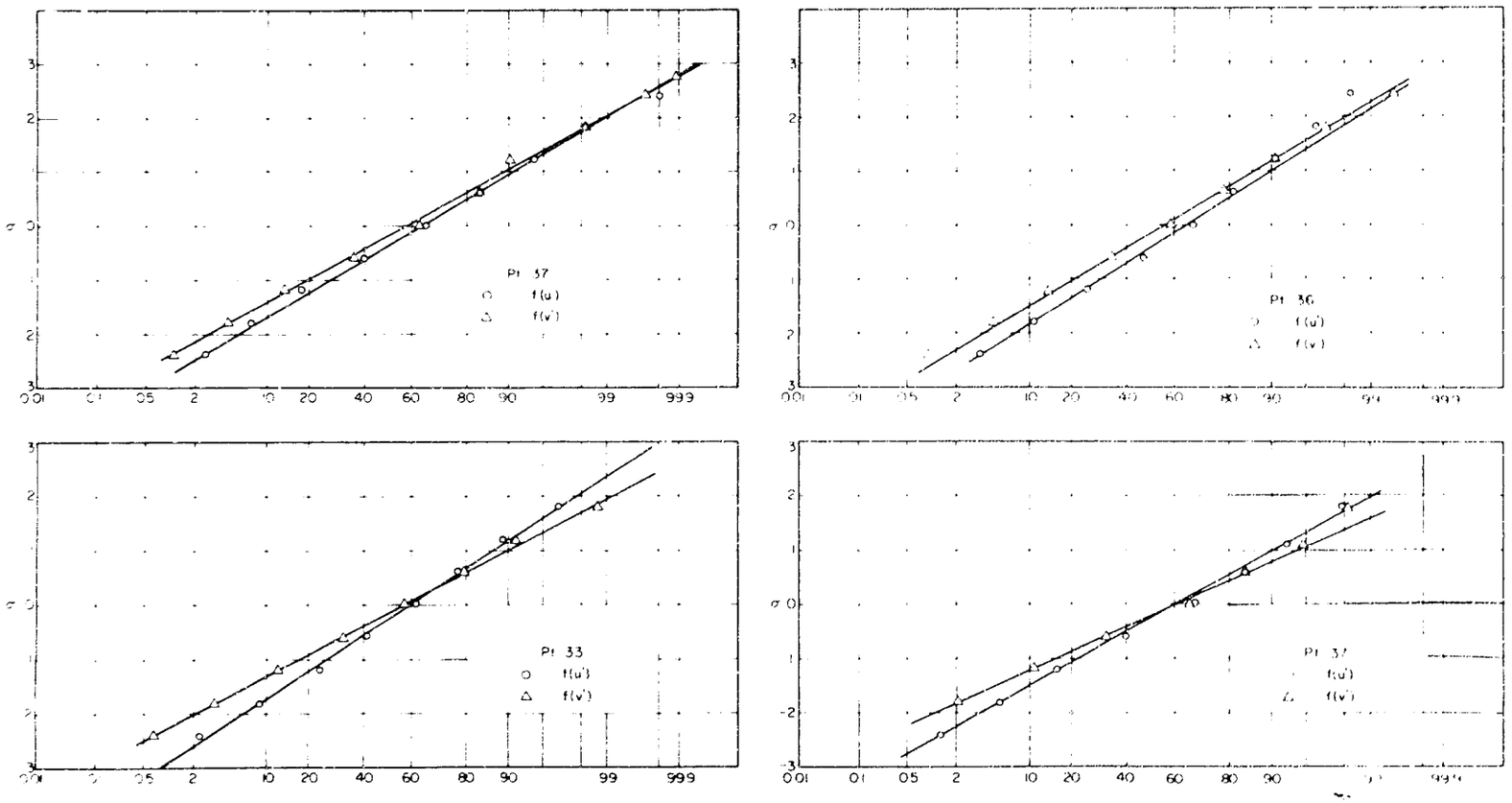

Fig. 53. Plots of the measured cumulative probability densities on the probability papers for test points No. 21, 33, 36, and 37.

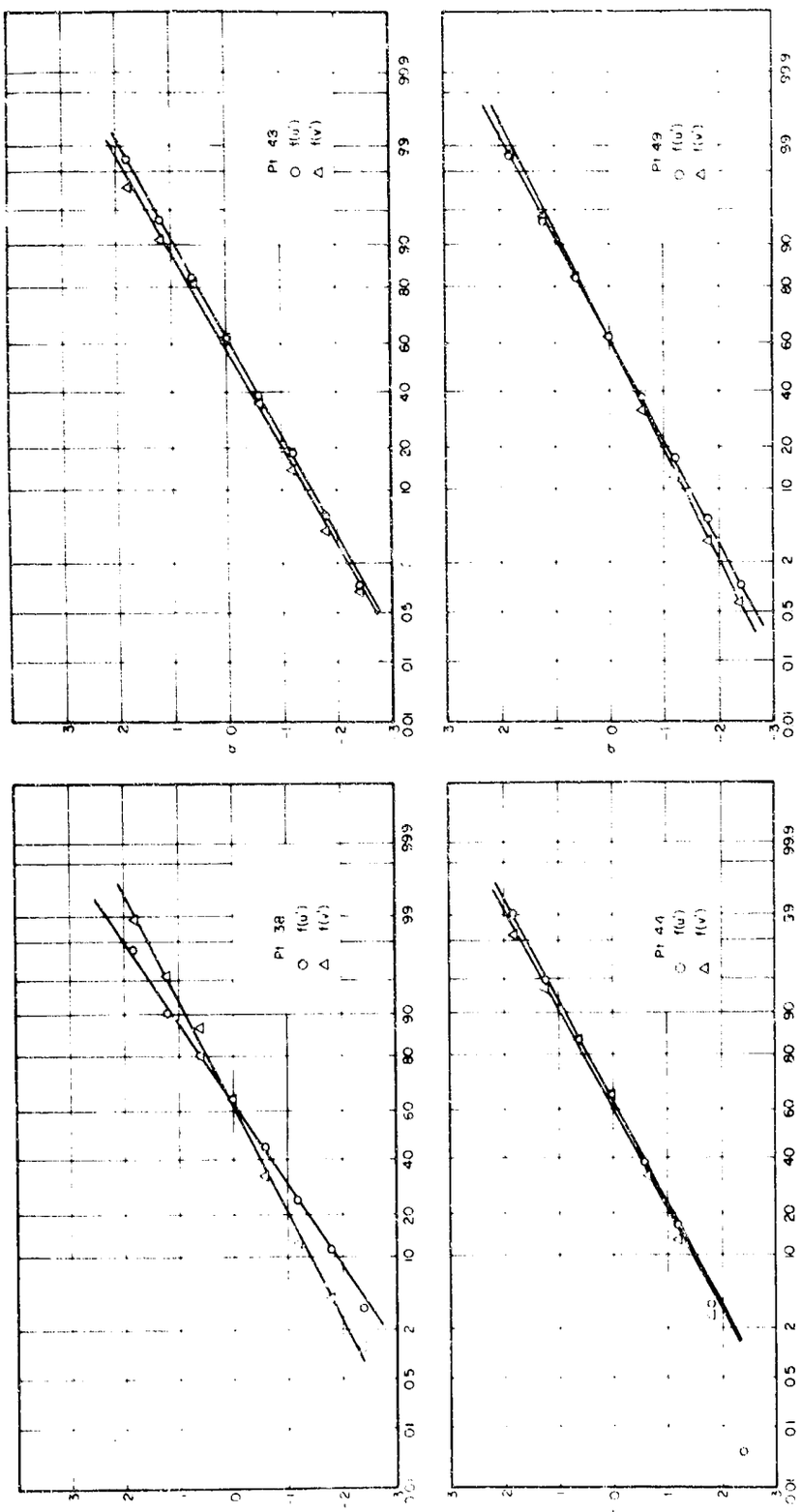

Fig. 54. Plots of the measured cumulative probability densities on the probability papers for test points No. 38, 44, 68, and 69.

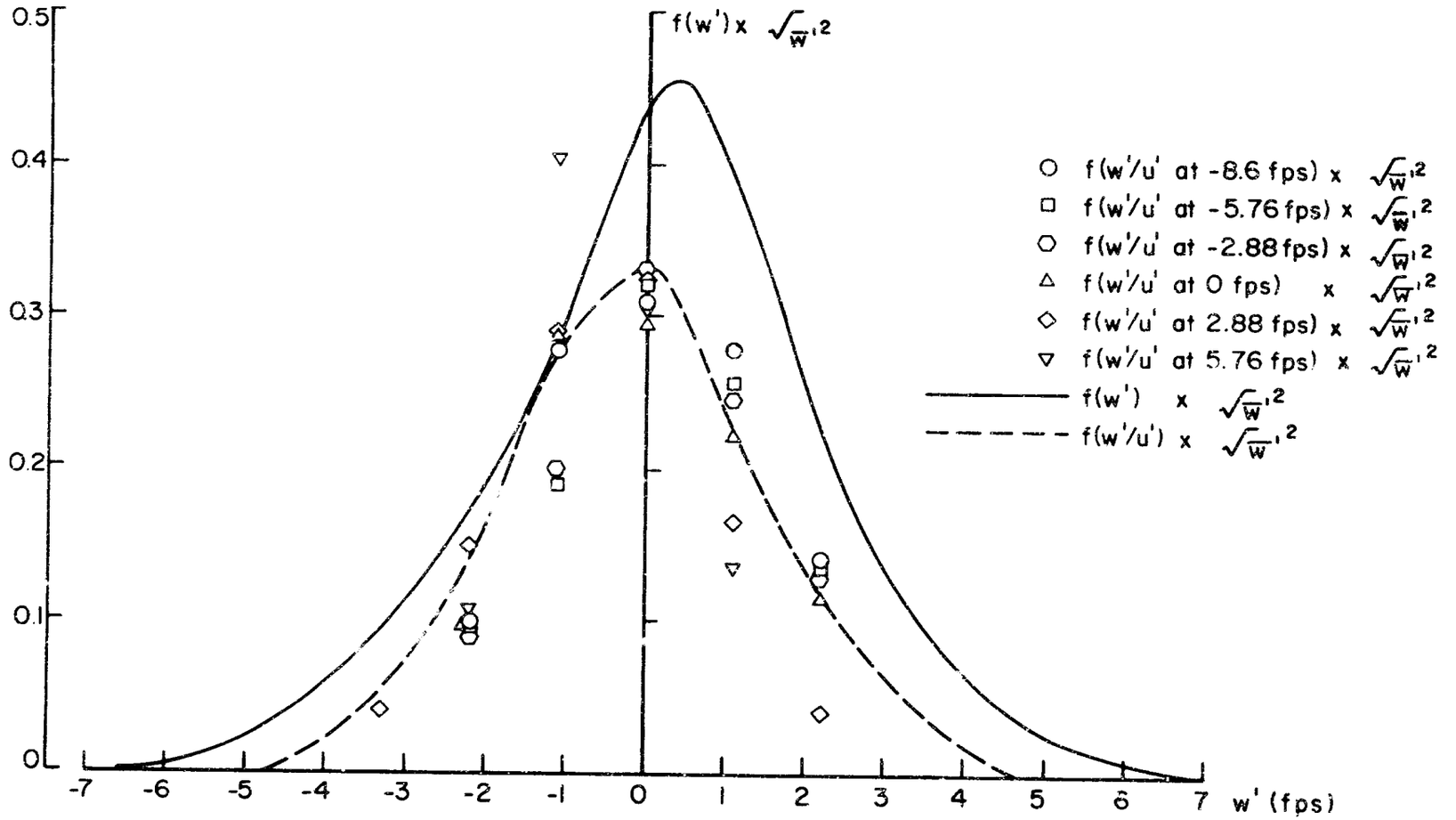

Fig. 55. Comparison between the probability density f(w') and the conditional probability densities f(w'/u') at test point no. 21.

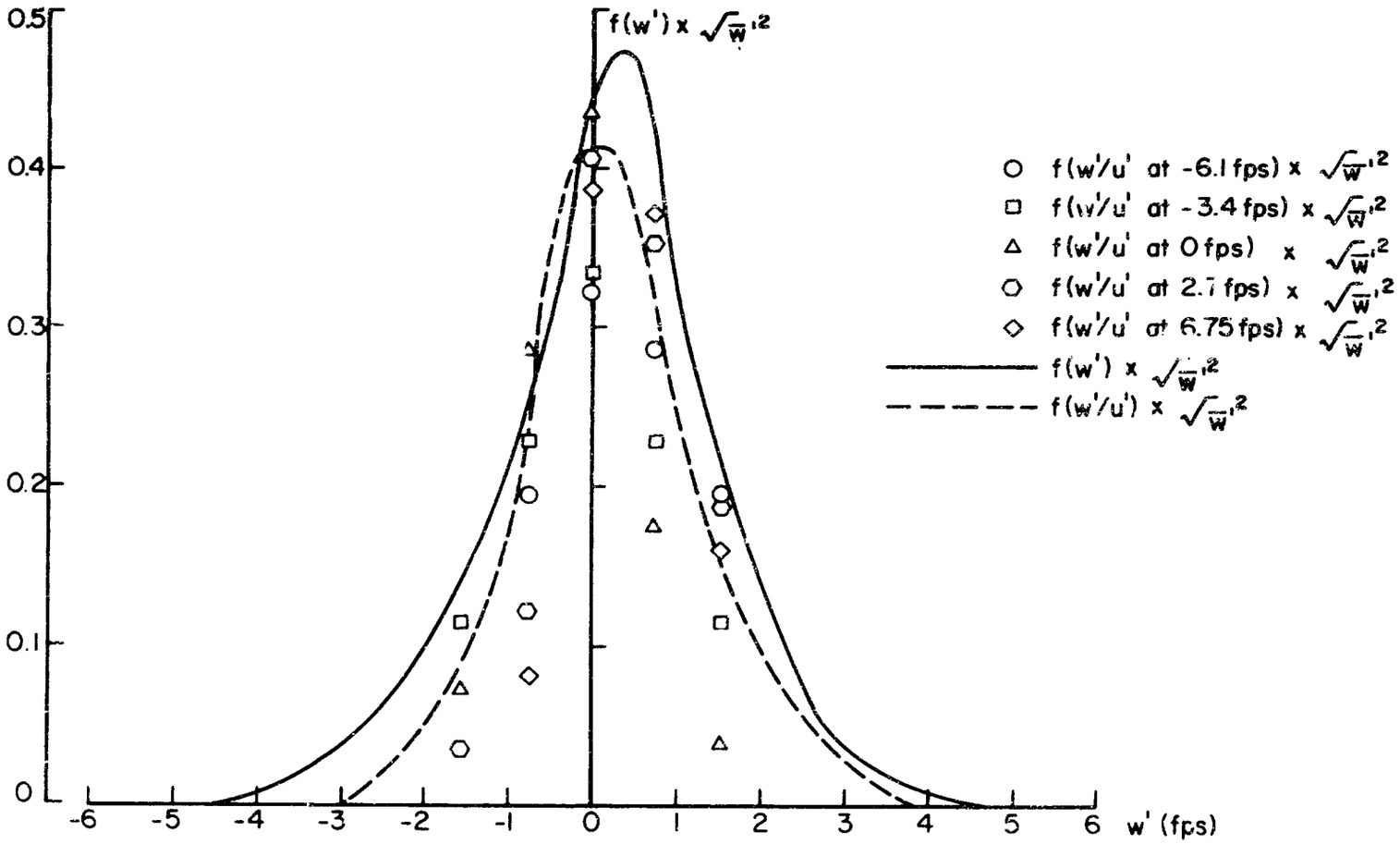

Fig. 56. Comparison between the probability density f(w') and the conditional probability densities f(w'/u') at test point no. 30.

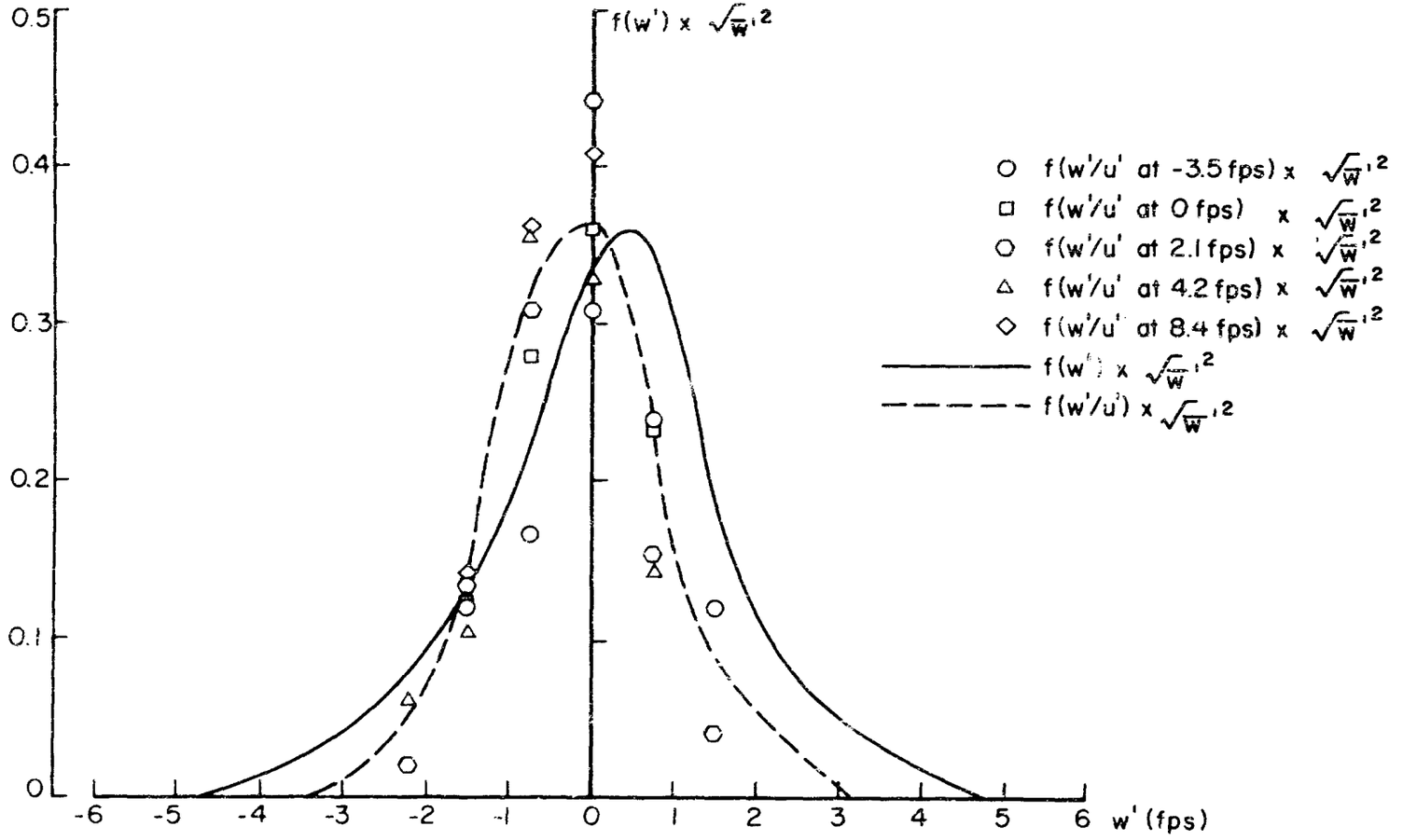

Fig. 57. Comparison between the probability density f(w') and the conditional probability densities f(w'/u') at test point no. 37.

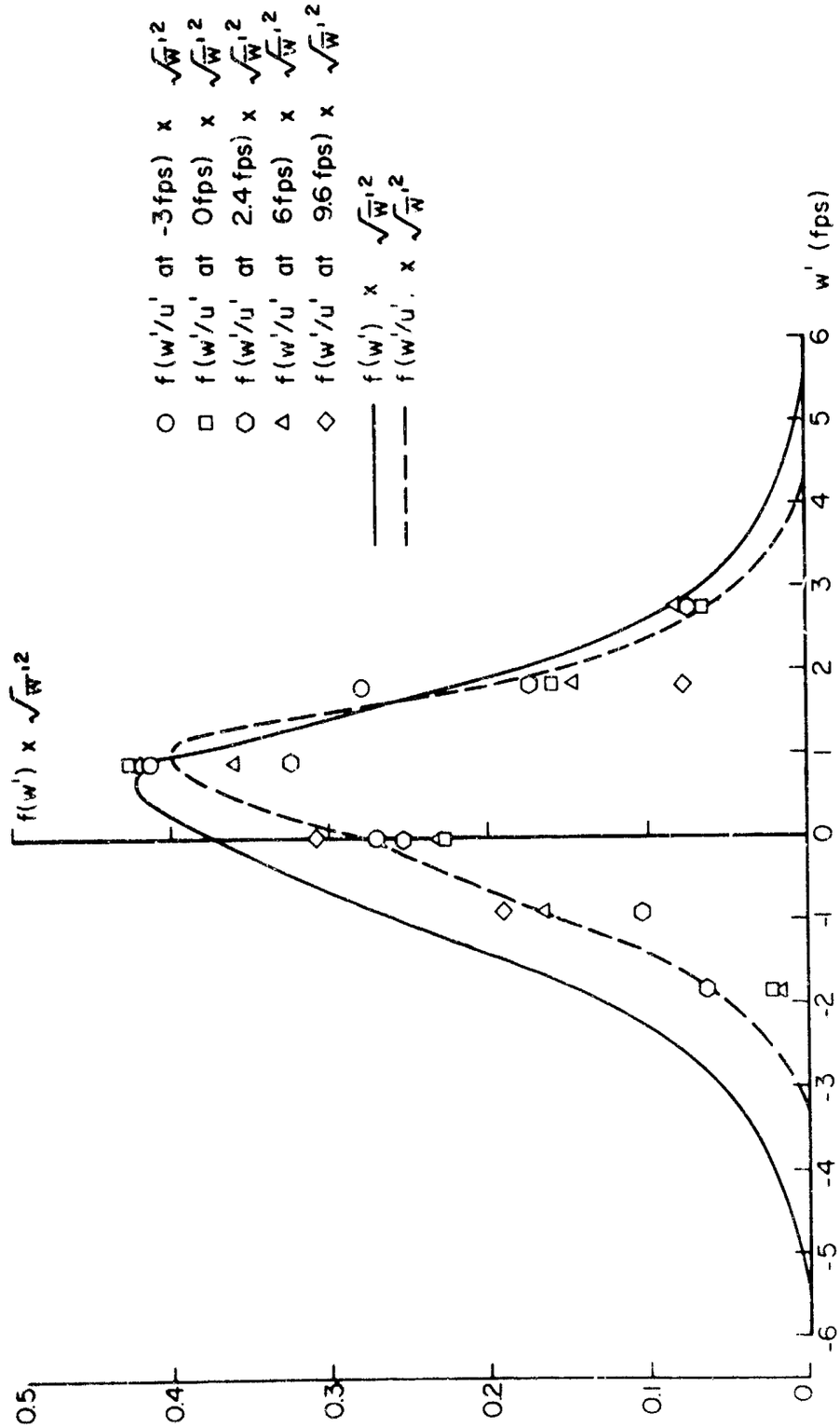

Fig. 58. Comparison between the probability density f(w') and the conditional probability densities f(w'/u') at test point no. 44.

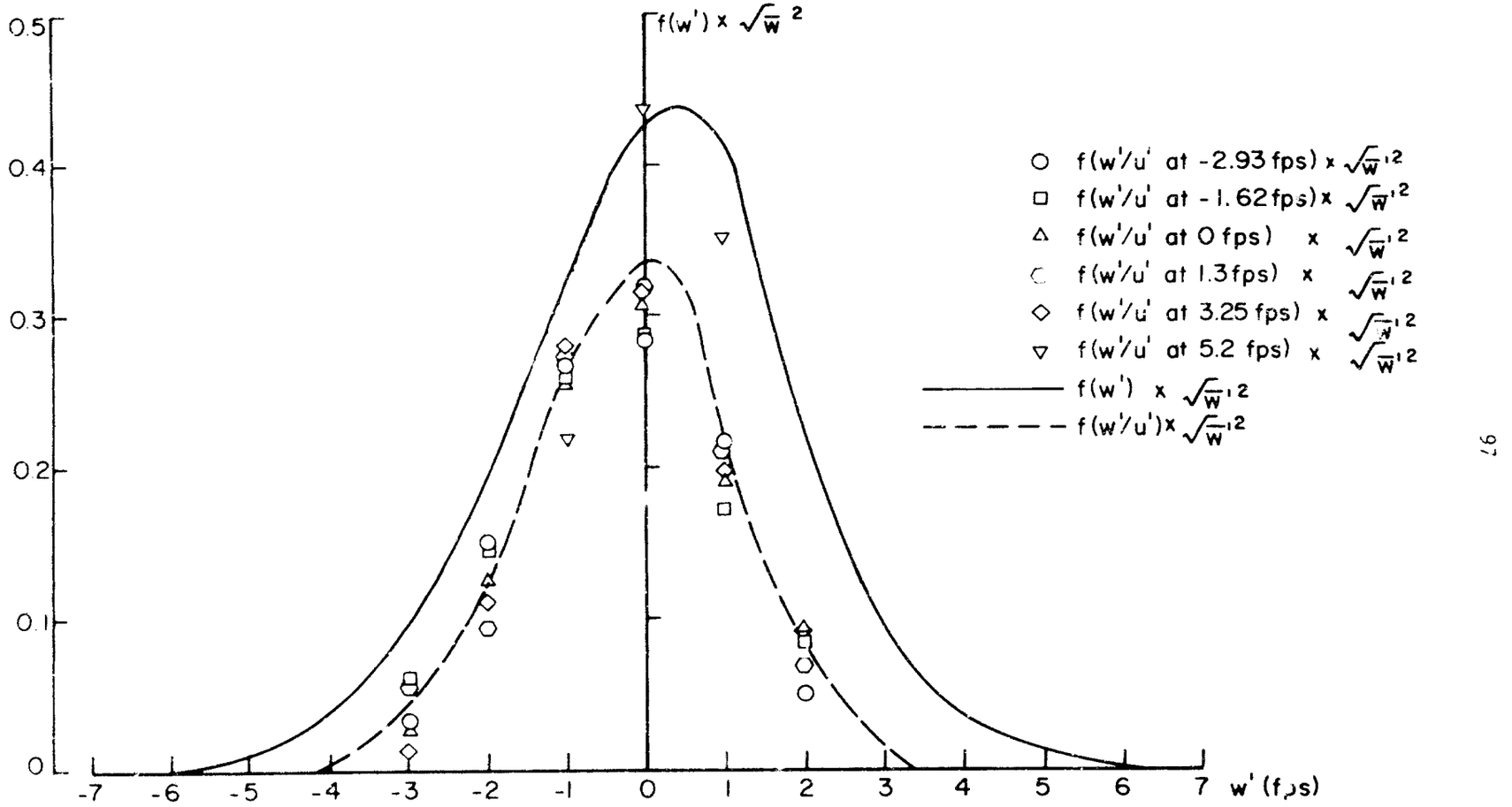

Fig. 59. Comparison between the probability density f(w') and the conditional probability densities f(w'/u') at test point no. 49.

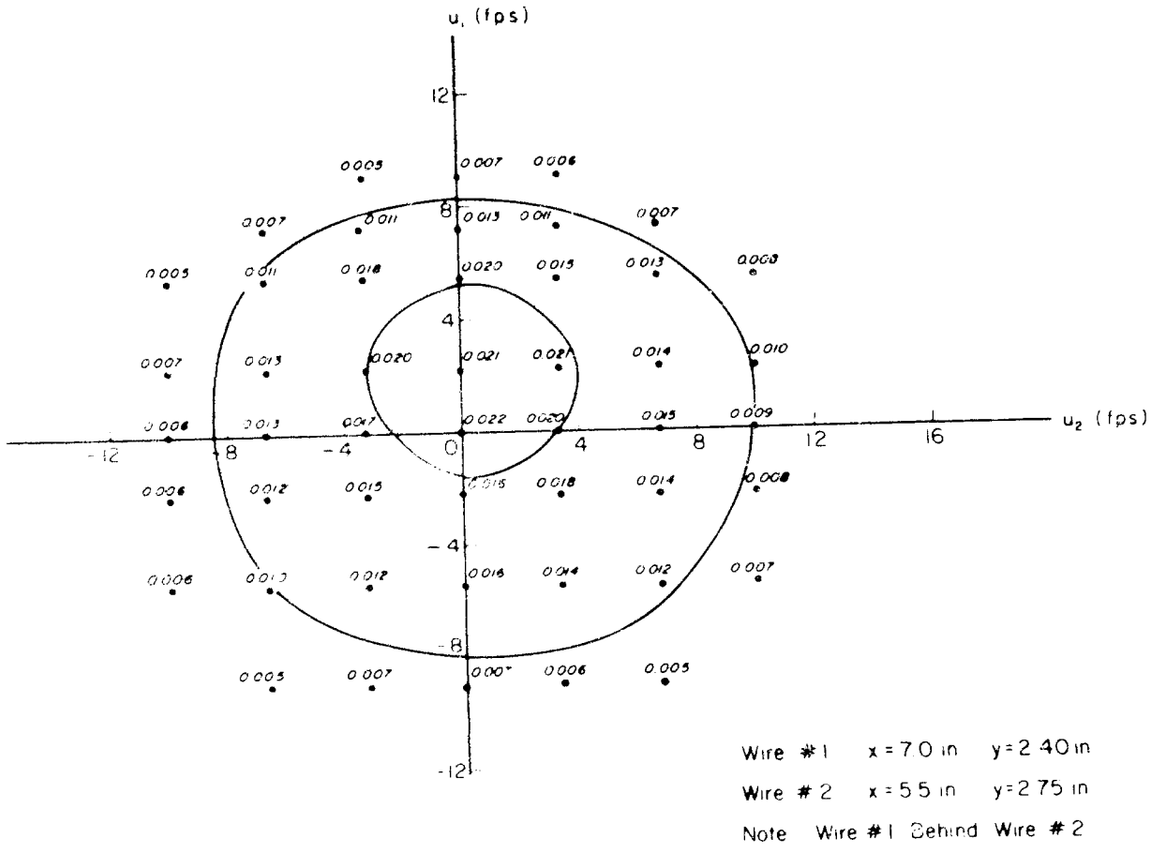

Fig. 60. Joint probability density of u_1' and u_2' along the trajectory launching from the top of the ridge with 60° azimuth (Numerical values on the contours = $f(u',v')\sqrt{\overline{u'^2}}\sqrt{\overline{v'^2}}$).

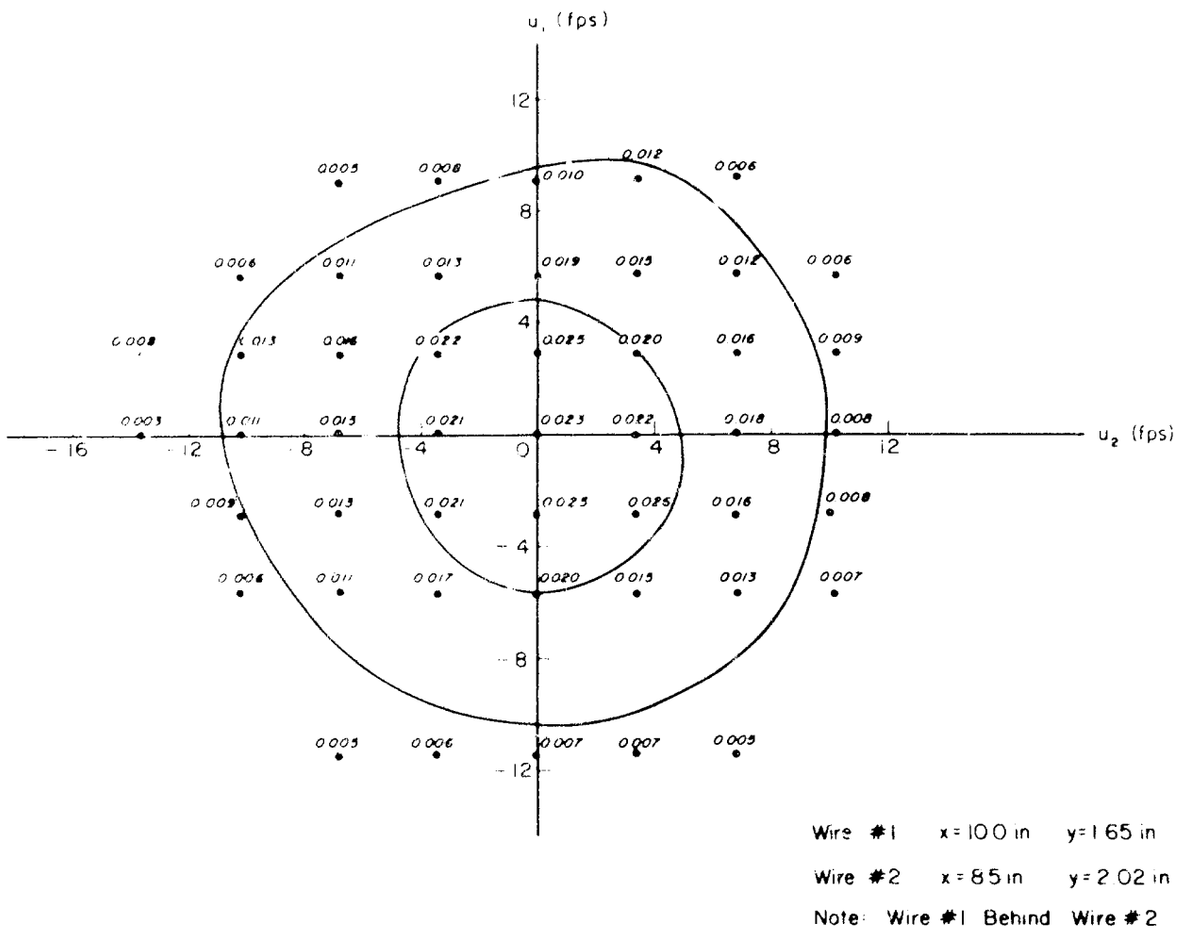

Fig. 61. Joint probability density of u_1' and u_2' along the trajectory launching from the t... of the ridge with 60° azimuth (Numerical values on the contours = $f(u',v') \sqrt{\overline{u'^2}}\ \sqrt{\overline{v'^2}}$).

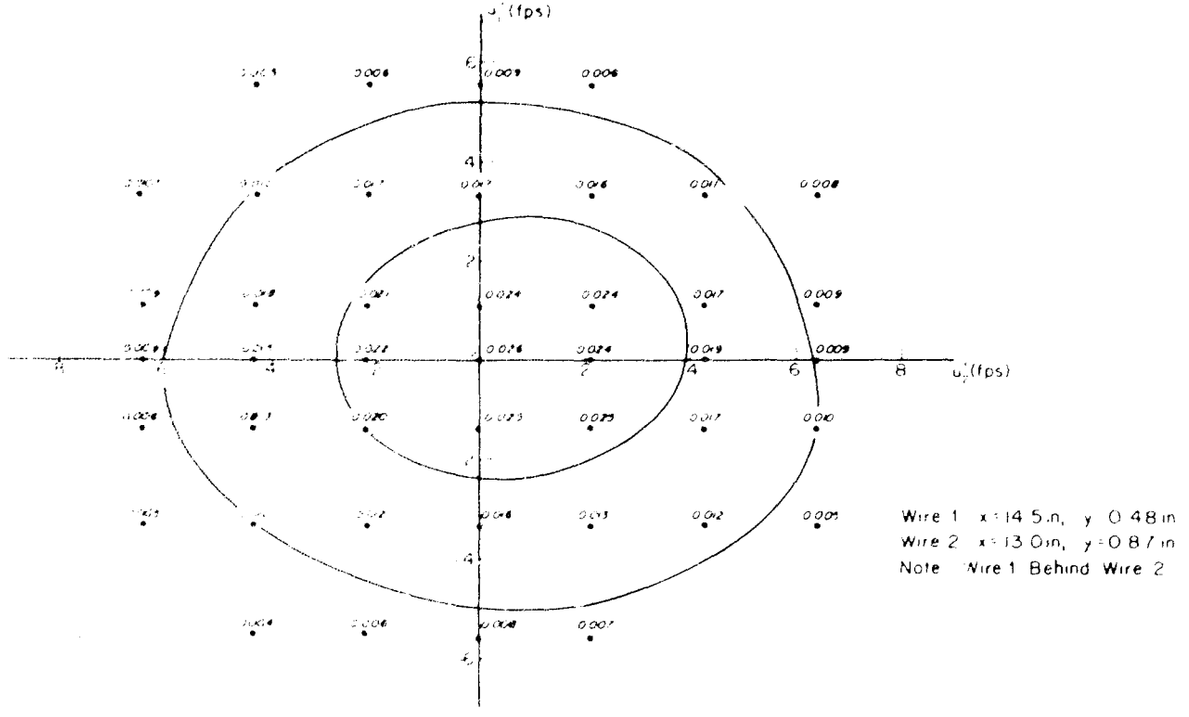

Fig. 62. Joint probability density of u_1' and u_2' along the trajectory launching from the top of the ridge with 60° azimuth (Numerical values on the contours = $f(u',v')\sqrt{\overline{u'^2}}\sqrt{\overline{v'^2}}$).

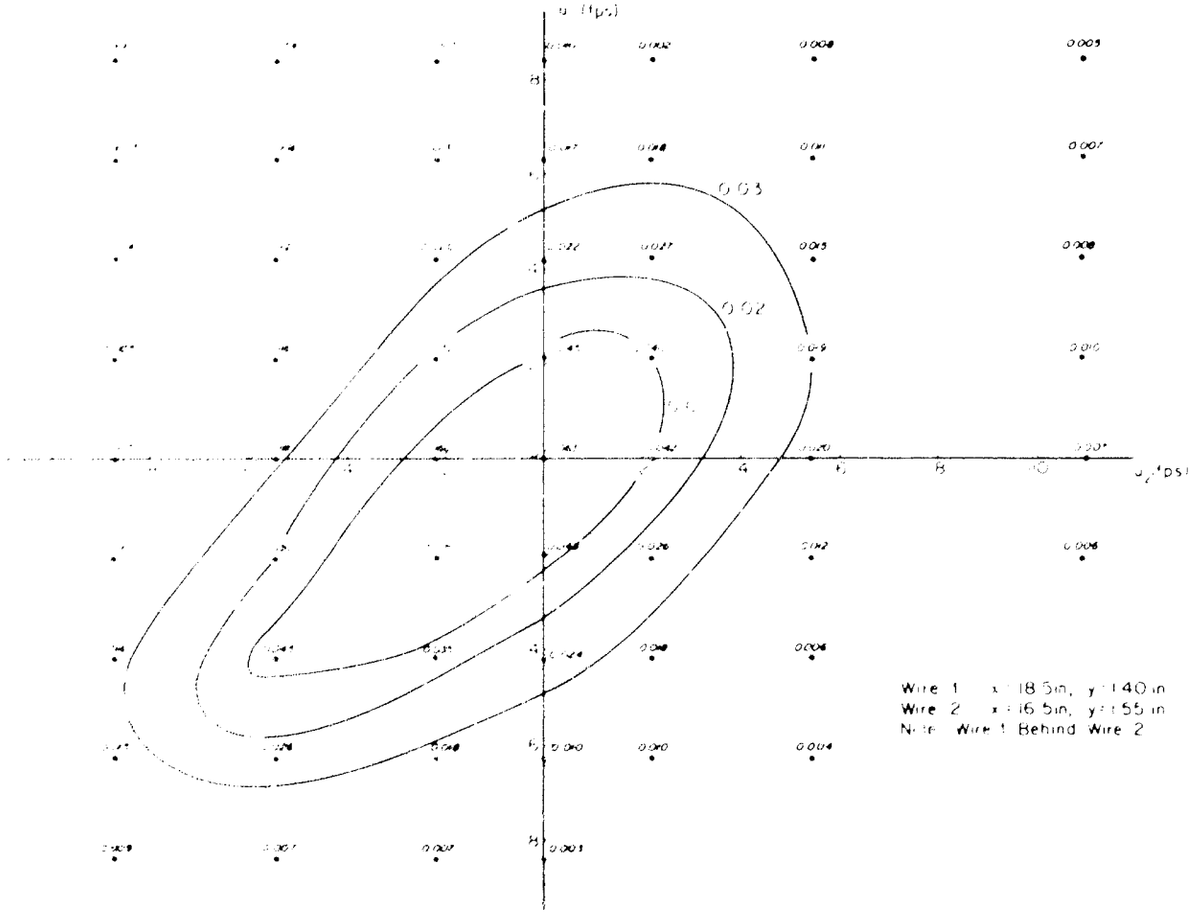

Fig. 65. Joint probability density of u_1' and u_2' along the trajectory launching from the halfway up the ridge with 0° azimuth (Numerical values on the contours = $f(u',v')\sqrt{\overline{u'^2}}\sqrt{\overline{v'^2}}$).

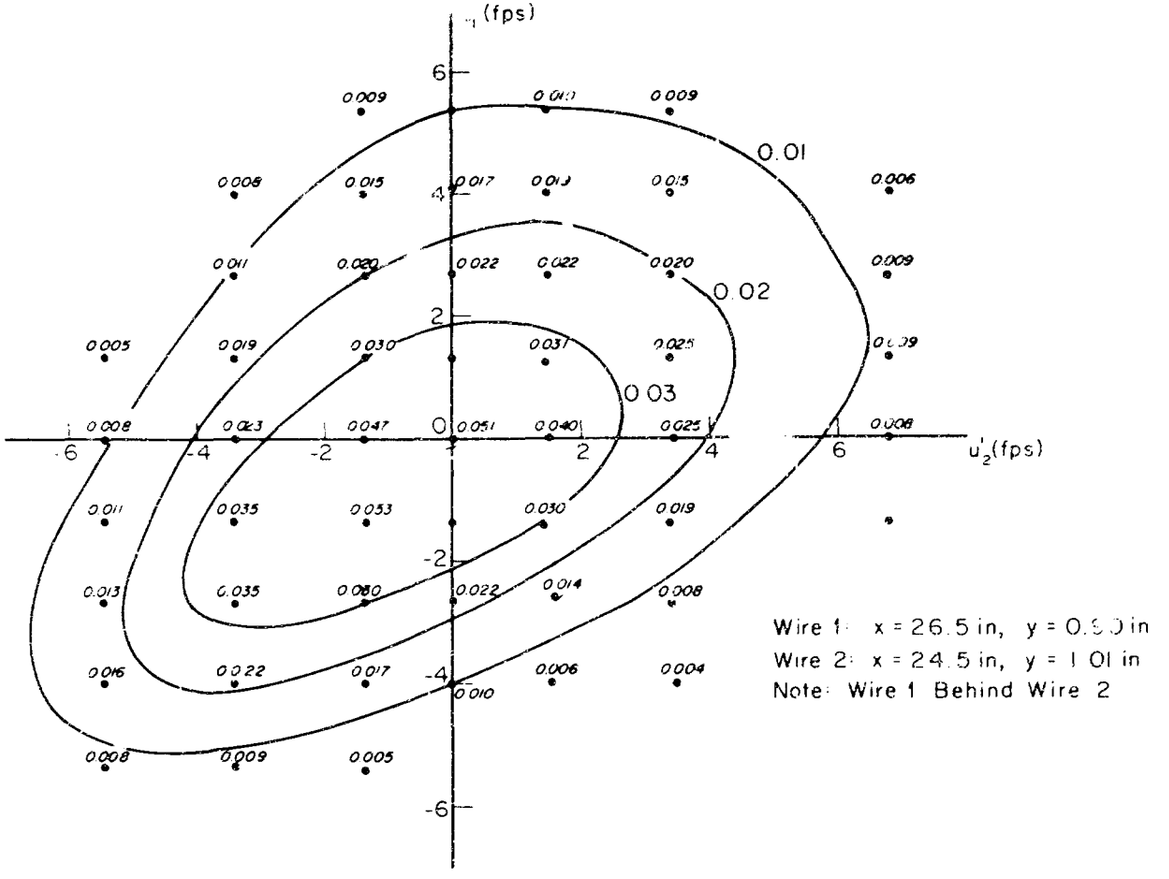

Fig. 64. Joint probability density of u_1' and u_2' along the trajectory launching from the halfway up the ridge with 0° azimuth (Numerical values on the contours = $f(u',v')\ \sqrt{\overline{u'^2}}\ \sqrt{\overline{v'^2}}$)

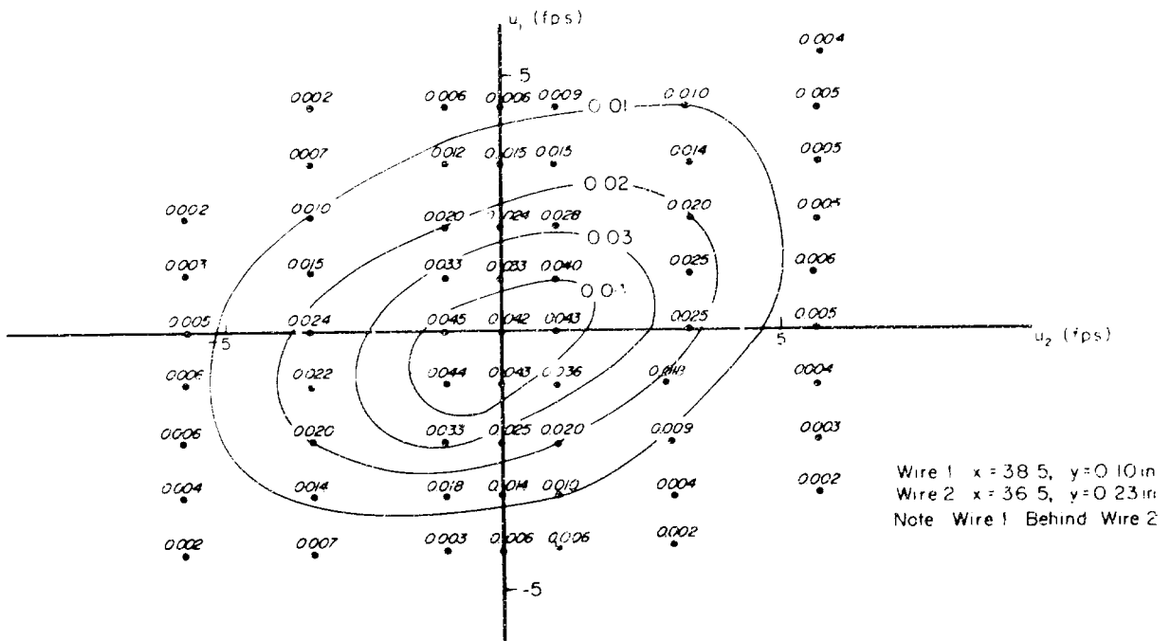

Fig. 65. Joint probability density of u_1' and u_2' along the trajectory launching from the halfway up the ridge with 0° azimuth (Numerical values on the contours = $f(u',v') \sqrt{\overline{u'^2}} \sqrt{\overline{v'^2}}$).

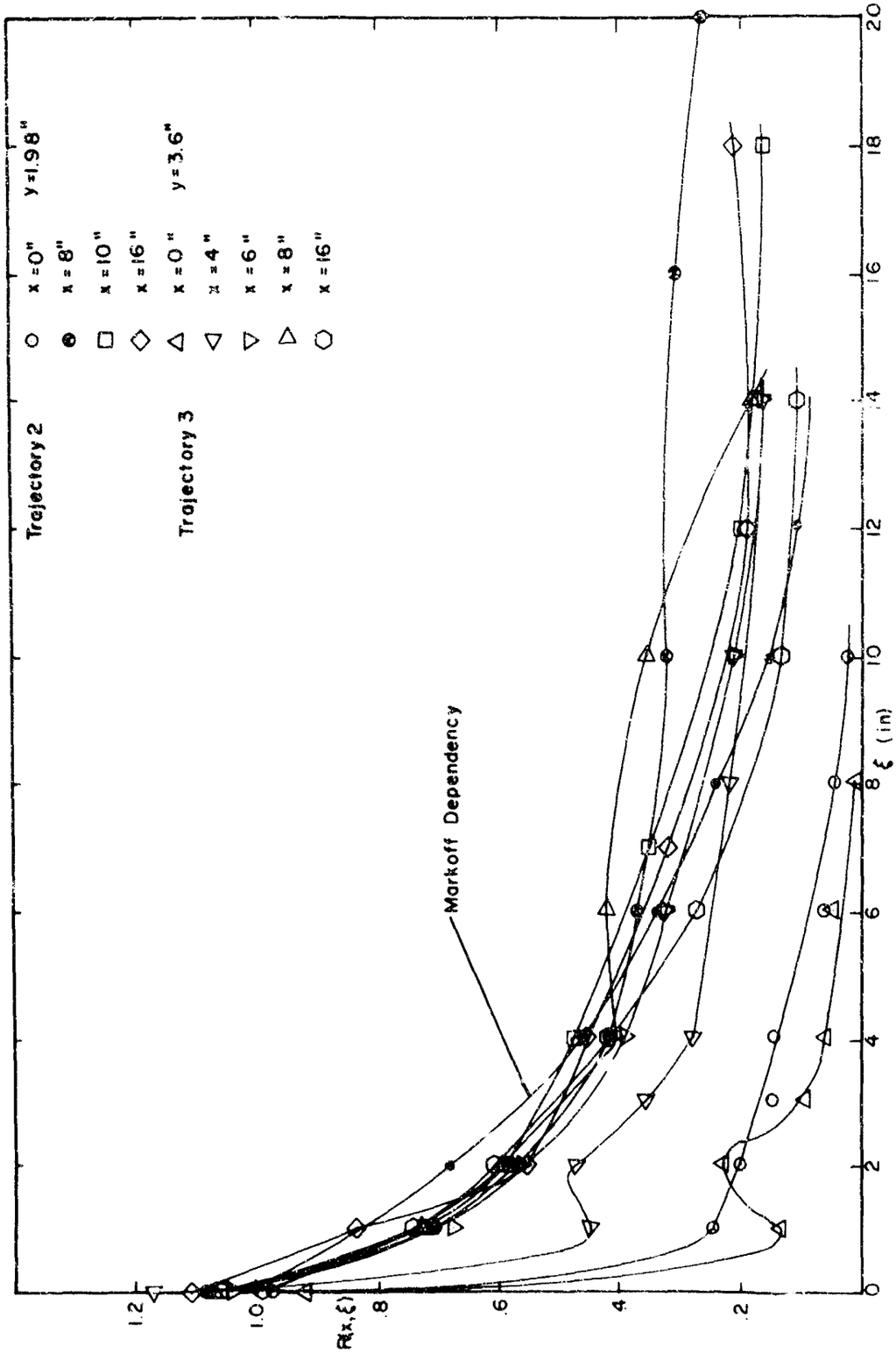

Fig. 66. Space correlation coefficients at various starting points along two selected trajectories with C^0 azimuth.

UNCLASSIFIED
Security Classification

DOCUMENT CONTROL DATA - R&D

(Security classification of title, body of abstract and indexing annotation must be entered when the overall report is classified)

1 ORIGINATING ACTIVITY (Corporate author)

FLUID DYNAMICS AND DIFFUSION LABORATORY
COLLEGE OF ENGINEERING, COLORADO STATE UNIVERSITY
FORT COLLINS, COLORADO 80521

2a REPORT SECURITY CLASSIFICATION: UNCLASSIFIED

2b GROUP:

3 REPORT TITLE

APPROXIMATE JOINT PROBABILITY DISTRIBUTIONS OF THE TURBULENCE ALONG A HYPOTHETICAL MISSILE TRAJECTORY DOWNWIND OF A SINUSOIDAL MODEL RIDGE

4 DESCRIPTIVE NOTES (Type of report and inclusive dates)

TECHNICAL REPORT

5 AUTHOR(S) (Last name, first name, initial)

Plate, E. J. Kung, R.

Yeh, F. F.

6 REPORT DATE	7a TOTAL NO. OF PAGES	7b NO. OF REFS
February, 1969	104	10

8a CONTRACT OR GRANT NO.	9a ORIGINATOR'S REPORT NUMBER(S)
DAAB07-68-C-0423	CER68-69EJP-FY-RK-4
b PROJECT NO. 1 TO. 14501B53A.08	
c	9b OTHER REPORT NO(S) (Any other numbers that may be assigned this report)
d	ECOM C-0423-2

10 AVAILABILITY/LIMITATION NOTICES

11 SUPPLEMENTARY NOTES	12 SPONSORING MILITARY ACTIVITY
	U.S. Army Electronics Command Fort Monmouth, N. J.

13 ABSTRACT

The wind field is investigated which is encountered by a missile traveling along a hypothetical trajectory downwind of a two-dimensional ridge. Reasons are given for studying this situation in a wind tunnel. The problem is reduced to the determination of turbulence spectra and of joint probabilities for the joint occurrence of two velocities simultaneously along the trajectory which corresponds to mean flow conditions.

In the theoretical part an attempt is made to obtain approximations to the joint probability density distributions which yield to experimental evaluation. The experimental part is concerned with measurements of profiles of mean velocities and turbulent intensities and with the determination of turbulence data for evaluating spectra and joint probability distributions.

DD FORM 1 JAN 64 1473

UNCLASSIFIED
Security Classification

14. KEY WORDS	LINK A		LINK B		LINK C	
	ROLE	WT	ROLE	WT	ROLE	WT
TURBULENCE BOUNDARY LAYER WIND TUNNEL MODELING						

INSTRUCTIONS

1. ORIGINATING ACTIVITY: Enter the name and address of the contractor, subcontractor, grantee, Department of Defense activity or other organization *(corporate author)* issuing the report.

2a. REPORT SECURITY CLASSIFICATION: Enter the overall security classification of the report. Indicate whether "Restricted Data" is included. Marking is to be in accordance with appropriate security regulations.

2b. GROUP: Automatic downgrading is specified in DoD Directive 5200.10 and Armed Forces Industrial Manual. Enter the group number. Also, when applicable, show that optional markings have been used for Group 3 and Group 4 as authorized.

3. REPORT TITLE: Enter the complete report title in all capital letters. Titles in all cases should be unclassified. If a meaningful title cannot be selected without classification, show title classification in all capitals in parenthesis immediately following the title.

4. DESCRIPTIVE NOTES: If appropriate, enter the type of report, e.g., interim, progress, summary, annual, or final. Give the inclusive dates when a specific reporting period is covered.

5. AUTHOR(S): Enter the name(s) of author(s) as shown on or in the report. Enter last name, first name, middle initial. If military, show rank and branch of service. The name of the principal author is an absolute minimum requirement.

6. REPORT DATE: Enter the date of the report as day, month, year; or month, year. If more than one date appears on the report, use date of publication.

7a. TOTAL NUMBER OF PAGES: The total page count should follow normal pagination procedures, i.e., enter the number of pages containing information.

7b. NUMBER OF REFERENCES. Enter the total number of references cited in the report.

8a. CONTRACT OR GRANT NUMBER: If appropriate, enter the applicable number of the contract or grant under which the report was written.

8b, 8c, & 8d. PROJECT NUMBER: Enter the appropriate military department identification, such as project number, subproject number, system numbers, task number, etc.

9a. ORIGINATOR'S REPORT NUMBER(S): Enter the official report number by which the document will be identified and controlled by the originating activity. This number must be unique to this report.

9b. OTHER REPORT NUMBER(S): If the report has been assigned any other report numbers *(either by the originator or by the sponsor)*, also enter this number(s).

10. AVAILABILITY/LIMITATION NOTICES: Enter any limitations on further dissemination of the report, other than those imposed by security classification, using standard statements such as:

(1) "Qualified requesters may obtain copies of this report from DDC."

(2) "Foreign announcement and dissemination of this report by DDC is not authorized."

(3) "U. S. Government agencies may obtain copies of this report directly from DDC. Other qualified DDC users shall request through _____."

(4) "U. S. military agencies may obtain copies of this report directly from DDC. Other qualified users shall request through _____."

(5) "All distribution of this report is controlled. Qualified DDC users shall request through _____."

If the report has been furnished to the Office of Technical Services, Department of Commerce, for sale to the public, indicate this fact and enter the price, if known.

11. SUPPLEMENTARY NOTES: Use for additional explanatory notes.

12. SPONSORING MILITARY ACTIVITY. Enter the name of the departmental project office or laboratory sponsoring *(paying for)* the research and development. Include address.

13 ABSTRACT. Enter an abstract giving a brief and factual summary of the document indicative of the report, even though it may also appear elsewhere in the body of the technical report. If additional space is required, a continuation sheet shall be attached.

It is highly desirable that the abstract of classified reports be unclassified. Each paragraph of the abstract shall end with an indication of the military security classification of the information in the paragraph, represented as *(TS)*, *(S)*, *(C)*, or *(U)*.

There is no limitation on the length of the abstract. However, the suggested length is from 150 to 225 words.

14. KEY WORDS: Key words are technically meaningful terms or short phrases that characterize a report and may be used as index entries for cataloging the report. Key words must be selected so that no security classification is required. Identifiers, such as equipment model designation, trade name, military project code name, geographic location, may be used as key words but will be followed by an indication of technical context. The assignment of links, rules, and weights is optional.